III

Dynamics and Control of Aerospace Systems

Robert E. Skelton

17

An Introduction to the Mechanics of Tensegrity Structures

Robert E. Skelton
University of California, San Diego

J. William Helton
University of California, San Diego

Rajesh Adhikari
University of California, San Diego

Jean-Paul Pinaud
University of California, San Diego

Waileung Chan
University of California, San Diego

Abstract

Tensegrity structures consist of strings (in tension) and bars (in compression). Strings are strong, light, and foldable, so tensegrity structures have the potential to be light but strong and deployable. Pulleys, NiTi wire, or other actuators to selectively tighten some strings on a tensegrity structure can be used to control its shape. This chapter describes some principles we have found to be true in a detailed study of mathematical models of several tensegrity structures. We describe properties of these structures which appear to have a good chance of holding quite generally. We describe how pretensing all strings of a tensegrity makes its shape robust to various loading forces. Another property (proven analytically) asserts that the shape of a tensegrity structure can be changed substantially with little change in the potential energy of the structure. Thus, shape control should be inexpensive. This is in contrast to control of classical structures which require substantial energy to change their shapes. A different aspect of the chapter is the presentation of several tensegrities that are light but extremely strong. The concept of self-similar structures is used to find minimal mass subject to a specified buckling constraint. The stiffness and strength of these structures are determined.

17.1 Introduction

Tensegrity structures are built of bars and strings attached to the ends of the bars. The bars can resist compressive force and the strings cannot. Most bar–string configurations which one might conceive are not in equilibrium, and if actually constructed will collapse to a different shape. Only bar–string configurations in a stable equilibrium will be called **tensegrity structures**.

If well designed, the application of forces to a tensegrity structure will deform it into a slightly different shape in a way that supports the applied forces. Tensegrity structures are very special cases of trusses, where members are assigned special functions. Some members are always in tension and others are always in compression. We will adopt the words "strings" for the tensile members, and "bars" for compressive members. (The different choices of words to describe the tensile members as "strings," "tendons," or "cables" are motivated only by the scale of applications.) A tensegrity structure's bars cannot be attached to each other through joints that impart torques. The end of a bar can be attached to strings or ball jointed to other bars.

The artist Kenneth Snelson[1] (Figure 17.1) built the first tensegrity structure and his artwork was the inspiration for the first author's interest in tensegrity. Buckminster Fuller[2] coined the word "tensegrity" from two words: "tension" and "integrity."

17.1.1 The Benefits of Tensegrity

A large amount of literature on the geometry, artform, and architectural appeal of tensegrity structures exists, but there is little on the dynamics and mechanics of these structures.[2-19] Form-finding results for simple symmetric structures appear[10,20-24] and show an array of stable tensegrity units is connected to yield a large stable system, which can be deployable.[14] Tensegrity structures for civil engineering purposes have been built and described.[25-27] Several reasons are given below why tensegrity structures should receive new attention from mathematicians and engineers, even though the concepts are 50 years old.

17.1.1.1 Tension Stabilizes

A compressive member loses stiffness as it is loaded, whereas a tensile member gains stiffness as it is loaded. Stiffness is lost in two ways in a compressive member. In the absence of any bending moments in the axially loaded members, the forces act exactly through the mass center, the material spreads, increasing the diameter of the center cross section; whereas the tensile member reduces its cross-section under load. In the presence of bending moments due to offsets in the line of force application and the center of mass, the bar becomes softer due to the bending motion. For most materials, the tensile strength of a longitudinal member is larger than its buckling (compressive)

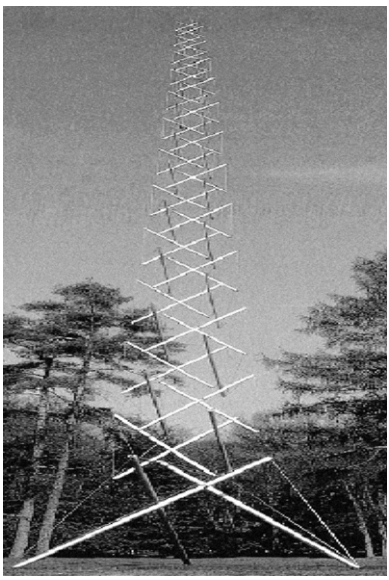

FIGURE 17.1 Snelson's tensegrity structure. (From Connelly, R. and Beck, A., *American Scientist,* 86(2), 143, 1998. Kenneth Snelson, Needle Tower 11, 1969, Kröller Müller Museum. With permission.)

strength. (Obviously, sand, masonary, and unreinforced concrete are exceptions to this rule.) Hence, a large stiffness-to-mass ratio can be achieved by increasing the use of tensile members.

17.1.1.2 Tensegrity Structures are Efficient

It has been known since the middle of the 20th century that continua cannot explain the strength of materials. The geometry of material layout is critical to strength at all scales, from nanoscale biological systems to megascale civil structures. Traditionally, humans have conceived and built structures in rectilinear fashion. Civil structures tend to be made with orthogonal beams, plates, and columns. Orthogonal members are also used in aircraft wings with longerons and spars. However, evidence suggests that this "orthogonal" architecture does not usually yield the minimal mass design for a given set of stiffness properties.[28] Bendsoe and Kikuchi,[29] Jarre,[30] and others have shown that the optimal distribution of mass for specific stiffness objectives tends to be neither a solid mass of material with a fixed external geometry, nor material laid out in orthogonal components. Material is needed only in the essential load paths, not the orthogonal paths of traditional manmade structures. *Tensegrity structures* use longitudinal members arranged in very unusual (and nonorthogonal) patterns to achieve strength with small mass. Another way in which tensegrity systems become mass efficient is with self-similar constructions replacing one tensegrity member by yet another tensegrity structure.

17.1.1.3 Tensegrity Structures are Deployable

Materials of high strength tend to have a very limited displacement capability. Such piezoelectric materials are capable of only a small displacement and "smart" structures using sensors and actuators have only a small displacement capability. Because the compressive members of tensegrity structures are either disjoint or connected with ball joints, large displacement, deployability, and stowage in a compact volume will be immediate virtues of tensegrity structures.[8,11] This feature offers operational and portability advantages. A portable bridge, or a power transmission tower made as a tensegrity structure could be manufactured in the factory, stowed on a truck or helicopter in a small volume, transported to the construction site, and deployed using only winches for erection through cable tension. Erectable temporary shelters could be manufactured, transported, and deployed in a similar manner. Deployable structures in space (complex mechanical structures combined with active control technology) can save launch costs by reducing the mass required, or by eliminating the requirement for assembly by humans.

17.1.1.4 Tensegrity Structures are Easily Tunable

The same deployment technique can also make small adjustments for fine tuning of the loaded structures, or adjustment of a damaged structure. Structures that are designed to allow tuning will be an important feature of next generation mechanical structures, including civil engineering structures.

17.1.1.5 Tensegrity Structures Can be More Reliably Modeled

All members of a tensegrity structure are axially loaded. Perhaps the most promising scientific feature of tensegrity structures is that while the *global* structure bends with external static loads, none of the *individual* members of the tensegrity structure experience bending moments. (In this chapter, we design all compressive members to experience loads well below their Euler buckling loads.) Generally, members that experience deformation in two or three dimensions are much harder to model than members that experience deformation in only one dimension. The Euler buckling load of a compressive member is from a bending instability calculation, and it is known in practice to be very unreliable. That is, the actual buckling load measured from the test data has a larger variation and is not as predictable as the tensile strength. Hence, increased use of tensile members is expected to yield more robust models and more efficient structures. More reliable models can be expected for axially loaded members compared to models for members in bending.[31]

17.1.1.6 Tensegrity Structures Facilitate High Precision Control

Structures that can be more precisely modeled can be more precisely controlled. Hence, tensegrity structures might open the door to quantum leaps in the precision of controlled structures. The architecture (geometry) dictates the mathematical properties and, hence, these mathematical results easily scale from the nanoscale to the megascale, from applications in microsurgery to antennas, to aircraft wings, and to robotic manipulators.

17.1.1.7 Tensegrity is a Paradigm that Promotes the Integration of Structure and Control Disciplines

A given tensile or compressive member of a tensegrity structure can serve multiple functions. It can simultaneously be a load-carrying member of the structure, a sensor (measuring tension or length), an actuator (such as nickel-titanium wire), a thermal insulator, or an electrical conductor. In other words, by proper choice of materials and geometry, a grand challenge awaits the tensegrity designer: How to control the electrical, thermal, and mechanical energy in a material or structure? For example, smart tensegrity wings could use shape control to maneuver the aircraft or to optimize the air foil as a function of flight condition, without the use of hinged surfaces. Tensegrity structures provide a promising paradigm for integrating structure and control design.

17.1.1.8 Tensegrity Structures are Motivated from Biology

Figure 17.2 shows a rendition of a spider fiber, where amino acids of two types have formed hard β–pleated sheets that can take compression, and thin strands that take tension.[32,33] The β–pleated sheets are discontinuous and the tension members form a continuous network. Hence, the nanostructure of the spider fiber is a tensegrity structure. Nature's endorsement of tensegrity structures warrants our attention because per unit mass, spider fiber is the strongest natural fiber.

Articles by Ingber[7,34,35] argue that tensegrity is the fundamental building architecture of life. His observations come from experiments in cell biology, where prestressed truss structures of the tensegrity type have been observed in cells. It is encouraging to see the similarities in structural building blocks over a wide range of scales. If tensegrity is nature's preferred building architecture, modern analytical and computational capabilities of tensegrity could make the same incredible efficiency possessed by natural systems transferrable to manmade systems, from the nano- to the megascale. This is a grand design challenge, to develop scientific procedures to create smart tensegrity structures that can regulate the flow of thermal, mechanical, and electrical energy in a material system by proper choice of materials, geometry, and controls. This chapter contributes to this cause by exploring the mechanical properties of simple tensegrity structures.

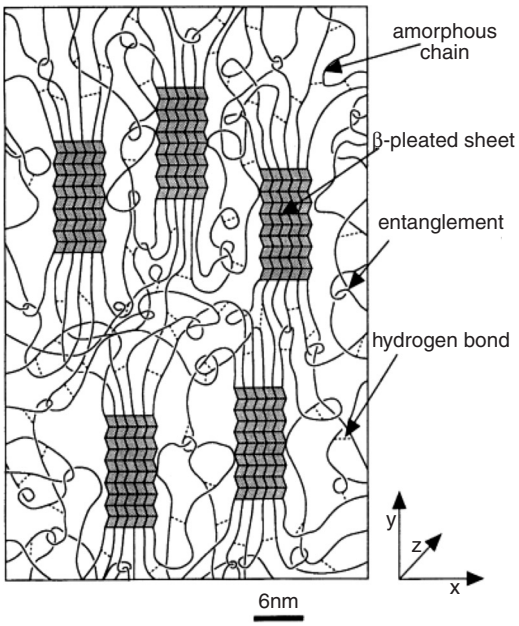

FIGURE 17.2 Structure of the Spider Fiber. (From Termonia, Y., *Macromolecules*, 27, 7378–7381, 1994. Reprinted with permission from the American Chemical Society.)

The remainder of the introduction describes the main results of this chapter. We start with formal definitions and then turn to results.

17.1.2 Definitions and Examples

This is an introduction to the mechanics of a class of prestressed structural systems that are composed only of axially loaded members. We need a couple of definitions to describe tensegrity scientifically.

Definition 17.1 *We say that the geometry of a material system is in a stable equilibrium if all particles in the material system return to this geometry, as time goes to infinity, starting from any initial position arbitrarily close to this geometry.*

In general, a variety of boundary conditions may be imposed, to distinguish, for example, between bridges and space structures. But, for the purposes of this chapter we characterize only the material system with free–free boundary conditions, as for a space structure. We will herein characterize the bars as rigid bodies and the strings as one-dimensional elastic bodies. Hence, a material system is in equilibrium if the nodal points of the bars in the system are in equilibrium.

Definition 17.2 *A* Class k tensegrity structure *is a stable equilibrium of axially loaded elements, with a maximum of k compressive members connected at the node(s).*

Fact 17.1 Class k tensegrity structures *must have tension members*.

Fact 17.1 follows from the requirement to have a stable equilibrium.

Fact 17.2 *Kenneth Snelson's structures of which* Figure *17.1 is an example are all* Class 1 tensegrity structures, *using Definition 17.1. Buckminster Fuller coined the word tensegrity to imply a connected set of tension members and a disconnected set of compression members. This fits our "Class 1" definition.*

A Class 1 tensegrity structure has a connected network of members in tension, while the network of compressive members is disconnected. To illustrate these various definitions, Figure 17.3(a)

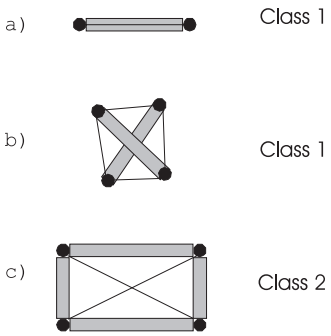

FIGURE 17.3 Tensegrity structures.

illustrates the simplest tensegrity structure, composed of one bar and one string in tension. Thin lines are strings and shaded bars are compressive members. Figure 17.3(b) describes the next simplest arrangement, with two bars. Figure 17.3(c) is a Class 2 tensegrity structure because two bars are connected at the nodes. Figure 17.3(c) represents a Class 2 tensegrity in the plane. However, as a three-dimensional structure, it is not a tensegrity structure because the equilibrium is unstable (the tensegrity definition requires a stable equilibrium).

From these definitions, the existence of a tensegrity structure having a specified geometry reduces to the question of whether there exist finite tensions that can be applied to the tensile members to hold the system in that geometry, in a stable equilibrium.

We have illustrated that the geometry of the nodal points and the connections cannot be arbitrarily specified. The role that geometry plays in the mechanical properties of tensegrity structures is the focus of this chapter.

The planar tensegrity examples shown follow a naming convention that describes the number of compressive members and tension members. The number of compressive members is associated with the letter C, while the number of tensile members is associated with T. For example, a structure that contains two compressive members and four tension members is called a *C*2*T*4 tensegrity.

17.1.3 The Analyzed Structures

The basic examples we analyzed are the structures shown in Figure 17.4, where thin lines are the strings and the thick lines are bars. Also, we analyzed various structures built from these basic structural units. Each structure was analyzed under several types of loading. In particular, the top and bottom loads indicated on the *C*2*T*4 structure point in opposite directions, thereby resulting in bending. We also analyzed a *C*2*T*4 structure with top and bottom loads pointing in the same direction, that is, a compressive situation. The *C*4*T*2 structure of Figure 17.4(b) reduces to a *C*4*T*1 structure when the horizontal string is absent. The mass and stiffness properties of such structures will be of interest under compressive loads, *F*, as shown. The 3-bar SVD (defined in 17.4.1) was studied under two types of loading: axial and lateral. Axial loading is compressive while lateral loading results in bending.

17.1.4 Main Results on Tensegrity Stiffness

A reasonable test of any tensegrity structure is to apply several forces each of magnitude F at several places and plot how some measure of its shape changes. We call the plot of $dF/dshape$ vs. F a stiffness profile of the structure. The chapter analyzes stiffness profiles of a variety of tensegrity structures. We paid special attention to the role of pretension set in the strings of the tensegrity. While we have not done an exhaustive study, there are properties common to these examples which we now describe. How well these properties extend to all tensegrity structures remains to be seen.

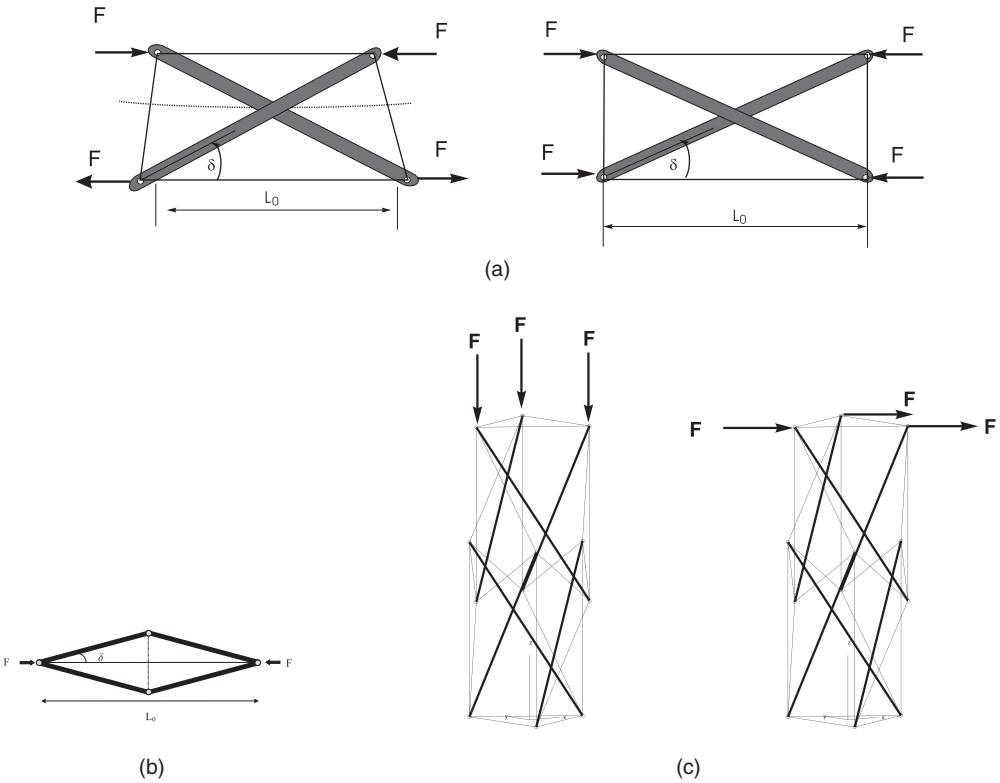

FIGURE 17.4 Tensegrities studied in this chapter (not to scale), (a) *C2T*4 bending loads (left) and compressive loads (right), (b) *C*4*T*2, and (c) 3-bar SVD axial loads (left) and lateral loads (right).

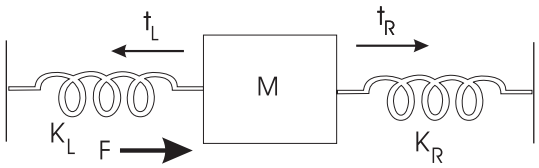

FIGURE 17.5 Mass–spring system.

However, laying out the principles here is an essential first step to discovering those universal properties that do exist.

The following example with masses and springs prepares us for two basic principles which we have observed in the tensegrity paradigm.

17.1.4.1 Basic Principle 1: Robustness from Pretension

As a parable to illustrate this phenomenon, we resort to the simple example of a mass attached to two bungy cords. (See Figure 17.5.)

Here K_L, K_R are the spring constants, F is an external force pushing right on the mass, and t_L, t_R are tensions in the bungy cords when $F = 0$. The bungy cords have the property that when they are shorter than their rest length they become inactive. If we set any positive pretensions t_L, t_R, there is a corresponding equilibrium configuration, and we shall be concerned with how the shape of this configuration changes as force F is applied. Shape is a peculiar word to use here when we mean position of the mass, but it forshadows discussions about very general tensegrity structures. The effect of the stiffness of the structure is seen in Figure 17.6.

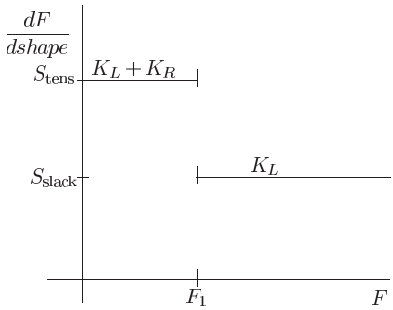

FIGURE 17.6 Mass–spring system stiffness profile.

There are two key quantities in this graph which we see repeatedly in tensegrity structures. The first is the critical value F_1 where the stiffness drops. It is easy to see that F_1 equals the value of F at which the right cord goes slack. Thus, F_1 increases with the pretension in the right cord. The second key parameter in this figure is the size of the jump as measured by the ratio

$$r := \frac{S_{tens}}{S_{slack}}$$

When $r = 1$, the stiffness plot is a straight horizontal line with no discontinuity. Therefore, the amount of pretension affects the value of F_1, but has no influence on the stiffness. One can also notice that increasing the value of r increases the size of the jump. What determines the size of r is just the ratio κ of the spring constants $\kappa := K_R/K_L$, since $r = 1 + \kappa$, indeed r is an increasing function of κ

$$r \cong \infty \quad \text{if} \quad \kappa \cong \infty.$$

Of course, pretension is impossible if $K_R = 0$. Pretension increases F_1 and, hence, allows us to stay in the high stiffness regime given by S_{tens}, over a larger range of applied external force F.

17.1.4.2 Robustness from Pretension Principle for Tensegrity Structures

Pretension is known in the structures community as a method of increasing the load-bearing capacity of a structure through the use of strings that are stretched to a desired tension. This allows the structure to support greater loads without as much deflection as compared to a structure without any pretension.

For a tensegrity structure, the role of pretension is monumental. For example, in the analysis of the planar tensegrity structure, the slackening of a string results in dramatic nonlinear changes in the bending rigidity. Increasing the pretension allows for greater bending loads to be carried by the structure while still exhibiting near constant bending rigidity. In other words, the slackening of a string occurs for a larger external load. We can loosely describe this as a robustness property, in that the structure can be designed with a certain pretension to accomodate uncertainties in the loading (bending) environment. Not only does pretension have a consequence for these mechanical properties, but also for the so-called prestressable problem, which is left for the statics problem. The prestressable problem involves finding a geometry which can sustain its shape without external forces being applied and with all strings in tension.[12,20]

17.1.4.2.1 Tensegrity Structures in Bending

What we find is that bending stiffness profiles for all examples we study have levels S_{tens} when all strings are in tension, S_{slack1} when one string is slack, and then other levels as other strings go slack or as strong forces push the structure into radically different shapes (see Figure 17.7). These very high force regimes can be very complicated and so we do not analyze them. Loose motivation for

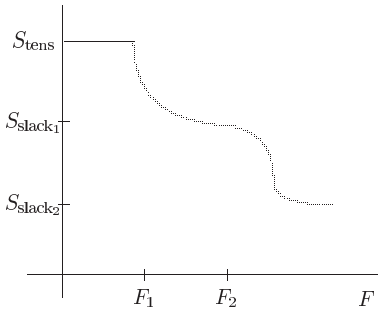

FIGURE 17.7 Gedanken stiffness profile.

the form of a bending stiffness profile curve was given in the mass and two bungy cord example, in which case we had two stiffness levels.

One can imagine a more complicated tensegrity geometry that will possibly yield many stiffness levels. This intuition arises from the possibility that multiple strings can become slack depending on the directions and magnitudes of the loading environment. One hypothetical situation is shown in Figure 17.7 where three levels are obtained. All tensegrity examples in the chapter have bending stiffness profiles of this form, at least until the force F radically distorts the figure. The specific profile is heavily influenced by the geometry of the tensegrity structure as well as of the stiffness of the strings, K_{string}, and bars, K_{bar}. In particular, the ratio

$$K := \frac{K_{string}}{K_{bar}}$$

is an informative parameter.

General properties common to our bending examples are

1. When no string is slack, the geometry of a tensegrity and the materials used have much more effect on its stiffness than the amount of pretension in its strings.
2. As long as all strings are in tension (that is, $F < F_1$), stiffness has little dependence on F or on the amount of pretension in the strings.
3. A larger pretension in the strings produces a larger F_1.
4. As F exceeds F_1 the stiffness quickly drops.
5. The ratio

$$r_1 := \frac{S_{tens}}{S_{slack}}$$

is an increasing function of K. Moreover, $r_1 \to \infty$ as $K \to \infty$ (if the bars are flabby, the structure is flabby once a string goes slack). Similar parameters, r_2, can be defined for each change of stiffness.

Examples in this chapter that substantiate these principles are the stiffness profile of *C2T*4 under bending loads as shown in Figure 17.12. Also, the laterally loaded 3-bar SVD tensegrity shows the same behavior with respect to the above principles, Figure 17.54 and Figure 17.55.

17.1.4.2.2 Tensegrity Structures in Compression

For compressive loads, the relationships between stiffness, pretension, and force do not always obey the simple principles listed above. In fact, we see three qualitatively different stiffness profiles in our compression loading studies. We now summarize these three behavior patterns.

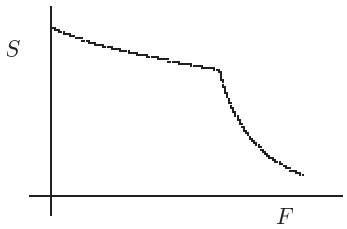

FIGURE 17.8 Stiffness profile for *C*4*T*2 in compression.

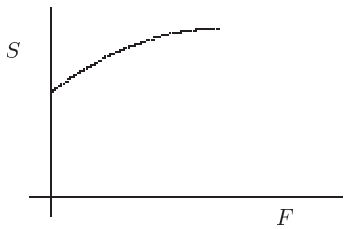

FIGURE 17.9 Stiffness profile of 3-bar SVD in compression.

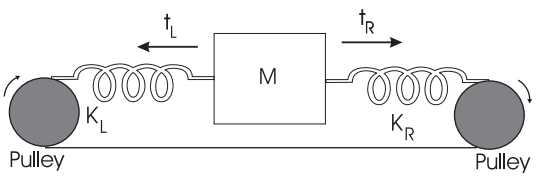

FIGURE 17.10 Mass–spring control system.

The *C*2*T*4 planar tensegrity exhibits the pretension robustness properties of Principles I, II, III, as shown in Figure 17.6. The pretension tends to prevent slack strings.

The *C*4*T*2 structure has a stiffness profile of the form in Figure 17.8. Only in the *C*4*T*1 and *C*4*T*2 examples does stiffness immediately start to fall as we begin to apply a load.

The axially loaded 3-bar-SVD, the stiffness profile even for small forces, is seriously affected by the amount of pretension in the structure. Rather than stiffness being constant for $F < F_1$ as is the case with bending, we see in Figure 17.9 that stiffness increases with F for small and moderate forces. The qualitative form of the stiffness profile is shown in Figure 17.9. We have not systematically analyzed the role of the stiffness ratio K in compression situations.

17.1.4.2.3 Summary

Except for the *C*4*T*2 compression situation, when a load is applied to a tensegrity structure the stiffness is essentially constant as the loading force increases unless a string goes slack.

17.1.4.3 Basic Principle 2: Changing Shape with Small Control Energy

We begin our discussion not with a tensegrity structure, but with an analogy. Imagine, as in Figure 17.10, that the rigid boundary conditions of Figure 17.5 become frictionless pulleys. Suppose we are able to actuate the pulleys and we wish to move the mass to the right, we can turn each pulley clockwise. The pretension can be large and yet very small control torques are needed to change the position of the nodal mass.

Tensegrity structures, even very complicated ones, can be actuated by placing pulleys at the nodes (ends of bars) and running the end of each string through a pulley. Thus, we think of two pulleys being associated with each string and the rotation of the pulleys can be used to shorten or loosen the string. The mass–spring example foreshadows the fact that even in tensegrity structures, shape changes (moving nodes changes the shape) can be achieved with little change in the potential energy of the system.

17.1.5 Mass vs. Strength

The chapter also considers the issue of the strength vs. mass of tensegrity structures. We find our planar examples to be very informative. We shall consider two types of strength. They are the size of the bending forces and the size of compressive forces required to break the object.

First, in 17.2 we study the ratio of bending strength to mass. We compare this for our $C2T4$ unit to a solid rectangular beam of the same mass. As expected, reasonably constructed $C2T4$ units will be stronger. We do this comparison to a rectangular beam by way of illustrating the mass vs. strength question, because a thorough study would compare tensegrity structures to various kinds of trusses and would require a very long chapter.

We analyze compression stiffness of the $C2T4$ tensegrity. The $C2T4$ has worse strength under compression than a solid rectangular bar. We analyze the compression stiffness of $C4T2$ and $C4T1$ structures and use self-similar concepts to reduce mass, while constraining stiffness to a desired value. The $C4T1$ structure has a better compression strength-to-mass ratio than a solid bar when $\delta < 29°$. The $C4T1$, while strong (not easily broken), may not have an extremely high stiffness.

17.1.5.1 A 2D Beam Composed of Tensegrity Units

After analyzing one $C2T4$ tensegrity unit, we lay n of them side by side to form a beam. We derive in 17.2.3 that the Euler buckling formula for a beam adapts directly to this case. From this we conclude that the strength of the beam under compression is determined primarily by the bending rigidity $(EI)_n$ of each of its units. In principle, one can build beams with arbitrarily great bending strength. In practice this requires more study. Thus, the favorable bending properties found for $C2T4$ bode well for beams made with tensegrity units.

17.1.5.2 A 2D Tensegrity Column

In 17.3 we take the $C4T2$ structure in Figure 17.4(b) and replace each bar with a smaller $C4T2$ structure, then we replace each bar of this new structure with a yet smaller $C4T2$ structure. In principle, such a self-similar construction can be repeated to any level. Assuming that the strings do not fail and have significantly less mass than the bars, we find that the compression strength increases without bound if we keep the mass of the total bars constant. This completely ignores the geometrical fact that as we go to finer and finer levels in the fractal construction, the bars increasingly overlap. Thus, at least in theory, we have a class of tensegrity structures with unlimited compression strength to mass ratio. Further issues of robustness to lateral and bending forces would have to be investigated to insure practicality of such structures. However, our dramatic findings based on a pure compression analysis are intriguing. The self-similar concept can be extended to the third dimension in order to design a realistic structure that could be implemented in a column.

The chapter is arranged as follows: Section 17.2 analyzes a very simple planar tensegrity structure to show an efficient structure in bending; Section 17.3 analyzes a planar tensegrity structure efficient in compression; Section 17.4 defines a shell class of tensegrity structures and examines several members of this class; Section 17.5 offers conclusions and future work. The appendices explain nonlinear and linear analysis of planar tensegrity.

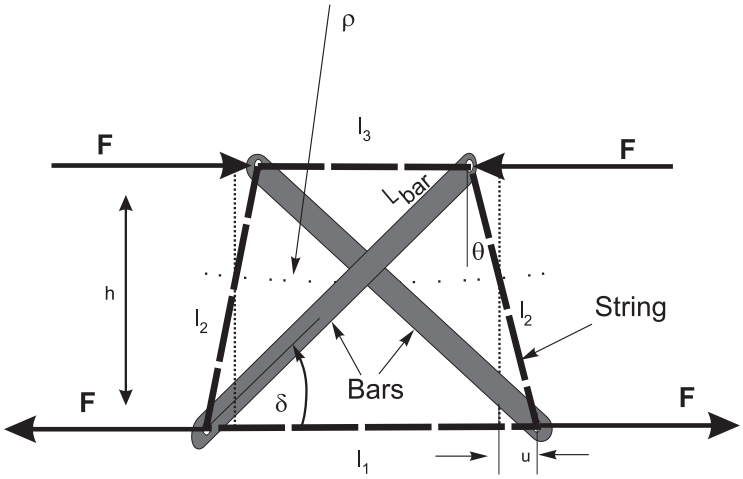

FIGURE 17.11 Planar one-stage tensegrity unit under pure bending.

17.2 Planar Tensegrity Structures Efficient in Bending

In this section, we examine the bending rigidity of a single tensegrity unit, a planar tensegrity model under pure bending as shown in Figure 17.11, where thin lines are the four strings and the two thick lines are bars. Because the structure in Figure 17.11 has two compressive and four tensile members, we refer to it as a *C2T*4 structure.

17.2.1 Bending Rigidity of a Single Tensegrity Unit

To arrive at a definition of bending stiffness suitable to *C2T*4, note that the moment M acting on the section is given by

$$M = FL_{bar} \sin \delta, \tag{17.1}$$

where F is the magnitude of the external force, L_{bar} is the length of the bar, and δ is the angle that the bars make with strings in the deformed state, as shown in Figure 17.11.

In Figure 17.11, ρ is the radius of curvature of the tensegrity unit under bending deformation. It can be shown from Figure 17.11 that

$$\rho = \left(\frac{L_{bar}}{2}\right)^2 \cos\delta \sin\delta \frac{1}{u}, \quad u = \frac{1}{2} L_{bar} \sin\delta \tan\theta. \tag{17.2}$$

The *bending rigidity* is defined by $EI = M\rho$. Hence,

$$EI = FL_{bar} \sin\delta\rho = FL_{bar} \sin^2\delta \left(\frac{L_{bar}}{2}\right)^2 \cos\delta \frac{1}{u}. \tag{17.3}$$

where EI is the equivalent bending rigidity of the planar one-stage tensegrity unit and u is the nodal displacement. The evaluation of the bending rigidity of the planar unit requires the evaluation of u, which will follow under various hypotheses. The bending rigidity will later be obtained by substituting u in (17.3).

17.2.1.1 Effective Bending Rigidity with Pretension

In the absence of external forces **f**, let $\mathbf{A}_0$ be the matrix defined in Appendix 17.A in terms of the initial prestressed geometry, and let $\mathbf{t}_0$ be the initial pretension applied on the members of the tensegrity. Then,

$$\mathbf{A_0 t_0} = \mathbf{0}, \quad \mathbf{t}_0^T = [\mathbf{t}_{0\_bars}\ \mathbf{t}_{0\_strings}], \quad \mathbf{t}_{0\_strings} \geq 0. \tag{17.4}$$

For a nontrivial solution of Equation (17.4), $\mathbf{A}_0$ must have a right null space. Furthermore, the elements of $\mathbf{t}_0$ obtained by solving Equation (17.4) must be such that the strings are always in tension, where $\mathbf{t}_{0\text{-}strings} \geq 0$ will be used to denote that each element of the vector is nonnegative. For this particular example of planar tensegrity, the null space of $\mathbf{A}_0$ is only one dimensional. $\mathbf{t}_0$ always exists, satisfying (17.4), and $\mathbf{t}_0$ can be scaled by any arbitrary positive scalar multiplier. However, the requirement of a stable equilibrium in the tensegrity definition places one additional constraint to the conditions (17.4); the geometry from which $\mathbf{A_0}$ is constructed must be a stable equilibrium.

In the following discussions, E_s, $(EA)_s$, and A_s denote the Young's modulus of elasticity, the axial rigidity and the cross-sectional area of the strings, respectively, whereas E_b, $(EA)_b$, and A_b, denote those of the bars, respectively. $(EI)_b$ denotes the bending rigidity of the bars.

The equations of the static equilibrium and the bending rigidity of the tensegrity unit are nonlinear functions of the geometry δ, the pretension $\mathbf{t}_0$, the external force **F**, and the stiffnesses of the strings and bars. In this case, the nodal displacement u is obtained by solving nonlinear equations of the static equilibrium (see Appendix 17.A for the underlying assumptions and for a detailed derivation)

$$\mathbf{A\ (u)\ KA\ (u)}^T\ \mathbf{u} = \mathbf{F} - \mathbf{A\ (u)t_0} \tag{17.5}$$

Also, $\mathbf{t}_0$ is the pretension applied in the strings, **K** is a diagonal matrix containing axial stiffness of each member, i.e., $K_{ii} = (EA)_i/L_i$, where L_i is the length of the i-th member; **u** represents small nodal displacements in the neighborhood of equilibrium caused by small increments in the external forces. The standard Newton–Raphson method is applied to solve (17.5) at each incremental load step $\mathbf{F}_k = \mathbf{F}_{k-1} + \Delta\mathbf{F}$. Matrix $\mathbf{A}(\mathbf{u}_k)$ is updated at each iteration until a convergent solution for $\mathbf{u}_k$ is found.

Figure 17.12 depicts EI as a function of the angle δ, pretension of the top string, and the rigidity ratio K which is defined as the ratio of the axial rigidity of the strings to the axial rigidity of the bars, i.e., $K = (EA)_s/(EA)_b$. The pretension is measured as a function of the prestrain in the top string Σ_0. In obtaining Figure 17.12, the bars were assumed to be equal in diameter and the strings were also assumed to be of equal diameter. Both the bars as well as the strings were assumed to be made of steel for which Young's modulus of elasticity E was taken to be $2.06 \times 10^{11} N/m^2$, and the yield strength of the steel σ_y was taken to be $6.90 \times 10^8 N/m^2$. In Figure 17.12, EI is plotted against the ratio of the external load F to the yield force of the string. The yield force of the string is defined as the force that causes the strings to reach the elastic limit. The yield force for the strings is computed as

$$\text{Yield force of string} = \sigma_y A_s,$$

where σ_y is the yield strength and A_s is the cross-sectional area of the string. The external force F was gradually increased until at least one of the strings yielded.

The following conclusions can be drawn from Figure 17.12:

1. Figure 17.12(a) suggests that the bending rigidity EI of a tensegrity unit with all taut strings increases with an increase in the angle δ, up to a maximum at $\delta = 90°$.
2. Maximum bending rigidity EI is obtained when none of the strings is slack, and the EI is approximately constant for any external force until one of the strings go slack.

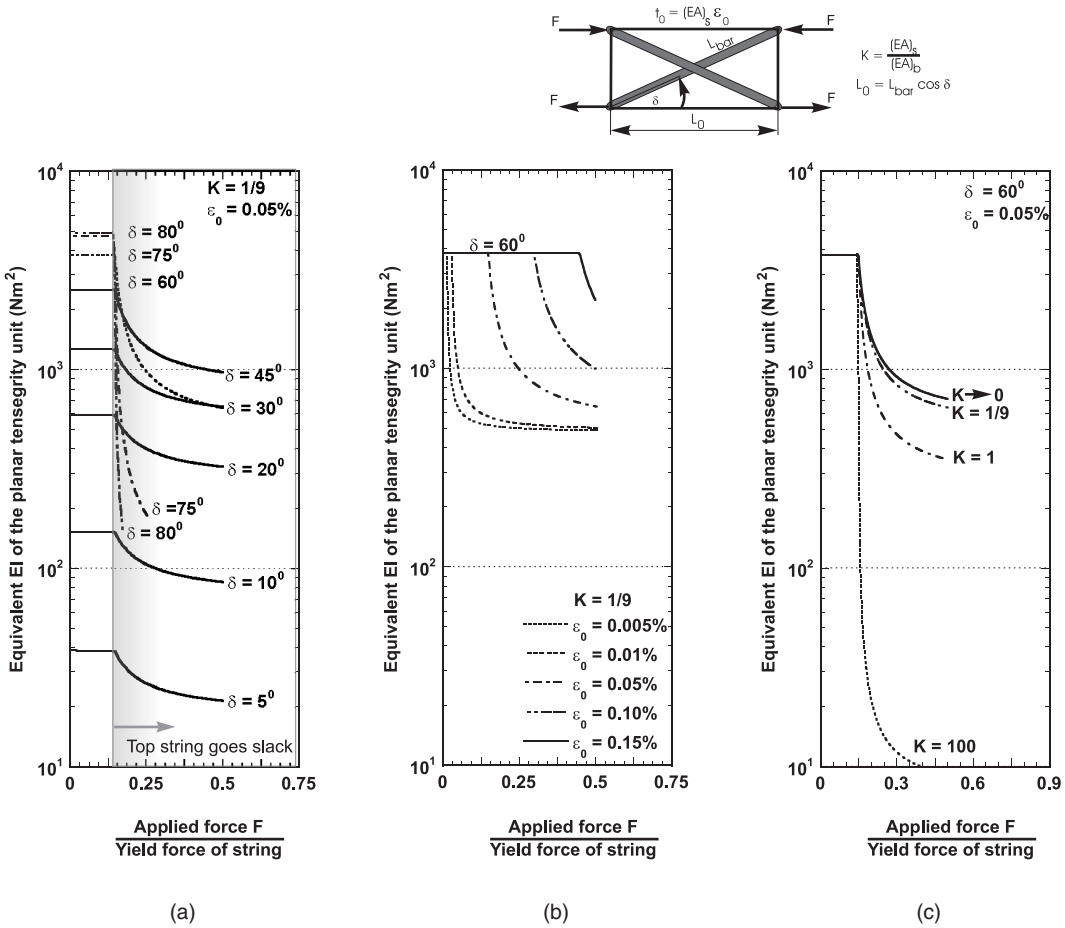

FIGURE 17.12 Bending rigidity *EI* of the planar tensegrity unit for (a) different initial angle δ with rigidity ratio $K = 1/9$ and prestrain in the top string $\varepsilon_0 = 0.05\%$, (b) different ε_0 with $K = 1/9$, (c) different K with $\delta = 60°$ and $\varepsilon_0 = 0.05\%$. L_{bar} for all cases is 0.25 m.

3. Figure 17.12(b) shows that the pretension does not have much effect on the magnitude of *EI* of a planar tensegrity unit. However, pretension does play a remarkable role in preventing the string from going slack which, in turn, increases the range of the constant *EI* against external loading. This provides robustness of *EI* predictions against uncertain external forces. This feature provides robustness against uncertainties in external forces.
4. In Figure 17.12(c) we chose structures having the same geometry and the same total stiffness, but different *K*, where *K* is the ratio of the axial rigidity of the bars to the axial rigidity of the strings. We then see that *K* has little influence on *EI* as long as none of the strings are slack. However, the bending rigidity of the tensegrity unit with slack string influenced *K*, with maximum *EI* occurring at $K = 0$ (rigid bars).

It was also observed that as the angle δ is increased or as the stiffness of the bar is decreased, the force-sharing mechanism of the members of the tensegrity unit changes quite noticeably. This phenomena is seen only in the case when the top string is slack. For example, for $K = 1/9$ and $\varepsilon_0 = 0.05\%$, for small values of δ, the major portion of the external force is carried by the bottom string, whereas after some value of δ (greater than 45°), the major portion of the external force is carried by the vertical side strings rather than the bottom string. In such cases, the vertical side strings

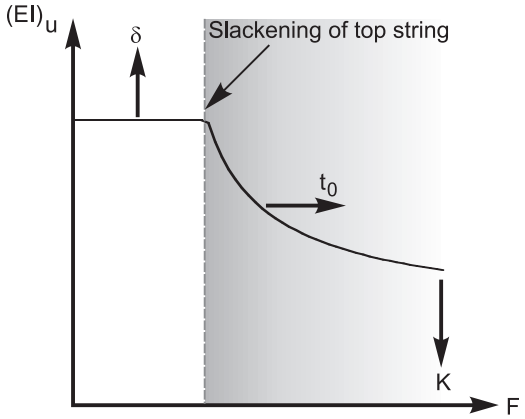

FIGURE 17.13 Trends relating geometry δ, prestress t_0, and material K.

could reach their elastic limit prior to the bottom string. Similar phenomena were also observed for a case of $K = 100$, $\delta = 60°$, and $\varepsilon_0 = 0.05\%$. In such cases, as shown in Figure 17.12(a) for $\delta = 70°$ and $\delta = 75°$, the EI drops drastically once the top string goes slack. Figure 17.13 summarizes the conclusions on bending rigidity, where the arrows indicate increasing directions of δ, $\mathbf{t}_0$, or K.

Note that when t_0 is the pretension applied to the top string, the pretension in the vertical side strings is equal to $t_0/\tan\delta$. The cases of $\delta > 80°$ were not computed, but it is clear that the bending rigidity is a step function as δ approaches 90°, with EI constant until the top string becomes slack, then the EI goes to zero as the external load increases further.

17.2.1.2 Bending Rigidity of the Planar Tensegrity for the Rigid Bar Case ($K = 0$)

The previous section briefly described the basis of the calculations for Figure 17.11. The following sections consider the special case $K = 0$ to show more analytical insight. The nonslack case describes the structure when all strings exert force. The slack case describes the structure when string 3 exerts zero force, due to the deformation of the structure. Therefore, the force in string 3 must be computed to determine when to switch between the slack and nonslack equations.

17.2.1.2.1 Some Relations from Geometry and Statics

Nonslack Case: Summing forces at each node we obtain the equilibrium conditions

$$f_c \cos\delta = F + t_3 - t_2 \sin\theta \tag{17.6}$$

$$f_c \cos\delta = t_1 + t_2 \sin\theta - F \tag{17.7}$$

$$f_c \sin\delta = t_2 \cos\theta, \tag{17.8}$$

where f_c is the compressive load in a bar, F is the external load applied to the structure, and t_i is the force exerted by string i defined as

$$t_i = k_i(l_i - l_{i0}). \tag{17.9}$$

The following relations are defined from the geometry of Figure 17.11:

$$\begin{aligned} l_1 &= L_{bar}\cos\delta + L_{bar}\tan\theta\sin\delta \\ l_2 &= L_{bar}\sin\delta\sec\theta \\ l_3 &= L_{bar}\cos\delta - L_{bar}\sin\delta\tan\theta \\ h &= L_{bar}\sin\delta, \end{aligned} \tag{17.10}$$

where l_i denote the geometric length of the strings. We will find the relation between δ and θ by eliminating f_c and F from (17.6)–(17.8)

$$\cos\theta = \frac{t_1 + t_3}{2t_2}\tan\delta. \tag{17.11}$$

Substitution of relations (17.10) and (17.9) into (17.11) yields

$$\cos\ \theta = \frac{k_1(L_{bar}\ \cos\delta\ +\ L_{bar}\tan\theta\sin\delta - l_{10}) + k_3(L_{bar}\cos\delta - L_{bar}\tan\theta\sin\delta - l_{30})}{2k_2(L_{bar}\sin\delta\sec\theta - l_{20})}\tan\delta. \tag{17.12}$$

If $k_i = k$, then (17.12) simplifies to

$$\tan\delta = \frac{2l_{20}}{l_{10} + l_{30}}\cos\theta\ =\ \beta\cos\theta. \tag{17.13}$$

Slack Case: In order to find a relation between δ and θ for the slack case when t_3 has zero tension, we use (17.12) and set k_3 to zero. With the simplification that we use the same material properties, we obtain

$$0 = L_{bar}\tan\theta\sin\delta\tan\delta + 2l_{20}\cos\theta - l_{10}\tan\delta - L_{bar}\sin\delta. \tag{17.14}$$

This relationship between δ and θ will be used in (17.22) to describe bending rigidity.

17.2.1.2.2 Bending Rigidity Equations

The bending rigidity is defined in (17.3) in terms of ρ and F. Now we will solve the geometric and static equations for ρ and F in terms of the parameters θ, δ of the structure. For the nonslack case, we will use (17.13) to get an analytical formula for the EI. For the slack case, we do not have an analytical formula. Hence, this must be done numerically.

From geometry, we can obtain ρ,

$$\tan\theta = \frac{l_1}{2(\rho + \frac{h}{2})}.$$

Solving for ρ we obtain

$$\begin{aligned}\rho &= \frac{l_1}{2\tan\theta} - \frac{h}{2}\\ &= \frac{L_{bar}\cos\delta + L_{bar}\tan\theta\sin\delta}{2\tan\theta} - \frac{L_{bar}\sin\delta}{2}\\ &= \frac{L_{bar}}{2}\frac{\cos\delta}{\tan\theta}.\end{aligned} \tag{17.15}$$

Nonslack Case: In the nonslack case, we now apply the relation in (17.13) to simplify (17.15)

$$\rho = \frac{L_{bar}}{2}\frac{1}{\tan\theta\sqrt{1 + \beta^2\cos^2\theta}}. \tag{17.16}$$

From (17.6)–(17.8) we can solve for the equilibrium external F

$$\begin{aligned} F &= \frac{1}{2}(t_1 + 2t_2 \sin\theta - t_3) \\ &= \frac{1}{2}(k_1 L_{bar} \cos\delta + k_1 L_{bar} \tan\theta \sin\delta - k_1 l_{10} \\ &\quad + 2k_2 L_{bar} \sin\delta \tan\theta - 2k_2 l_{20} \sin\theta \\ &\quad - k_3 L_{bar} \cos\delta + k_3 L_{bar} \sin\delta \tan\theta + k_3 l_{30}). \end{aligned} \tag{17.17}$$

Again, using (17.13) and $k_i = k$, Equation (17.17) simplifies to

$$F = \frac{2kL_{bar}\beta \sin\theta}{\sqrt{1+\beta^2 \cos^2\theta}} - \frac{k}{2}(l_{10} - l_{30} + 2l_{20} \sin\theta). \tag{17.18}$$

We can substitute (17.18) and (17.16) into (17.3)

$$El = \frac{L_{bar}^2 \beta \cos^2\theta}{2(1+\beta^2 \cos^2\theta)(\sin\theta)} \left(\frac{2kL_{bar}\beta \sin\theta}{\sqrt{1+\beta^2 \cos^2\theta}} - \frac{k}{2}(l_{10} - l_{30} + 2l_{20} \sin\theta) \right), \tag{17.19}$$

and we obtain the bending rigidity of the planar structure with no slack strings present. The expression for string length l_3 in the nonslack case reduces to

$$l_3 = L_{bar} \frac{1 - \beta \sin\theta}{\sqrt{1 + \beta^2 \cos^2\theta}}. \tag{17.20}$$

This expression can be used to determine the angle which causes l_3 to become slack.

Slack Case: Similarly, for the case when string 3 goes slack, we set $k_3 = 0$ and $k_i = k$ in (17.17), which yield simply

$$\begin{aligned} F_{slack} &= \frac{1}{2}(t_1 + 2t_2 \sin\theta) \\ &= \frac{1}{2}(kL_{bar} \cos\delta + 3kL_{bar} \tan\theta \sin\delta - kl_{10} - 2kl_{20} \sin\theta) \end{aligned} \tag{17.21}$$

and

$$EI_{slack} = \frac{L_{bar}^2 \sin\delta \cos\delta}{4 \tan\theta}(kL_{bar} \cos\delta + 3kL_{bar} \tan\theta \sin\delta - kl_{10} - 2kl_{20} \sin\theta). \tag{17.22}$$

See Figure 17.12(c) for a plot of EI for the $K = 0$ (rigid bar) case.

17.2.1.2.3 Constants and Conversions

All plots shown are generated with the following data which can then be converted as follows if necessary.

$$\textit{Young's Modulus, } E = 2.06 \times 10^{11}\ N/m^2$$

$$\textit{Yield Stress, } \sigma = 6.9 \times 10^{8}\ N/m^2$$

$$\textit{Diameter of Tendons} = 1\ \text{mm}$$

$$\textit{Cross-Sectional Area of Tendon} = 7.8540 \times 10^{-7}\ m^2$$

$$\textit{Length of Bar, } L_{bar} = .25\ m$$

$$\textit{Prestress} = e_0$$

$$\textit{Initial Angle} = \delta_0$$

The spring constant of a string is

$$k = \frac{EA}{L_{bar}\cos(\delta_0)}. \tag{17.23}$$

The following equation can be used to compute the equivalent rest length given some measure of prestress t_0

$$t_0 = (\mathrm{EA})_s\ e_0 = k(l - l_0)$$

$$l_0 = L_{bar}\cos(\delta_0) - \frac{EAe_0}{k}. \tag{17.24}$$

17.2.1.3 Effective Bending Rigidity with Slack String ($K > 0$)

As noted earlier, the tensegrity unit is a statically indeterminate structure (meaning that matrix **A** is not full column rank) as long as the strings remain taut during the application of the external load. However, as soon as one of the strings goes slack, the tensegrity unit becomes statically determinate. In the following, an expression for bending rigidity of the tensegrity unit with an initially slack top string is derived. Even in the case of a statically determinate tensegrity unit with slack string, the problem is still a large displacement and nonlinear problem. However, a linear solution, valid for small displacements only, resulting in a quite simple and analytical form can be found. Based on the assumptions of small displacements, an analytical expression for *EI* of the tensegrity unit with slack top string has been derived in Appendix 17.B and is given below.

$$EI \approx \frac{1}{2}\frac{L_{bar}^{\ 2}(EA)_s \sin^2\delta\cos^3\delta}{(\sin^3\delta + 2\cos^3\delta + K)}. \tag{17.25}$$

The *EI* obtained from nonlinear analysis, i.e., from (17.3) together with (17.5), is compared with the *EI* obtained from linear analysis, i.e., from (17.25), and is shown in Figure 17.14. Figure 17.14 shows that the linear analysis provides a lower bound to the actual bending rigidity. The linear estimation of *EI*, i.e., (17.25), is plotted in Figure 17.15 as a function of the initial angle δ for different values of the stiffness ratio *K*. Both bars and the strings are assumed to be made of steel, as before. It is seen in Figure 17.15 that the *EI* of the tensegrity unit with slack top string attains a maximum value for some value of δ. The decrease of *EI* (after the maximum) is due to the change in the force sharing mechanism of the members of the tensegrity unit, as discussed earlier. For small values of δ, the major portion of the external force is carried by the bottom string, whereas for larger values of δ, the vertical side strings start to share the external force. As δ is further

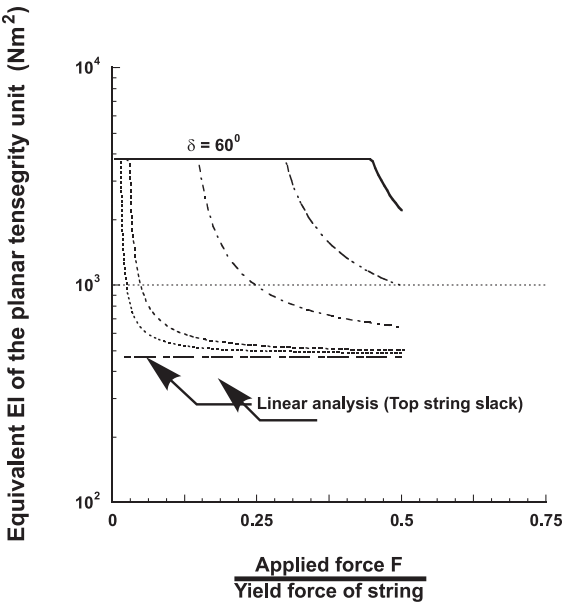

FIGURE 17.14 Comparison of *EI* from nonlinear analysis with the *EI* from linear analysis with slack top string (L_{bar} = 0.25 m, δ = 60° and K = 1/9).

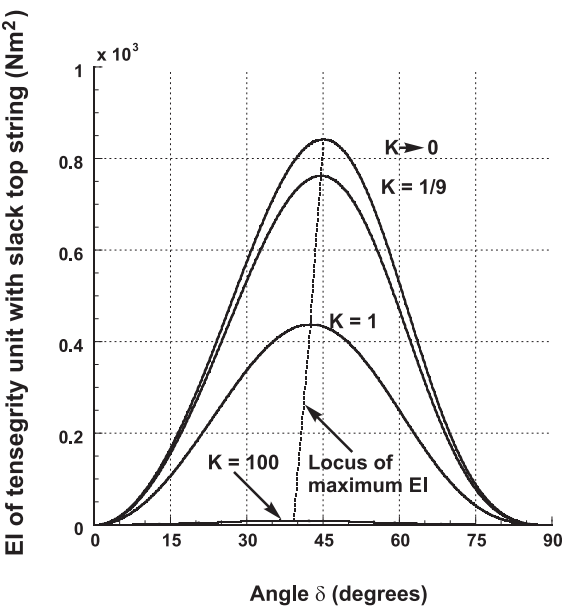

FIGURE 17.15 *EI* with slack top string with respect to the angle δ for L_{bar} = 0.25m.

increased, the major portion of the external force is carried by the vertical side strings rather than the bottom string. This explains the decrease in *EI* with the increase in δ after some values of δ for which *EI* is maximum.

The locus of the maximum *EI* is also shown in Figure 17.15. The maximum value of *EI* and the δ for which *EI* is maximum depend on the relative stiffness of the string and the bars, i.e., they depend on *K*. From Figure 17.15 note that the maximum *EI* is obtained when the bars are much

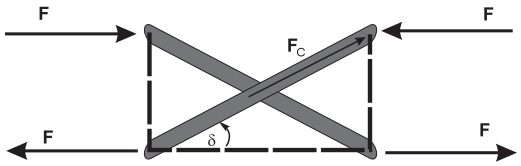

FIGURE 17.16 *C2T4* tensegrity with slack top string.

stiffer than the strings. *EI* is maximum when the bars are perfectly rigid, i.e., $K \to 0$. It is seen in Figure 17.15 and can also be shown analytically from (17.25) that for the case of bars much stiffer than the strings, $K \to 0$, the maximum *EI* of the tensegrity unit with slack top string is obtained when $\delta = 45°$. In constrast, note from Figure 17.12(a) that when no strings are slack, the maximum bending rigidity occurs with $\delta = 90°$.

17.2.2 Mass Efficiency of the *C2T4* Class 1 Tensegrity in Bending

This section demonstrates that beams composed of tensegrity units can be more efficient than continua beams. We make this point with a very specific example of a single-unit *C2T4* structure. In a later section we allow the number of unit cells to approach infinity to describe a long beam. Let Figure 17.16 describe the configuration of interest. Note that the top string is slack (because the analysis is easier), even though the stiffness will be greater before the string is slack. The compressive load in the bar, F_c.

$$F_c = F/\cos\,\delta$$

Designing the bar to buckle at this force yields

$$F_c = \frac{\pi^3 E_1 r_{bar}^4}{4L_{bar}^2},\ (L_{bar},\ r_{bar})\ =\ \text{length, radius of bar.}$$

where the mass of the two bars is (ρ_1 = bar mass density)

$$m_b = \ 2m_1 = 2\pi\,\rho_1\,L_{bar}\,r_{bar}^2 \Rightarrow r_{bar}^2 = \frac{m_b}{2\pi\rho_1 L_{bar}}.$$

Hence, eliminating r_{bar} gives for the force

$$F_c = \frac{\pi^3\,E_1}{4L_{bar}^2}\left(\frac{m_b^2}{4\pi^2\rho_1^2 L_{bar}^2}\right) = \left(\frac{\pi E_1}{16\rho_1^2 L_{bar}^4}\right) m_b^2$$

The moment applied to the unit is

$$M = F\,L_{bar}\sin\delta = \frac{\pi E_1}{16\rho_1^2 L_{bar}^3} m_b^2\cos\delta\sin\delta. \tag{17.30}$$

To compare this structure with a simple classical structure, suppose the same moment is applied to a single bar of a rectangular cross section with *b* units high and *a* units wide and yield strength σ_y such that

$$M = \frac{\sigma_y I}{C}, I = \frac{1}{12}ab^3, C = \frac{b}{2}, m_0 = \rho_0\,L_0\,ab, \tag{17.31}$$

then, for the rectangular bar

$$M = \frac{\sigma_y \, m_0^2}{6a \, \rho_0^2 \, L_0^2}. \tag{17.32}$$

Equating (17.30) and (17.32), using $L_0 = L_{bar} \cos \delta$, yields the material/geometry conservation law ($\bar{\sigma}$ is a material property and g is a property of the geometry)

$$\mu^2 \triangleq \left(\frac{m_b}{m_0} \right)^2 = \frac{\delta}{3\pi} \bar{\sigma} g, \quad \bar{\sigma} \triangleq \frac{\sigma_y}{E_1}, \quad g \triangleq \frac{L_0}{a \cos^4 \delta \sin \delta} \tag{17.33}$$

The mass ratio μ is infinity if $\delta = 0°, 90°$, and the lower bound on the mass ratio is achieved when $\delta = \tan^{-1}(1/2) = 26.565°$.

Lemma 17.1 Let σ_y denote the yield stress of a bar with modulus of elasticity E_1 and dimension $a \times b \times L_0$. Let M denote the bending moment about an axis perpendicular to the b dimension. M is the moment at which the bar fails in bending. Then, the *C2T*4 tensegrity fails at the same M but has less mass if $\bar{\sigma} g < (3\pi/\delta)$, and minimal mass is achieved at $\delta = \tan^{-1}(1/2)$.

Proof: From (17.33),

$$\mu^2 = \frac{\delta}{3\pi} \bar{\sigma} g, \geq \frac{\delta}{3\pi} \bar{\sigma} \bar{g}, \bar{g} = 3.493856 \frac{L_0}{a} \tag{17.34}$$

where the lower bound $(\delta/3\pi)\bar{\sigma}\bar{g}$ is achieved at $\delta = \tan^{-1}(1/2)$ by setting $\partial g / \partial \delta = 0$ and solving $\cos^2 \delta = 4 \sin^2 \delta$, or $\tan \delta = 1/2$. ❑

For steel with $(\sigma_y, E_1) = (6.9 \times 10^8, 2 \times 10^{11})$ (N/m^2),

$$\mu^2 = \frac{\delta}{3\pi} \bar{\sigma} g \geq 0.008035869 \frac{L_0}{a} \tag{17.35}$$

where the lower bound is achieved for $\tan^{-1}(1/2) = 26.565°$. Hence, for geometry of the steel comparison bar given by $\{L_0/a = 50, \text{and } \delta = \tan^{-1}(1/2) = 26.565^o\}$, then $m_b = 0.51 \, m_0$, showing 49% improvement in mass for a given yield moment. For the geometry $\{L_0/a = 20 \text{ and } \delta = 26.565^o\}$, $m_b = 0.2 m_0$, showing 80% improvement in mass for a given yield moment, M. The main point here is that strength and mass efficiency are achieved by geometry ($\delta = 26.565°$), not materials.

It can be shown that the compressive force in a bar when the system *C2T*4 is under a pure bending load exhibits a similar robustness property that was shown with the bending rigidity. The force in a bar is constant until a string becomes slack, which is shown in Figure 17.17.

17.2.3 Global Bending of a Beam Made from *C2T*4 Units

The question naturally arises "what is the bending rigidity of a beam made from many tensegrity cells?" 17.2.3.2 answers that question. First, in Section 17.2.3.1 we review the standard beam theory.

17.2.3.1 Bucklings Load

For a beam loaded as shown in Figure 17.18, we have

$$EI \frac{d^2 v}{dz^2} = -Fv - Fe \tag{17.36}$$

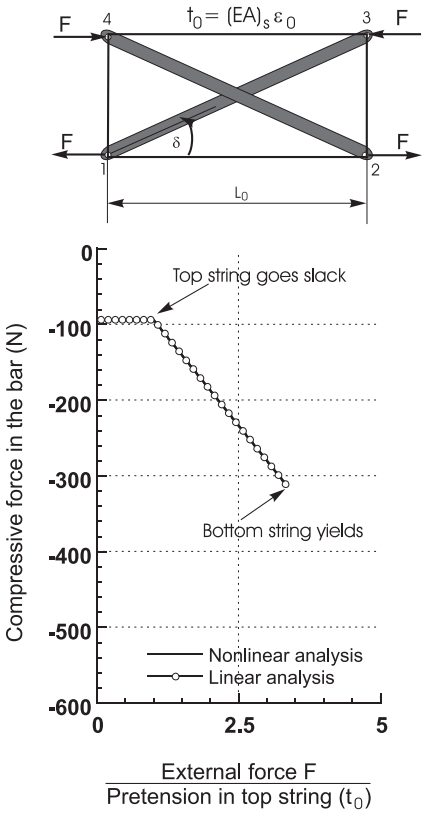

FIGURE 17.17 Comparison of force in the bar obtained from linear and nonlinear analysis for pure bending loading. (Strings and bars are made of steel, Young's modulus $E = 2.06 \times 10^{11}$ N/m^2, yield stress $\sigma_y = 6.90 \times 10^8$ N/m^2, diameter of string = 1 mm, diameter of bar = 3 mm, $K = 1/9$, $\delta = 30°$, $\varepsilon_0 = 0.05\%$ and $L_0 = 1.0$ m.)

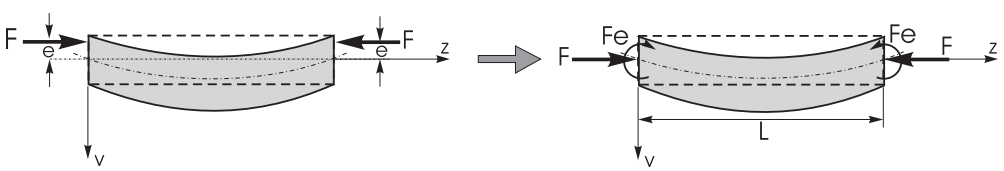

FIGURE 17.18 Bending of a beam with eccentric load at the ends.

equivalently,

$$\frac{d^2v}{dz^2} + p^2 v = -p^2 e \tag{17.37}$$

where

$$p^2 = F/EI, \tag{17.38}$$

where EI is the bending rigidity of the beam, v is the transverse displacement measured from the neutral axis (denoted by the dotted line in Figure 17.18), z represents the longitudinal axis, L is

the length of the beam, e is the eccentricity of the external load F. The eccentricity of the external load is defined as the distance between the point of action of the force and the neutral axis of the beam.

The solution of the above equation is

$$v = A \sin pz + B \cos pz - e \tag{17.39}$$

where constants A and B depend on the boundary conditions. For a pin–pin boundary condition, A and B are evaluated to be

$$A = e \tan \frac{pL}{2}, \quad \text{and} \quad B = e \tag{17.40}$$

Therefore, the deflection is given by

$$v = e\left[\tan \frac{pL}{2} \sin pz + \cos pz - 1\right] \tag{17.41}$$

17.2.3.2 Buckling of Beam with Many *C2T4* Tensegrity Cells

Assume that the beam as shown in Figure 17.18 is made of n small tensegrity units similar to the one shown in Figure 17.11, such that $L = nL_0$, and the bending rigidity EI appearing in (17.36) and (17.38) is replaced by EI given by (17.25). Also, since we are analyzing a case when the beam breaks, we shall assume that the applied force is large compared to the pretension. The beam buckles at the unit receiving the greatest moment. Because the moment varies linearly with the bending and the bending is greatest at the center of the beam, the tensegrity unit at the center buckles. The maximum moment $M_{\max}$ leading to the worst case scenario is related to the maximum deflection at the center $v_{\max}$. From (17.41),

$$v_{\max} = e\left[\tan \frac{pL}{2} \sin \frac{pL}{2} + \cos \frac{pL}{2} - 1\right]. \tag{17.42}$$

Simple algebra converts this to

$$v_{\max} = e\left(\frac{1}{\cos \dfrac{pL}{2}} - 1\right) \tag{17.43}$$

The worst case $M_{\max}$ is equal to $Fv_{max} + Fe$ and is given by

$$M_{\max} = \frac{F}{\cos\left(\dfrac{nL_0}{2}\sqrt{\dfrac{F}{EI}}\right)} e \tag{17.44}$$

Now we combine this with the buckling formula for one tensegrity unit to get its breaking moment

$$M_{break} = eF_B = e\frac{\pi^2 (EI)_b}{L_0^2} \cos^3 \delta \tag{17.45}$$

Thus, from Equations (17.44) and (17.45), if F exceeds F_{gB} given by

$$\frac{F_{gB}}{\cos\left(\frac{nL_0}{2}\sqrt{\frac{F_{gB}}{EI}}\right)} = \frac{\pi^2 (EI)_b}{L_0^2}\cos^3\delta \tag{17.46}$$

the central unit buckles, and F_{gB} is called the global buckling load.

Multiplying both sides of (17.46) by $(nL_0)^2$ and introducing three new variables,

$$\mathcal{F} = F_{gB}(nL_0)^2, \quad \mathcal{P} = \frac{\pi^2 (EI)_b}{L_0^2}\cos^3\delta, \qquad \mathcal{K} = \frac{1}{2}\sqrt{\frac{1}{EI}}, \tag{17.47}$$

we rewrite (17.46) as

$$\frac{\mathcal{F}}{\cos\left(\mathcal{K}\sqrt{\mathcal{F}}\right)} = \mathcal{P}n^2 L_0^2 \tag{17.48}$$

Equivalently,

$$\eta(\mathcal{F}) = \mathcal{P}n^2 L_0^2, \tag{17.49}$$

where η is a function defined as

$$\eta(\mathcal{F}) = \frac{\mathcal{F}}{\cos\left(\mathcal{K}\sqrt{\mathcal{F}}\right)}. \tag{17.50}$$

η is a monotonically increasing function in

$$0 \le \mathcal{F} \le \left(\frac{\pi}{2}\right)^2 \frac{1}{\mathcal{K}^2}, \tag{17.51}$$

satisfying

$$\eta \ge \mathcal{F} \tag{17.52}$$

It is interesting to know the buckling properties of the beam as the number of the tensegrity elements become large. As $n \to \infty$, $(nL_0)^2 \to \infty$, and from (17.49) and (17.51)

$$\mathcal{F} = \eta^{-1}\left[\mathcal{P}n^2 L_0^2\right] \to \left(\frac{\pi}{2}\right)^2 \frac{2}{\mathcal{K}^2} \tag{17.53}$$

and $\mathcal{F}$ approaches the limit from below. From Equations (17.47) and (17.49),

$$F_{gB} = \frac{1}{n^2}\frac{1}{L_0^2}\left[\eta^{-1}\left(\mathcal{P}n^2 L_0^2\right)\right] \tag{17.54}$$

Thus, for large n, using (17.53), we get

$$F_{gB} \approx \frac{1}{n^2}\frac{1}{L_0^2}\left(\frac{\pi}{2}\right)^2 \frac{1}{\mathcal{K}^2}$$
$$\approx \frac{1}{n^2}\frac{1}{L_0^2}\left(\frac{\pi}{2}\right)^2 \frac{1}{\frac{1}{4}\frac{1}{EI}} \tag{17.55}$$
$$\approx \frac{1}{n^2}\frac{\pi^2 EI}{L_0^2}$$

The global buckling load as given by (17.55) is exactly the same as the classical Euler's buckling equation evaluated for the bending rigidity EI of the tensegrity unit. Therefore, asymptotically the buckling performance of the beam depends only on the characteristics of EI and L_0^2 just as a classical beam.

Note, for each n

$$F_{gB} \le \frac{1}{n^2}\frac{\pi^2 EI}{L_0^2}.$$

The implication here is that the standard Euler buckling formula applies where EI is a function of the geometrical properties of the tensegrity unit. Figure 17.12(a) shows that EI can be assigned any finite value. Hence, the beam can be arbitrarily stiff if the tensegrity unit has horizontal length arbitrarily small. This is achieved by using an arbitrarily large number of tensegrity units with large δ (arbitrarily close to 90°). More work is needed to define practical limits on stiffness.

17.2.4 A Class 1 *C*2*T*4 Planar Tensegrity in Compression

In this section we derive equations that describe the stiffness of the Class 1 *C*2*T*4 planar tensegrity under compressive loads. The nonslack case describes the structure when all strings exert force. The slack case describes the structure when string 3 and string 1 exert zero force, due to the deformation of the structure. Therefore, the force in string 3 and string 1 must be computed in order to determine when to switch between the slack and nonslack equations. We make the assumption that bars are rigid, that is, $K = 0$.

17.2.4.1 Compressive Stiffness Derivation

Nonslack Case: Summing forces at each node we obtain the equilibrium conditions

$$f_c \cos\delta = F + t_3 \tag{17.56}$$

$$f_c \cos\delta = F + t_1 \tag{17.57}$$

$$f_c \sin\delta = t_2\,, \tag{17.58}$$

where f_c is the compressive load in a bar, F is the external load applied to the structure, and t_i is the force exerted by string i defined as

$$t_i = k_i\left(l_i - l_{i0}\right).$$

The following relations are defined from the geometry of Figure 17.19:

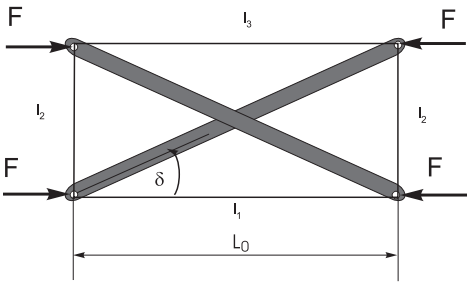

FIGURE 17.19 *C2T4* in compression.

$$l_1 = L_{bar}\cos\delta$$

$$l_2 = L_{bar}\sin\delta$$

$$l_3 = L_{bar}\cos\delta \tag{17.59}$$

Solving for F we obtain

$$F = k(l_{10} - \frac{l_{20}}{\tan\delta}). \tag{17.60}$$

Using the relation $L_0 = L_{\text{bar}}\cos\delta$ and $\tan\delta = \dfrac{\sqrt{L_{bar}^2 - L_0^2}}{L_0}$ results in

$$F = kl_{10} - \frac{kl_{20}L_0}{\sqrt{L_{bar}^2 - L_0^2}} \tag{17.61}$$

We will also make the assumption now that all strings have the same material properties, specifically, $l_{i0} = l_0$. Now, the stiffness can be computed as

$$K \stackrel{\Delta}{=} -\frac{dF}{dL_0} = \frac{kl_0}{\sqrt{L_{bar}^2 - L_0^2}} + \frac{kl_0L_0^2}{\left(L_{bar}^2 - L_0^2\right)^{\frac{3}{2}}} = \frac{kl_0L_{bar}^2}{\left(L_{bar}^2 - L_0^2\right)^{\frac{3}{2}}}. \tag{17.62}$$

Similarly, for the slack case, when t_1 and t_3 are slack, we follow the same derivation setting $t_1 = t_3 = 0$ in (17.56)–(17.58)

$$F_{slack} = kL_{bar}\cos\delta - \frac{kl_0}{\tan\delta}. \tag{17.63}$$

Substitution of $L_0 = L_{bar}\cos\delta$ yields

$$F_{slack} = kL_0 - \frac{kl_0L_0}{\sqrt{L_{bar}^2 - L_0^2}}. \tag{17.64}$$

Taking the derivative with respect to L_0 gives

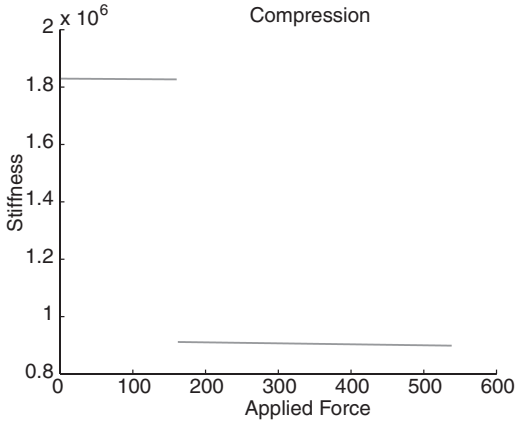

FIGURE 17.20 Stiffness of *C2T4* vs. applied load, plotted until strings yield.

$$K_{slack} = -\frac{dF_{slack}}{dL_0} = -k + \frac{kl_0}{\sqrt{L_{bar}^2 - L_0^2}} + \frac{kl_0 L_0^2}{\left(L_{bar}^2 - L_0^2\right)^{\frac{3}{2}}}$$

$$= k\left(\frac{l_0 L_{bar}^2}{\left(L_{bar}^2 - L_0^2\right)^{\frac{3}{2}}} - 1\right). \tag{17.65}$$

A plot of stiffness for the nonslack and slack case vs. applied force is given in Figure 17.20, where $k = 9.1523 \times 10^5$ *N/m*, $\delta = 45°$, $L_{bar} = 0.25$ *m*, and the force, *F*, ranges between 0 and 600 *N*.

17.2.5 Summary

Tensegrity structures have geometric structure that can be designed to achieve desirable mechanical properties. First, this chapter demonstrates how bending rigidity varies with the geometrical parameters. The bending rigidity is reduced when a string goes slack, and pretension delays the onset of slack strings. The important conclusions made in this section are

- Beams made from tensegrity units can be stiffer than their continuous beam counterparts.
- Pretension can be used to maintain a constant bending rigidity over a wider range of external loads. This can be important to robustness, when the range of external loads can be uncertain.
- For larger loads the bending stiffness is dominated by geometry, not pretension. This explains the mass efficiency of tensegrity structures since one can achieve high stiffness by choosing the right geometry.
- The ratio of mass to bending rigidity of the *C2T4* tensegrity is shown to be smaller than for a rectangular cross-section bar, provided the geometry is chosen properly (angle between bars must be less than 53°). Comparisons to a conventional truss would be instructive. There are many possibilities.

17.3 Planar Class K Tensegrity Structures Efficient in Compression

It is not hard to show that the Class 1 *C2T4* tensegrity of Figure 17.19 is not as mass efficient as a single rigid bar. That is, the mass of the structure in Figure 17.19 is greater than the mass of a

FIGURE 17.21 A bar under compression.

single bar which buckles at the same load 2*F*. This motivates the examination of Class 2 tensegrity structures which have the potential of greater strength and stiffness due to ball joints that can efficiently transfer loads from one bar to another. Compressive members are disconnected in the traditional definition[2] of tensegrity structures, which we call Class 1 tensegrity. However, if stiff tendons connecting two nodes are very short, then for all practical purposes, the nodes behave as though they are connected. Hence, Class 1 tensegrity generates Class k tensegrity structures as special cases when certain tendons become relatively short. Class k tensegrity describes a network of axially loaded members in which the ends of not more than k compressive members are connected (by ball joints, of course, because torques are not permitted) at nodes of the network.

In this section, we examine one basic structure that is efficient under compressive loads. In order to design a structure that can carry a compressive load with small mass we employ Class k tensegrity together with the concept of self-similarity. Self-similar structures involve replacing a compressive member with a more efficient compressive system. This algorithm, or fractal, can be repeated for each member in the structure. The basic principle responsible for the compression efficiency of this structure is geometrical advantage, combined with the use of tensile members that have been shown to exhibit large load to mass ratios. We begin the derivation by starting with a single bar and its Euler buckling conditions. Then this bar is replaced by four smaller bars and one tensile member. This process can be generalized and the formulae are given in the following sections. The objective is to characterize the mass of the structure in terms of strength and stiffness. This allows one to design for minimal mass while bounding stiffness. In designing this structure there are trade-offs; for example, geometrical complexity poses manufacturing difficulties.

The materials of the bars and strings used for all calculations in this section are steel, which has the mass density $\rho = 7.862\ \ g/cm^3$, Young's modulus $E = 2.06^{11}\ \ N/m^2$ and yield strength $\sigma = 6.9^8\ \ N/m^2$. Except when specified, we will normalize the length of the structures $L_0 = 1$ in numerical calculations.

17.3.1 Compressive Properties of the *C4T2* Class 2 Tensegrity

Suppose a bar of radius r_0 and length L_0, as shown in Figure 17.21 buckles at load *F*. Then,

$$F = \frac{E_0 \pi^3 r_0^4}{L_0^2}, \tag{17.66}$$

where E_0 is the Young's modulus of the bar material.

The mass of the bar is

$$m_0 = \rho_0 \pi r_0^2 L_0, \tag{17.67}$$

where ρ_0 is the mass density of the bar.

Equations (17.66) and (17.67) yield the force–mass relationship

$$F = \frac{E_0 \pi m_0^2}{4\rho_0^2 L_0^4}. \tag{17.68}$$

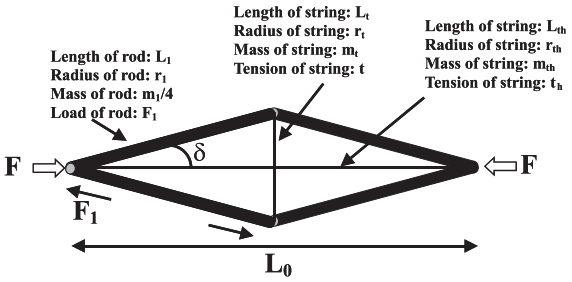

FIGURE 17.22 A *C4T2* planar Class 2 tensegrity structure.

Now consider the four-bar pinned configuration in Figure 17.22, which is designed to buckle at the same load *F*. Notice that the Class 2 tensegrity of Figure 17.22 is in the dual (where bars are replaced by strings and vice versa) of the Class 1 tensegrity of Figure 17.3(b), and is of the same type as the Class 2 tensegrity in Figure 17.3(c).

We first examine the case when tendon t_h is slack. The four identical bars buckle at the bar compressive load F_1 and the mass of each of the four bars is $1/4\, m_1$. Hence,

$$F_1 = \frac{E_1 \pi^2 r_1^4}{4L_1^2}, \quad m_1 = 4\rho_1 \pi r_1^2 L_1, \quad F_1 = \frac{E_1 \pi m_1^2}{64\rho_1^2 L_1^4}, \tag{17.69}$$

where (r_1, L_1, E_1, ρ_1) is respectively, the radius, length, Young's modulus, and mass density of each bar, and the mass of the system *C4T1* in Figure 17.22 is

$$m_1 = 4\rho_1 \pi r_1^2 L_1.$$

Since from the Figure 17.22, the length of each bar is L_1 and the compressive load in each bar is F_1 given by,

$$L_1 = \frac{L_0}{2\cos\delta}, \quad F_1 = \frac{F + t_h}{2\cos\delta}, \tag{17.70}$$

then, from (17.68)–(17.70)

$$F_1 = \frac{E_1 \pi m_1^2}{64\rho_1^2 L_1^4} = \frac{F + t_h}{2\cos\delta}. \tag{17.71}$$

Note from (17.70) that the *C4T2* structure with no external force *F* and tension $t_h = F_x$ in the horizontal string, places every member of the structure under the same load as a *C4T1* structure (which has no horizontal string) with an external load $F = F_x$. In both cases, $F_1 = F_x/2\cos\delta$.

Solving for the mass ratio, from (17.71)

$$\mu_1 \triangleq \left(\frac{m_1}{m_0}\right) = \frac{\rho_1}{\rho_0}\sqrt{\frac{E_0}{E_1}}\left(\frac{1 + \frac{t_h}{F}}{2\cos^5\delta}\right)^{\frac{1}{2}} \tag{17.72}$$

For slack tendon $t_h = 0$, note that $\mu_1 < 1$ if $\delta < \cos^{-1}\left(\frac{1}{2}\right)^{\frac{1}{5}} = 29.477°$. Of course, in the slack case (when $t_h = 0$), one might refer to Figure 17.22 as a *C4T1* structure, and we will use this designation to describe the system of Figure 17.22 when t_h is slack. Increasing pretension in t_h to generate the nonslack case can be examined later. The results are summarized as follows:

Proposition 17.1 *With slack horizontal string $t_h = 0$, assume that strings are massless, and that the C4T1 system in* Figure 17.22 *is designed to buckle at the same load F as the original bar of mass m_0 in* Figure 17.21. *Then, the total mass m_1 of the C4T1 system is $m_1 = m_0(2\cos^5\delta)^{-\frac{1}{2}}$, which is less than m_0 whenever $\delta < 29.477$ degrees.*

Proof: This follows by setting $\mu_1 = 1$ in (17.72).

TABLE 17.1 Properties of the *C4T*1 Structure[a]

	$\delta = 10°$	$\delta = 20°$
r_1	$.602r_0$	$.623r_0$
m_1	$.735m_0$	$.826m_0$
L_1	$.508L_0$	$.532L_0$
$\frac{L_1}{r_1}$	$.844\frac{L_0}{r_0}$	$.854\frac{L_0}{r_0}$

[a] Strings are assumed massless.

Some illustrative data that reflect the geometrical properties of the *C4T*1 in comparison with a bar which buckles with the same force *F* are shown in Table 17.1. For example, when $\delta = 10^\circ$, the *C4T*1 requires only 73.5% of the mass of the bar to resist the same compressive force. The data in Table 17.1 are computed from the following relationships for the *C4T*1 structure. The radius of each bar in the *C4T*1 system is r_1

$$r_1^2 = \frac{m_1}{4\rho_1\pi L_1},$$

and

$$r_0^2 = \frac{m_0}{\rho_0\pi L_0}.$$

From this point forward we will assume the same material for all bars. Hence,

$$\left(\frac{r_1}{r_0}\right)^4 = \frac{1}{8\cos^3\delta}.$$

Likewise,

$$\left(\frac{L_1}{L_0}\right) = \frac{1}{2\cos\delta},$$

and

$$\left(\frac{r_1}{r_0}\right)^4 = \left(\frac{L_1}{L_0}\right)^3.$$

Also,

$$\frac{L_1}{r_1} = \frac{L_0\left(8\cos^3\delta\right)^{\frac{1}{4}}}{2r_0\cos\delta} = \frac{L_0}{r_0}\left(\frac{1}{2\cos\delta}\right)^{\frac{1}{4}}.$$

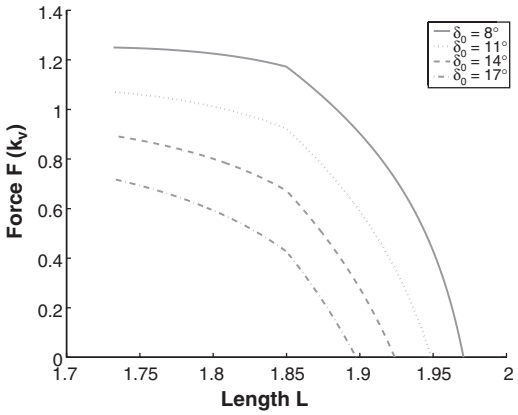

FIGURE 17.23 Load-deflection curve of *C4T*2 structure with different δ (K_e = 1, $K_h = 3K_t = 3$, L_l = 1).

17.3.2 *C4T*2 Planar Tensegrity in Compression

In this section we derive equations that describe the stiffness of the *C4T*2 planar tensegrity under compressive loads. Pretension would serve to increase the restoring force in the string, allowing greater loads to be applied with smaller deformations. This is clearly shown in the force balance Equation (17.70), where pretension can be applied through the use of the rest length L_{h0} of the string, and $t_h = k_h(L_0 - L_{h0})$, where k_h is the stiffness of the horizontal string.

17.3.2.1 Compressive Stiffness Derivation

From Figure 17.22, the equilibrium configuration can be expressed as

$$F = t\cot\delta - t_h = k_t(L_t - L_{t0})\frac{L_0}{L_t} - t_h = k_t\left(1 - \frac{L_{t0}}{L_t}\right)L_0 - t_h, \tag{17.73}$$

where t, L_0, L_t, and L_{t0} are the tension, length of the structure, length of the string, and the rest length of the vertical string, respectively. The length of the string can be written as

$$L_t^2 = 4L_1^2 - L_0^2,$$

where L_1 denotes the length of one bar. This relation simplifies the force balance equation to

$$F = k_t\left(1 - \frac{l_0}{\sqrt{4L_1^2 - L_0^2}}\right)L_0 - k_h(L_0 - l_{h0}). \tag{17.74}$$

Figure 17.23 shows the plot of the load deflection curve of a *C4T*2 structure with different δ. The compressive stiffness can be calculated by taking the derivative of (17.74) with respect to L_0 as follows,

$$\frac{dF}{dL_0} = k_t\left(1 - \frac{L_{t0}}{\sqrt{4L_1^2 - L_0^2}}\right) - k_t\frac{L_{t0}L_0^2}{\left(4L_1^2 - L_0^2\right)^{\frac{3}{2}}} - k_h$$

$$= k_t\left(1 - \frac{4L_{t0}L_1^2}{\left(4L_1^2 - L_0^2\right)^{\frac{3}{2}}}\right) - k_h. \tag{17.75}$$

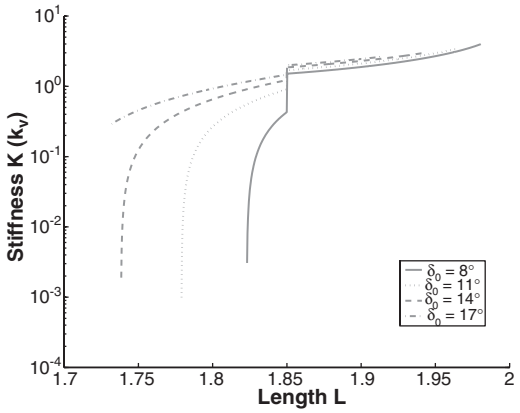

FIGURE 17.24 Stiffness vs. length of $C4T1^1$ structure with different δ_0 ($K_e = 1$, $K_h = 3K_e = 3$, $L_1 = 1$).

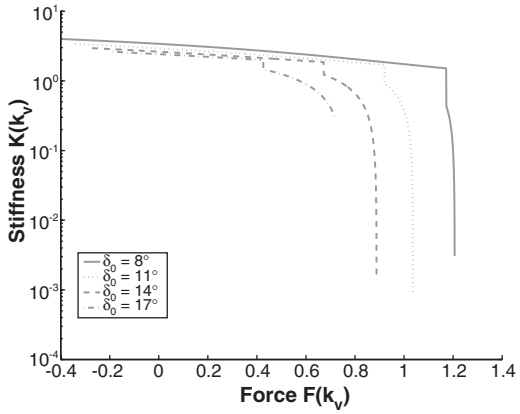

FIGURE 17.25 Stiffness vs. force of $C4T1$ structure with different δ ($K_e = 1$, $K_h = 3K_e = 3$, $L_1 = 1$).

Therefore, the stiffness is defined as

$$K \triangleq -\frac{dF}{dL_0} = k_t\left(\frac{4L_{t0}L_1^2}{\left(4L_1^2 - L_0^2\right)^{\frac{3}{2}}} - 1\right) + k_h = k_t\left(\frac{L_{t0}\cos\delta}{L_0\sin^3\delta} - 1\right) + k_h. \tag{17.76}$$

Figure 17.24 shows the plot of stiffness vs. the length of the structure and Figure 17.25 shows the plot of stiffness vs. the applied load F on the structure. Figures 17.23–17.25 demonstrate a step change in stiffness when tendon t_h goes slack. Note also that the $C4T1$ structure (t_h slack) demonstrates the property described in Figure 17.8. Structures which demonstrate robustness to external forces (that is, they maintain stiffness until strings go slack) do not preserve strength very well, whereas structures which demonstrate strength robustness have poor stiffness properties.

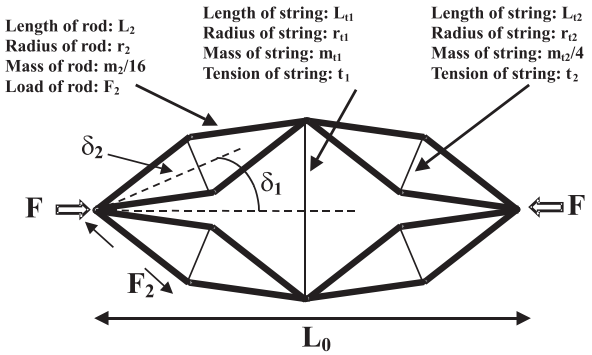

FIGURE 17.26 A $C4T1^2$ planar tensegrity structure. Points *A* are the same, and points *B* are the same, to illustrate that two identical bars overlap.

17.3.3 Self-Similar Structures of the *C4T*1 Type

Now let each of the four bars of the *C4T*1 system (that is, the *C4T*2 system with $t_h = 0$) in Figure 17.22 be replaced by another *C4T*1 system. The new 16 bar structure of Figure 17.26 is called $C4T1^2$, and is designed to buckle at the same load *F*. Hence, if F_2 represents the force in each of the 16 bars, with length L_2 and radius r_2, and mass $m_2/16$, then, for $\delta_1 = \delta_2 = \delta$ the relations below are obtained.

$$F_2 = \frac{E_0 \pi^3 r_2^4}{4L_2^2}, \quad m_2 = 16\rho_0 \pi r_2^2 L_2, \quad F_2 = \frac{E_0 \pi m_2^2}{64\rho_0^2 L_2^4} \tag{17.77}$$

$$L_2 = \frac{L_1}{2\cos\delta}, \quad F_2 = \frac{F_1}{2\cos\delta} \tag{17.78}$$

$$m_2^2 = \frac{m_1^2}{2\cos^5\delta} = \frac{m_0^2}{\left(2\cos^5\delta\right)^2} \tag{17.79}$$

$$\left(\frac{r_2}{r_1}\right)^4 = (2\cos\delta)^{-3} \tag{17.80}$$

$$\left(\frac{r_2}{r_0}\right)^4 = (2\cos\delta)^{-6} \tag{17.81}$$

$$\frac{L_2}{L_0} = \left(2\cos\delta\right)^{-1} \tag{17.82}$$

$$\frac{L_2}{L_0} = (2\cos\delta)^{-2} \tag{17.83}$$

$$\left(\frac{r_2}{r_1}\right)^4 = \left(\frac{L_2}{L_1}\right)^3 \tag{17.84}$$

$$\left(\frac{r_2}{r_0}\right)^4 = \left(\frac{L_2}{L_0}\right)^3 \tag{17.85}$$

$$\frac{L_2}{r_2} = \frac{L_1}{r_1}(2\cos\delta)^{-\frac{1}{4}} = \frac{L_0}{r_0}(2\cos\delta)^{-\frac{1}{2}} \tag{17.86}$$

Now let us replace each bar in the structure of Figure 17.26 by yet another *C4T*1 structure and continue this process indefinitely. To simplify the language for these instructions, we coin some names that will simplify the description of the process we consider later.

Definition 17.3 *Let the operation which replaces the bar of length L_0 with the design of Figure 17.22 be called the "C4T1 operator." This replaces one compressive member with four compressive members plus one tension member, where the bar radii obey (17.88). Let δ be the same for any i. Let the operation which replaces the design of the bar Figure 17.21 with the design of Figure 17.26 be called the "C4T1² operator." If this C4T1 operation is repeated i times, then call it the C4T1^i operator, yielding the C4T1^i system.*

Lemma 17.2 *Let the C4T1^i operator be applied to the initial bar, always using the same material and preserving buckling strength. Then, $\delta_1 = \delta$ the mass m_i, bar radius r_i, bar length L_i of the C4T1^i system satisfy:*

$$\frac{m_i}{m_0} = (2\cos^5\delta)^{-\frac{i}{2}} \tag{17.87}$$

$$\frac{r_i}{r_0} = (2\cos\delta)^{-\frac{3i}{4}} = \left(\frac{L_i}{L_0}\right)^{\frac{3}{4}} \tag{17.88}$$

$$\frac{L_i}{L_0} = (2\cos\delta)^{-i} \tag{17.89}$$

$$\frac{L_i}{r_i} = \frac{L_0}{r_0}(2\cos\delta)^{-\frac{i}{4}} \tag{17.90}$$

$$F_i = \frac{E_0\pi r_i^4}{L_i^2} = \frac{E_0 m_i^2}{4^{2i}\rho_0^2 L_i^4} \tag{17.91}$$

$$m_i = 4^i\rho_0\pi r_i^2 L_i\,. \tag{17.92}$$

Note from (17.90) that the length-to-diameter ratio of the bars decreases with i if $\delta < 60^\circ$.

Figure 17.27 illustrates *C4T*1^i structures for $i = 3, 4, 5, 6$. Taking the limit of (17.87) as $i \to \infty$ proves the following:

Theorem 17.1 *Suppose the compressive force which buckles a C4T1^i system is a specified value, F. Then if $\delta < 29.477^\circ$, the total mass of the bars in the C4T1^i system approaches zero as $i \to \infty$.*

Proof: Take i toward infinity in (17.87). ❑

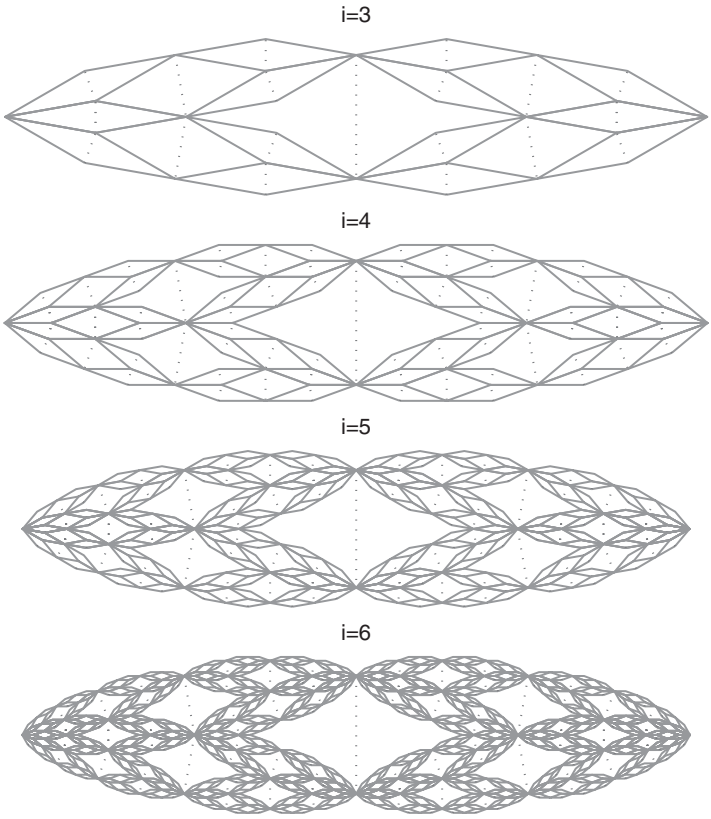

FIGURE 17.27 A $C4T1^i$ planar tensegrity structure for $i = 3, 4, 5, 6$.

Now suppose the number of self-similar iterations continue until the lengths of the bars are not longer than their diameters. Then, buckling cannot occur, and the structure is theoretically infinitely strong against buckling of the bars, but of course, the strings can still break. Therefore, ignoring the obvious overlapping of material as the iterations become large, we cite this result which is more intriguing than practical.

Proposition 17.2 *The $C4T1^i$ structure is infinitely strong against buckling if i, δ satisfy*

$$\left(2\cos\delta\right)^i \geq \left(\frac{L_0}{2r_0}\right)^4 \tag{17.93}$$

Proof: The Euler buckling formula $F_B = \pi^2 EI/L^2$ applies to beams whose diameter is smaller than the length. Otherwise, buckling cannot occur. From Lemma 17.2, the diameter equals the length of the bar when $L_i/2r_i = L_0/2r_0\left(2\cos\delta\right)^{-i/4} = 1$. From (17.90) the i such that $L_i/2r_i = 1$, satisfies

$$L_i/2r_i = L_0/2r_0\left(2\cos\delta\right)^{-i/4} = 1 \quad \text{❑} \tag{17.94}$$

As an example of (17.93) and (17.94), compared to a bar of length L_0 and radius r_0, the $C4T1^{18}$ structure with $\alpha = 10°$ buckles at the same load as the original bar, has .39% of the mass of the

original bar, and is infinitely stronger than the bar. For a given specified strength, this example suggests that solid materials are quite wasteful of mass. Of course, the above result has ignored the fact that the material overlaps, if one tried to place all elements in the same plane. However, multiple planar layers of elements can be pinned to give the desired planar effect mathematically described herein. A more important omission of the above analysis is the calculation of string mass. The string mass increases with self-similar iterations (increases with i) because strings are added in the process. The mass of the bars decrease with *i,* so obviously minimal mass of the system (bars plus strings) occurs at finite *i.* This calculation will be shown momentarily.

17.3.3.1 Robustness of the *C*4*T*1

In this section we discuss briefly the issue of stability under a lateral force $F_L = 0$ in Figure 17.22. We begin by mentioning two disastrous circumstances. First, if the applied force F is small and F_L is big, then the *C*4*T*1 will collapse. Second, if the angle δ is very small and F is big, then a modest lateral force F_L will collapse the structure. Of course, a larger pretension in t_h will protect against larger F_L. Three important points on more general structures of this type: first, big F always helps lateral robustness; second, larger δ helps lateral robustness; third, increasing t_h helps robustness.

17.3.3.2 Mass and Tension of String in a *C*4*T*1[1] Structure

The mass m_{t1}, length L_{t1} and tension t_1 of string in the *C*4*T*1[1] structure are expressed as

$$m_{t1} = \rho_{t1} L_{t1} \pi r_{t1}^2, \tag{17.95}$$

$$L_{t1} = L_0 \tan\delta, \tag{17.96}$$

and

$$t_1 = F \tan\delta = \sigma_{t1} \pi r_{t1}^2, \tag{17.97}$$

respectively.

With (17.95) and (17.97),

$$t_1 = F \tan\delta = \sigma_{t1} \pi r_{t1}^2 = \sigma_{t1} \frac{m_{t1}}{\rho_{t1} L_{t1}}.$$

Hence,

$$m_{t1} = \frac{\rho_{t1}}{\sigma_{t1}} L_{t1} F \tan\delta$$

$$= \frac{\rho t1}{\sigma t1} (L_0 \tan\delta) \left(\frac{E_0 \pi m_0^2}{4\rho_0^2 L_0^4} \right) \tan\delta$$

$$= \left(\frac{E_0 \pi \tan^2\delta}{4\sigma_{t1} L_0^3} \right) \left(\frac{\rho_{t1}}{\rho_0^2} \right) m_0^2$$

$$= \left(\frac{E_0 \pi \tan^2\delta}{4\sigma_{t1} L_0^3} \right) \left(\frac{\rho_{t1}}{\rho_0^2} \right) \rho_0 \pi r_0^2 L_0 m_0.$$

So, the mass of string m_{t1} is

$$m_{t1} = \left(\frac{E_0 \pi^2 \tan^2\delta}{16\sigma_{t1} l_0^2} \right) \left(\frac{\rho_{t1}}{\rho_0} \right) m_0. \tag{17.98}$$

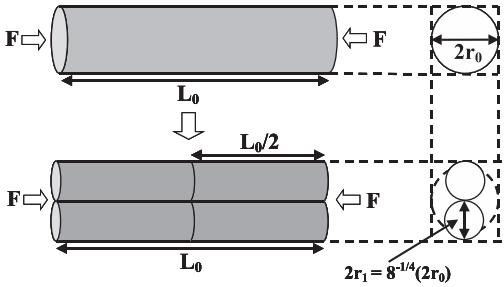

FIGURE 17.28 The minimal mass of $C4T1^1$ structure (bottom) that replaces the $C4T1^0$ structure (top) with a cross-section area comparison (right).

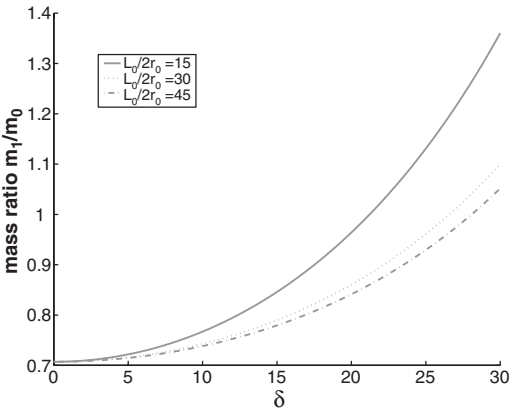

FIGURE 17.29 Mass ratio $\frac{m_1}{m_0}$ vs. δ for different length-to-diameter ratio $l_0 = \frac{L_0}{2r_o}$.

17.3.3.3 Total Mass of a $C4T1^1$ Structure

From (17.87) and (17.98), the total mass m_1 of the $C4T1^1$ structure is

$$m_1 = m_{t1} + m_{b1}$$

$$m_1 = \left[\left(\frac{E_0 \pi^2 \tan^2 \delta}{16 \sigma_{t1} l_0^2} \right) \left(\frac{\rho_{t1}}{\rho_o} \right) + \left(\frac{E_0}{E_1} \right)^{\frac{1}{2}} \left(\frac{\rho_1}{\rho_0} \right) \left(\frac{1}{2 \cos^5 \delta} \right)^{\frac{1}{2}} \right] m_0. \tag{17.99}$$

For the same material of bar and string as that of the original structure, (17.99) is reduced to

$$m_1 = \left[\left(\frac{E_0 \pi^2 \tan^2 \delta}{16 \sigma_{t1} l_0^2} \right) + \left(\frac{1}{2 \cos^5 \delta} \right)^{\frac{1}{2}} \right] m_0. \tag{17.100}$$

So, the minimal mass occurs at $\delta = 0^\circ$, yielding $m_1 = \frac{1}{\sqrt{2}} m_o$. This configuration is shown in Figure 17.28.

Figure 17.29 shows the plot of mass ratio m_1/m_0 vs. δ for different l_0. It can be seen that the upper bound of δ is less than 29.477318° for mass reduction and also depends on the length-to-diameter ratio l_0.

17.3.3.4 *C4T1*^{i} Structures

For bars, the Young's modulus, density, and length-to-diameter ratio in *C4T1*^{i} will be denoted as E_i, ρ_i, and l_i, respectively. For strings, the Young's modulus, density, and yield strength in every stage j of *C4T1*^{i} (where $j = 0, 1, 2 \ldots i-1, i$) will be denoted as E_{tj}, ρ_{tj}, and σ_{tj}, respectively. The extra subscript "t" is used to distinguish the string from the bar. Applying the *C4T1*^{i} operator to the original bar allows one to proceed from the *C4T1*^{0} to *C4T1*^{i} system. Similar to the analysis before, the total mass of bars is

$$m_{bi} = 4^i \rho_i L_i \pi r_i^2. \tag{17.101}$$

The buckling load of each bar is

$$F_i = \frac{E_i \pi^3 r_i^4}{4L_i^2} = \frac{E_i \pi m_{bi}^2}{4^{2i+1} \rho_i^2 L_i^4}. \tag{17.102}$$

From the geometry of the structure, the length and load of each bar are

$$L_i = \frac{L_{e-1}}{2\cos\delta_i} = \frac{L_0}{\Pi_{j=1}^i 2\cos\delta_j}, \tag{17.103}$$

and

$$F_i = \frac{F_{i-1}}{2\cos\delta_i} = \frac{F}{\Pi_{j=1}^i 2\cos\delta j}, \tag{17.104}$$

respectively, where δ_j is the angle described in the same way as in Figure 17.26 and all δ_j might be equal, or might be different.

17.3.3.5 Mass of Bars in a *C4T1*^{i} Structure

From (17.101), (17.102), (17.103), and (17.106), the total mass of the bars in *C4T1*^{i} can be related to the mass of *C4T1*^{0} through

$$F_i = \frac{E_i \pi m_{bi}^2}{4^{2i+1} \rho_i^2 L_i^4} = \frac{F}{\Pi_{j=1}^i 2\cos\delta_j} = \frac{E_0 m_0^2}{4\rho_0^2 L_0^4 \Pi_{j=1}^i 2\cos\delta_j}$$

$$m_{bi}^2 = \left(\frac{E_0}{E_i}\right)\left(\frac{\rho_i}{\rho_0}\right)^2 \frac{1}{\Pi_{j=1}^i 2\cos^5\delta_j} m_0^2. \tag{17.105}$$

17.3.3.6 Length to Diameter Ratio of Bar in a *C4T1*^{i} Structure

The length-to-diameter ratio of the bars in *C4T1*^{i} will be l_i given by

$$l_i = \frac{L_i}{2r_i} = \left(\frac{E_i}{E_0}\right)^{\frac{1}{4}} \left(\frac{1}{\Pi_{j=1}^i 2\cos\delta_j}\right)^{\frac{1}{4}} l_0. \tag{17.106}$$

17.3.3.7 Mass and Tension of Strings in a $C4T1^i$ Structure

Generalizing the concept from the previous section, the mass, length, and tension of the strings in the j-th iteration ($j = 1,2,3,\ldots i-1, i$) of $C4T1^i$ will be

$$m_{tj} = 4^{j-1}\rho_{tj}L_{tj}\pi r_{tj}^2, \tag{17.107}$$

where (r_{tj}, L_{tj}) is the radius and length of the strings,

$$L_{tj} = 2L_j \sin\delta_j = \frac{2L_0 \sin\delta_j}{\Pi_{r=1}^{j} 2\cos\delta_r}. \tag{17.108}$$

and

$$t_j = 2F_j \sin\delta_j = \frac{2F \sin\delta_j}{\Pi_{r=1}^{j} 2\cos\delta_j} = \sigma_{tj}\pi r_{tj}^2, \tag{17.109}$$

where σ_{tj} is the yield stress of the string.

With (17.107), (17.108), and (17.109), the mass of the each string in the i-th iteration can be related to the mass of $C4T1^0$

$$t_j = \frac{2\sin\delta_j}{\Pi_{r=1}^{j}\cos\delta_r}\left(\frac{E_0\pi m_0^2}{4\rho_0^2 L_0^4}\right) = \sigma_{tj}\left(\frac{4}{4i}\right)\left(\frac{m_{tj}\Pi_{s=1}^{j}2\cos\delta_s}{2\rho_{tj}L_0\sin\delta_j}\right)$$

$$m_{tj} = \frac{E_0\pi^2\sin^2\delta_j}{16\sigma_{tj}l_0^2\Pi_{r=1}^{j}\cos^2\delta_r}\left(\frac{\rho_{tj}}{\rho_0}\right)m_0. \tag{17.110}$$

17.3.3.8 Total Mass of $C4T1^i$ Structure

The total mass m_i of the $C4T1^i$ structure will be

$$m_i = m_{bi} + \sum_{j=1}^{i} m_{tj}.$$

With (17.105) and (17.110)

$$m_i = \left[\left(\frac{E_0}{E_i}\right)^{\frac{1}{2}}\left(\frac{\rho_i}{\rho_0}\right)\left(\frac{1}{\Pi_{j=1}^{i}2\cos^5\delta_j}\right)^{\frac{1}{2}} + \sum_{j=1}^{i}\frac{E_0\pi^2\sin^2\delta_j}{16\sigma_{tj}l_0^2\Pi_{r=1}^{j}\cos^2\delta_j}\left(\frac{\rho_{tj}}{\rho_0}\right)\right]m_0. \tag{17.111}$$

For the same angle $\delta_j = \delta$ and same material of bars and strings in every j-th stage, the total mass can be simplified to

$$m_i = \left[\left(\frac{1}{2\cos^5\delta}\right)^{\frac{i}{2}} + \frac{E_0\pi^2}{16\sigma_t l_0^2}\left(\frac{1}{\cos^{2i}\delta} - 1\right)\right]m_0. \tag{17.112}$$

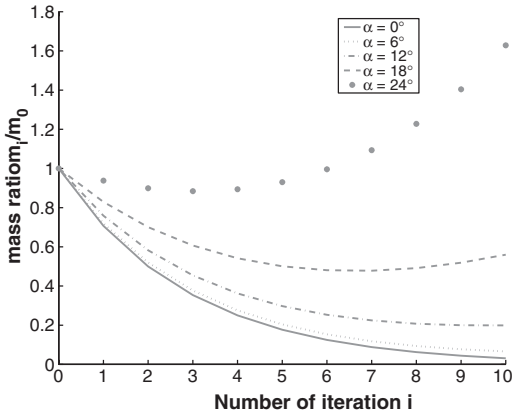

FIGURE 17.30 Mass ratio $\frac{m_i}{m_0}$ vs. number of iterations for length-to-diameter ratio $l_0 = 30$.

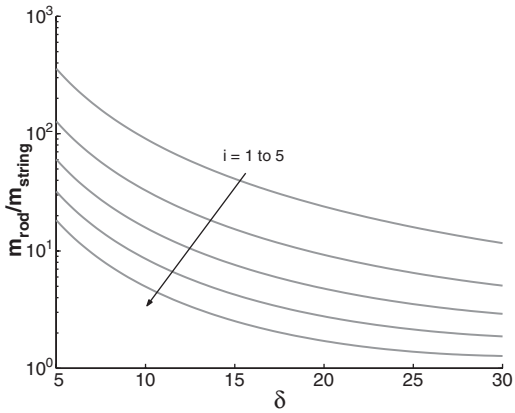

FIGURE 17.31 Mass ratio $\frac{m_{bar}}{m_{string}}$ vs. δ of $C4T1^i$ with $l_0 = \frac{L_0}{2r_0} = 30$.

Figure 17.30 shows the plot of mass ratio (m_i/m_0) vs. the number of iterations for different δ and $l_0 = 30$. From the figure, smaller angles δ will lead to larger mass reduction, and a larger length-to-diameter ratio l_0 also enhances the mass reduction effect.

Figure 17.31 shows the plot of the mass ratio of bars to strings vs. the angle δ for $l_0 = 30$. Bars will dominate the mass of structure at small δ and at a small number of iterations i.

Figure 17.32 shows the plot of δ vs. the number of iterations for different length-to-diameter ratios such that $m_i = m_0$. Regions below each curve are the allowed regions for mass reduction. Note that if $\delta \le 29.477318°$ and the use of materials are the same for every iteration, from (17.105), the mass of bars decreases as the number of iterations increases. However, the mass reduction will be offset by the increase of string mass as can be seen from (17.112). Therefore, maximum mass reduction can be achieved in some finite number of iterations that depends on the angle δ and length-to-diameter ratio l_0. In fact, from (17.112), the mass reduction will be maximum when the number of iterations i is given by the following theorem:

Theorem 17.2 *Assume all bars and strings are composed of the same material. Let the $C4T1^i$ operator be applied to the original bar to get the $C4T1^i$ system, where the iterations are designed*

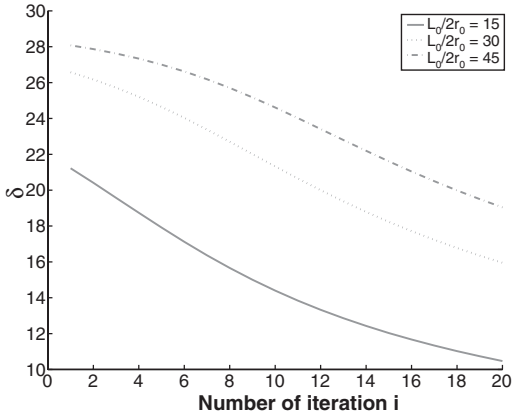

FIGURE 17.32 δ vs. number of iterations i for different for mass ratio $\frac{m_i}{m_0}$ = 1 of iteration i.

to preserve the buckling strength of the original bar. Minimum mass is achieved at a finite number of iterations and this number is given by either i_1 or i_2, where

$$i_1 = \left\lceil \frac{2}{In\left(\frac{1}{2\cos\delta}\right)} In\left(\frac{E_0\pi^2 In\cos\delta}{\sigma_t l_0^2 In\frac{1}{2\cos^5\delta}}\right)\right\rceil, \quad i_2 = \left\lfloor \frac{2}{In\left(\frac{1}{2\cos\delta}\right)} In\left(\frac{E_0\pi^2 In\cos\delta}{\sigma_t l_0^2 In\frac{1}{2\cos^5\delta}}\right)\right\rfloor, \tag{17.113}$$

where ⌈ ⌉ (⌊ ⌋) implies rounding up (down) to the closest integer. One must check the mass at both i_1 and i_2 to choose the smallest mass.

Proof: Let $\mu = m_i/m_0$, then, from (17.112),

$$\mu = \left(\frac{1}{2\cos^5\delta}\right)^{\frac{i}{2}} + \frac{E_0\pi^2}{16\sigma_t l_0^2}\left(\frac{\rho_t}{\rho_0}\right)\left(\frac{1}{\cos^{2i}\delta} - 1\right).$$

Take the derivative of μ w.r.t i by using the rule $da^x/dx = a^x In\, a$, and set it equal to zero to obtain

$$\frac{d\mu}{di} = \frac{1}{2}\left(\frac{1}{2\cos^5\delta}\right)^{\frac{i}{2}} In\left(\frac{1}{2\cos^5\delta}\right) + \frac{E_0\pi^2}{16\sigma_t l_0^2}\left(\frac{\rho_t}{\rho_0}\right)\frac{2}{\cos^{2i}\delta} In\left(\frac{1}{\cos\delta}\right) = 0.$$

Rearranging the equation gives

$$\left(\frac{1}{2\cos\delta}\right)^{\frac{1}{2}} = \frac{E_0\pi^2}{4\sigma_t l_0^2}\left(\frac{\rho_t}{\rho_0}\right)\frac{In\cos\delta}{In\left(\frac{1}{2\cos^5\delta}\right)}.$$

Solving for i yields (17.113). ❑

Figure 17.33 shows the plot of the optimal iteration in (17.113) vs. angle δ for maximum mass reduction.

Figure 17.34 shows the plot of the ratio of bar mass to string mass vs. δ at the optimal iteration given by (17.113). Note that at about δ= 17° and l_0= 30, the total bar mass and the total string mass are equal.

Figure 17.35 shows the corresponding plot of total mass ratio.

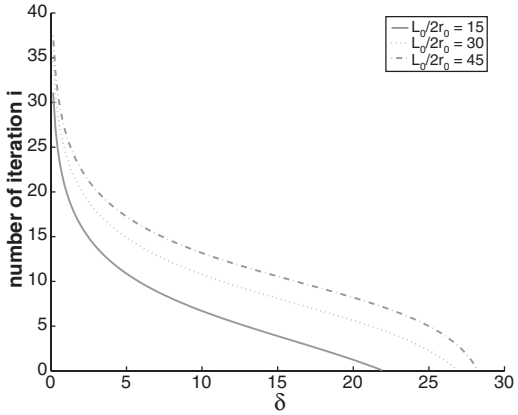

FIGURE 17.33 Optimal number of iterations i vs. δ for the maximum mass reduction.

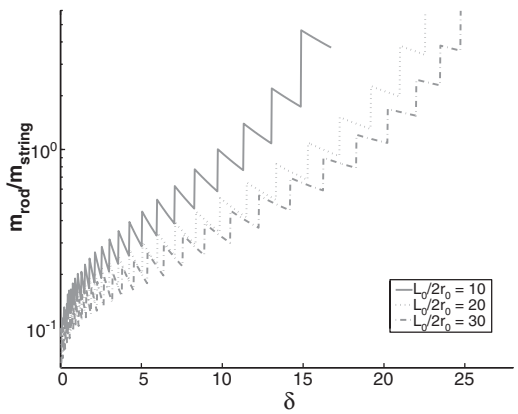

FIGURE 17.34 Mass ratio of bars to strings $\frac{m_{bar}}{m_{string}}$ vs. δ at the optimal iteration.

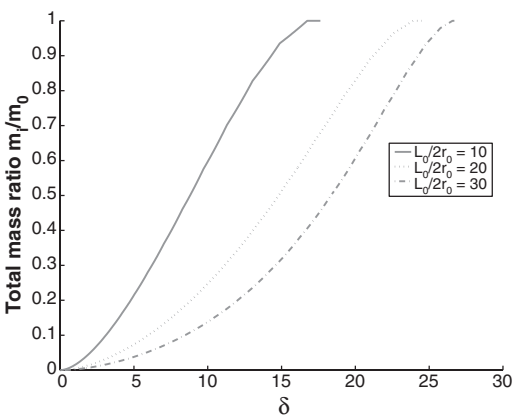

FIGURE 17.35 Total mass ratio $\frac{m_i}{m_0}$ vs. δ at the optimal iteration.

17.3.4 Stiffness of the $C4T1^i$ Structure

17.3.4.1 Stiffness Definition

For the $C4T1^i$, the structure will change its length (measured from two nodal points where external load is applied) in the same direction as the applied force. Therefore, the stiffness calculation is a one-dimensional problem. For an external load F applied to the structure of length L, the stiffness K of the structure is defined as

$$K = -\frac{dF}{dL}, \tag{17.114}$$

where the negative sign means the length of the structure decreases as the applied load increases. Since the external load can be related to the potential energy of the structure U by

$$F = -\frac{dU}{dL},$$

the stiffness can also be calculated from the potential energy by

$$K = \frac{d^2U}{dL^2}. \tag{17.115}$$

17.3.4.2 The Stiffness Equation of a $C4T1^i$ Structure

In the calculations of stiffness (see Appendix 17.C), it is assumed that the stiffness of bars k_{bi} and strings k_{tj}, where $1 \le j \le i$, is constant under deformation. This is not always a good assumption, but other string stiffness models, such as $k = EA/L$ can be analyzed in a straightforward manner. If L_{i0} and L_{tj0} are the rest lengths of bars in the i-th iteration and strings in the j-th iteration, respectively, the stiffness of $C4T1^i$ is given by

$$K_i = k_{t1}\left\{\left(\frac{L_{t10}}{L_{t1}} - 1\right) + \left[4^i \frac{k_{t1}}{k_{bi}} \frac{L_i}{L_{i0}} \left(\frac{L_i}{L_0}\right)^2 + \sum_{j=1}^{i} 4^{j-1} \frac{k_{t1}}{k_{tj}} \frac{L_{tj}}{L_{tjo}} \left(\frac{L_{tj}}{L_0}\right)^2\right]^{-1}\right\}, \tag{17.116}$$

where, in the buckling design (see Appendix 17.B)

$$L_0 = L_t \Pi_{s=1}^{i} 2\cos\delta_s$$

$$L_{tj} = 2L_i \sin\delta_j \Pi_{s=j+1}^{i} 2\cos\delta_s$$

$$\frac{k_{t1}}{k_{tj}} = \frac{E_{t1}\sigma_{tj}}{E_{tj}\sigma_{t1}}$$

$$\frac{k_{t1}}{k_{bi}} = \frac{E_{t1}\pi}{16\sigma_{t1}l_0^2}\sqrt{\frac{E_0}{E_i}}\left(\Pi_{s=1}^{i} 2\cos\delta_s\right)^{\frac{1}{2}}$$

$$\frac{L_{tjo}}{L_{tj}} = 1 - \frac{\sigma_{tj}}{E_{tj}}$$

$$k_{t1} = \frac{E_0 E_{t1} \pi^3 L_0}{16 \sigma_{t1} l_0^4}$$

$$\frac{L_{io}}{L_i} = 1 + \frac{\pi}{16 l_0^2} \left(\Pi_{s=1}^{i} 2 \cos \delta_s \right)^{\frac{1}{2}}.$$

In particular, if the materials of the bars and strings used are the same as those of original structure ($C4T1^0$) and $\delta_j = \delta$, the stiffness equation will be simplified to

$$\begin{aligned} K_i &= k_{t1} \left\{ -\frac{\sigma_t}{E_t} + \left[4^i \frac{k_{t1}}{k_{bi}} \frac{L_i}{L_{i0}} \left(\frac{L_i}{L_0} \right)^2 + \left(1 - \frac{\sigma_t}{E_t} \right)^{-1} \sum_{j=1}^{i} 4^{j-1} \left(\frac{L_{tj}}{L_0} \right)^2 \right]^{-1} \right\} \\ &= k_{t1} \left\{ -\frac{\sigma_t}{E_t} + \left[4^i \frac{k_{t1}}{k_{bi}} \frac{L_i}{L_{i0}} \left(\frac{L_i}{L_0} \right)^2 + \left(1 - \frac{\sigma_t}{E_t} \right)^{-1} \left(\frac{1}{\cos^{2i} \delta} - 1 \right) \right]^{-1} \right\} \end{aligned} \tag{17.117}$$

where

$$L_0 = L_i (2 \cos \delta)^i$$

$$\frac{k_{t1}}{k_{bi}} = \frac{E_t \pi^2}{16 \sigma_t l_0^2} (2 \cos \delta)^{\frac{i}{2}}$$

$$k_{t1} = \frac{E_0 E_t \pi^3 L_0}{64 \sigma_t l_0^4}$$

$$\frac{L_{i0}}{L_i} = 1 + \frac{\pi}{16 l_0^2} (2 \cos \delta)^{\frac{i}{2}}.$$

17.3.4.3 The Rigid Bar Case

If the bar has infinite rigidity (large compared to the stiffness of strings), this means

$$\frac{k_{ti}}{k_{bi}} \to 0,$$

then, the stiffness equation becomes

$$K_i = k_{t1} \left(\frac{\cos^{2i} \delta - \frac{\sigma_t}{E_t}}{1 - \cos^{2i} \delta} \right), \tag{17.118}$$

where

$$k_{t1} = \frac{E_0 E_t \pi^3 L_0}{64 \sigma_t l_0^4}.$$

Figure 17.36 shows the plot of the stiffness K_i vs. δ for length-to-diameter ratio $l_0 = 30$.

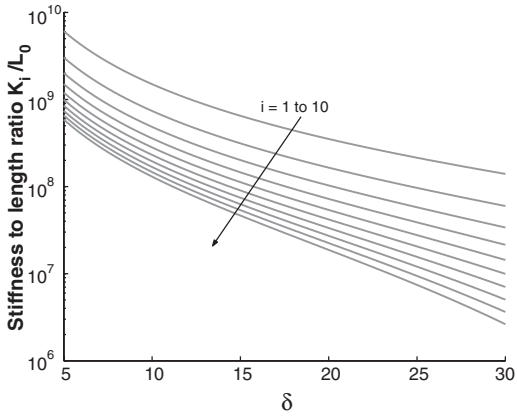

FIGURE 17.36 Stiffness K_i of $C4T1^i$ structure with rigid bars vs. δ for $l_0 = 30$.

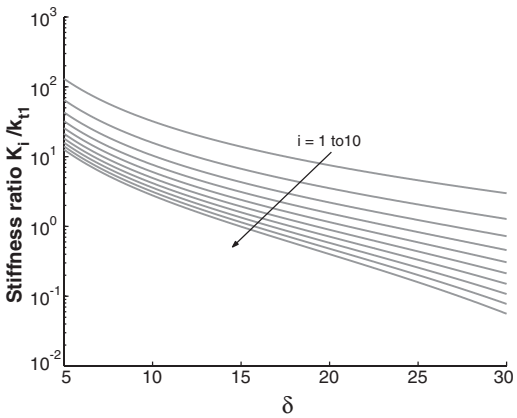

FIGURE 17.37 Stiffness ratio $\frac{K_i}{k_{t_1}}$ of $C4T1^i$ structure with rigid bars vs. δ.

Figure 17.37 shows the plot of the stiffness ratio K_i/k_{i1} vs. δ for the infinite rigid bar $C4T1^i$ structure. Note that the ratio is independent of l_0.

Because the stiffness reduces with each iteration i, it is of interest to know how many iterations may be taken before the stiffness violates a desired lower bound $\underline{K}$.

Proposition 17.3 *Given δ and a desired lower bound stiffness $\underline{K}$ of $C4T1^i$, that is, $\underline{K} \le K_i$, the number of iterations i which achieves this stiffness requirement is bounded by*

$$i \le \frac{\log \frac{\frac{\underline{K}}{k_{t1}} + \frac{\sigma_t}{E_t}}{1 + \frac{\underline{K}}{k_{t1}}}}{2 \log \cos\delta}. \tag{17.119}$$

Proof: From (17.118),

$$\underline{K} \le K_i$$

$$\le k_{t1}\left(\frac{\cos^{2i}\delta - \frac{\sigma_t}{E_t}}{1 - \cos^{2i}\delta}\right).$$

Rearrange the inequality to expose $\cos^{2i}\delta$ on one side and then take the log of both sides to obtain (17.119) ❑

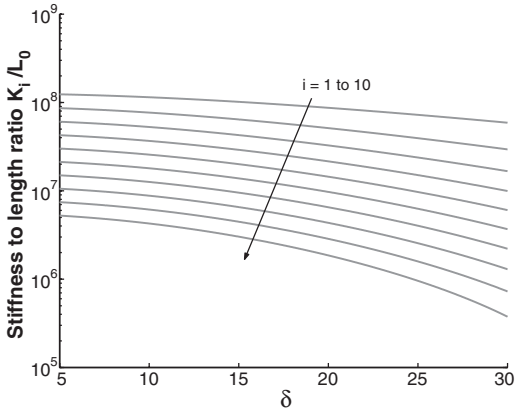

FIGURE 17.38 Stiffness-to-length ratio $\frac{K_i}{L_0}$ vs. δ for length-to-diameter ratio $l_0 = 30$, for elastic bars.

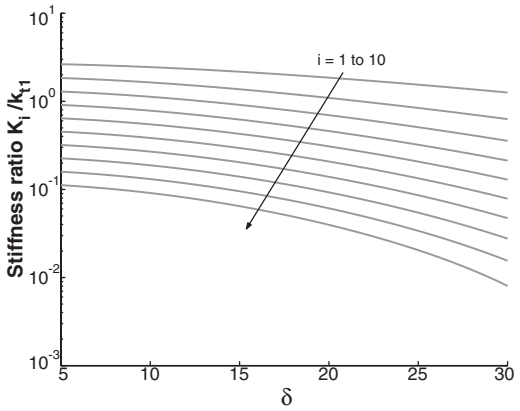

FIGURE 17.39 Stiffness ratio $\frac{K_i}{k_{t_1}}$ vs. δ for length-to-diameter ratio $l_0 = 30$, for elastic bars.

17.3.4.4 The Elastic Bar Case

If the bars in the $C4T1^i$ structure are elastic,

$$\frac{k_{ti}}{k_{bi}} \neq 0\,,$$

and hence (17.117) will be used for numerical calculations.

Figure 17.38 shows the plot of the stiffness K_i vs. δ for length-to-diameter ratio $l_0 = 30$.

Figure 17.39 shows the corresponding plot of the stiffness ratio K_i/K_{t1} vs. δ for Figure 17.38. A comparison of Figures 17.36 to 17.39 reveals that with elastic bars, system stiffness is much less than for a system made with rigid bars.

17.3.4.4.1 Stiffness Ratio K_i/K_0

The stiffness of $C4T1^0$ (a single bar) is

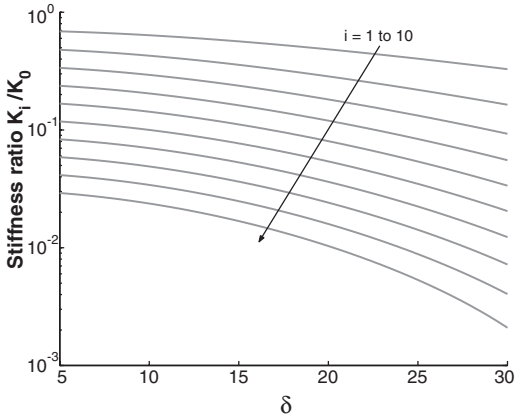

FIGURE 17.40 Stiffness ratio $\frac{K_i}{K_0}$ vs. δ for $l_0 = 30$, for elastic bars.

$$K_0 = \frac{E_0 \pi r_0^2}{L_0}. \tag{17.120}$$

With (17.117), the stiffness ratio K_i/K_0 is given by

$$\frac{K_i}{K_0} = \left(\frac{E_t \pi^2}{16\sigma_t l_0^2}\right)\left\{-\frac{\sigma_t}{E_t} + \left[4^i \frac{k_{ti}}{k_{bi}} \frac{L_i}{L_{i0}}\left(\frac{L_i}{L_{i0}}\right)^2 + \left(1-\frac{\sigma_t}{E_t}\right)^{-1}\left(\frac{1}{\cos^{2i}\delta} - 1\right)\right]^{-1}\right\}, \tag{17.121}$$

where other physical quantities are the same as those given in (17.117).

Figure 17.40 shows the plot of the stiffness ratio K_i/K_0 vs. δ for length-to-diameter ratio $l_0 = 30$.

Figures 17.37, 17.39, and 17.40 demonstrate that stiffness is much less sensitive to geometry (choice of δ) when bars are elastic than when the bars are rigid.

17.3.4.4.2 Stiffness to Mass Ratio

From (17.112) and (17.117), the stiffness-to-mass ratio is given by

$$\frac{K_i}{m_i} = \left(\frac{E_0 E_t \pi^2}{16\sigma_t \rho_0 l_0^2 L_0^2}\right)\left\{\frac{-\frac{\sigma_t}{E_t} + \left[4^i \frac{k_{ti}}{k_{bi}} \frac{L_i}{L_{i0}}\left(\frac{L_i}{L_0}\right)^2 + \left(1-\frac{\sigma_t}{E_t}\right)^{-1}\left(\frac{1}{\cos^{2i}\delta} - 1\right)^{-1}\right]}{\left(\frac{1}{2\cos^5\delta}\right)^{\frac{1}{2}} + \frac{E_0\pi}{16\sigma_t l_0^2}\left(\frac{1}{\cos^{2i}\delta} - 1\right)}\right\}, \tag{17.122}$$

where other physical quantities are the same as those given in (17.117).

Figures 17.41 plots the stiffness-to-mass ratio, K_i/m_i vs. δ, length-to-diameter ratio $l_0 = 30$. The stiffness-to-mass ratio remains constant with self-similar iteration i at $\delta = 0°$ and always decreases with the increase of iterations i and δ.

17.3.5 *C4T1*^{i} Structure with Elastic Bars and Constant Stiffness

Given a bar of radius r_0 and length L_0 under applied force F (not buckling load), this section shows how to design the *C4T1*^{i} structure to minimize the use of mass by replacing the bar with the *C4T1*^{i} structure such that the stiffness of the structure is the same as that of a bar under the same applied load F.

It is assumed that the stiffness of member bars and strings is constant and it is given by

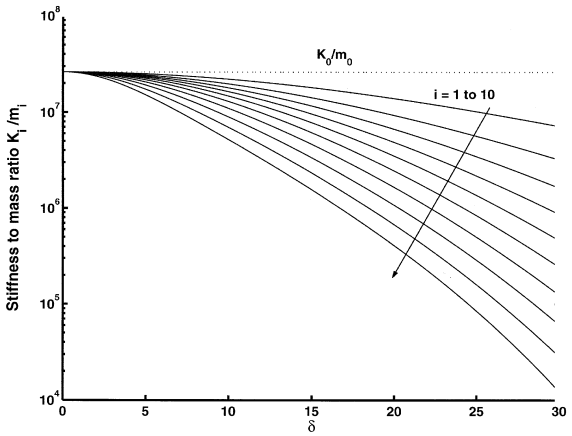

FIGURE 17.41 Stiffness-to-mass ratio $\frac{K_i}{m_i}$ vs. δ for $l_0 = 30$.

$$k = \frac{E\pi r^2}{L}, \tag{17.123}$$

where r and L are the cross-section radius and length of bars or strings when the $C4T1^i$ structure is under external load F.

17.3.5.1 $C4T1^1$ at δ = 0°

At δ = 0°, it is known from the previous section that the use of mass is minimum while the stiffness is maximum. Therefore, a simple analysis of $C4T1^1$ at δ = 0 will give an idea of whether it is possible to reduce the mass while preserving stiffness.

For the $C4T1^0$ structure, the stiffness is given by

$$K_0 = \frac{E\pi r_0^2}{L_0}. \tag{17.124}$$

For a $C4T1^1$ structure at δ = 0°, i.e., two pairs of parallel bars in series with each other, the length of each bar is $L_0/2$ and its stiffness is

$$k_b = \frac{E\pi r_1^2}{L_1} = \frac{2E\pi r_1^2}{L_0}. \tag{17.125}$$

For this four-bar arrangement, the equivalent stiffness is same as the stiffness of each bar, i.e.,

$$K_1 = \frac{2E\pi r_1^2}{L_0}. \tag{17.126}$$

To preserve stiffness, it is required that

$$K_1 = K_0$$

$$\frac{2E\pi r_1^2}{L_0} = \frac{E\pi r_0^2}{L_0}.$$

So,

$$r_0^2 = 2r_1^2. \tag{17.127}$$

Then, the mass of $C4T1^1$ at $\delta = 0°$ for stiffness preserving design is

$$m_1 = 4\rho\pi r_1^2 L_1 = 4\rho\pi \frac{r_0^2}{2}\frac{L_0}{2} = \rho\pi_0^2 L_0 = m_0, \tag{17.128}$$

which indicates, at $\delta = 0°$, that the mass of $C4T1^1$ is equal to that of $C4T1^0$ in a stiffness-preserving design. Therefore, the mass reduction of $C4T1^i$ structure in a stiffness-preserving design is unlikely to happen. However, if the horizontal string t_h is added in the $C4T1^1$ element to make it a $C4T2$ element, then stiffness can be improved, as shown in (17.76).

17.3.6 Summary

The concept of self-similar tensegrity structures of Class k has been illustrated. For the example of massless strings and rigid bars replacing a bar with a Class 2 tensegrity structure $C4T1$ with specially chosen geometry, $\delta < 29°$, the mass of the new system is less than the mass of the bar, the strength of the bar is matched, and a stiffness bound can be satisfied. Continuing this process for a finite member of iterations yields a system mass that is minimal for these stated constraints. This optimization problem is analytically solved and does not require complex numerical codes. For elastic bars, analytical expressions are derived for the stiffness, and choosing the parameters to achieve a specified stiffness is straightforward numerical work. The stiffness and stiffness-to-mass ratio always decrease with self-similar iteration, and with increasing angle δ, improved with the number of self-similar iterations, whereas the stiffness always decreases.

17.4 Statics of a 3-Bar Tensegrity

17.4.1 Classes of Tensegrity

The tensegrity unit studied here is the simplest three-dimensional tensegrity unit which is comprised of three bars held together in space by strings to form a tensegrity unit. A tensegrity unit comprising three bars will be called a 3-bar tensegrity. A 3-bar tensegrity is constructed by using three bars in each stage which are twisted either in clockwise or in counter-clockwise direction. The top strings connecting the top of each bar support the next stage in which the bars are twisted in a direction opposite to the bars in the previous stage. In this way any number of stages can be constructed which will have an alternating clockwise and counter-clockwise rotation of the bars in each successive stage. This is the type of structure in Snelson's Needle Tower, Figure 17.1. The strings that support the next stage are known as the "saddle strings (S)." The strings that connect the top of bars of one stage to the top of bars of the adjacent stages or the bottom of bars of one stage to the bottom of bars of the adjacent stages are known as the "diagonal strings (D)," whereas the strings that connect the top of the bars of one stage to the bottom of the bars of the same stage are known as the "vertical strings (V)."

Figure 17.42 illustrates an unfolded tensegrity architecture where the dotted lines denote the vertical strings in Figure 17.43 and thick lines denote bars. Closure of the structure by joining points A, B, C, and D yields a tensegrity beam with four bars per stage as opposed to the example in Figure 17.43 which employs only three bars per stage. Any number of bars per stage may be employed by increasing the number of bars laid in the lateral direction and any number of stages can be formed by increasing the rows in the vertical direction as in Figure 17.42.

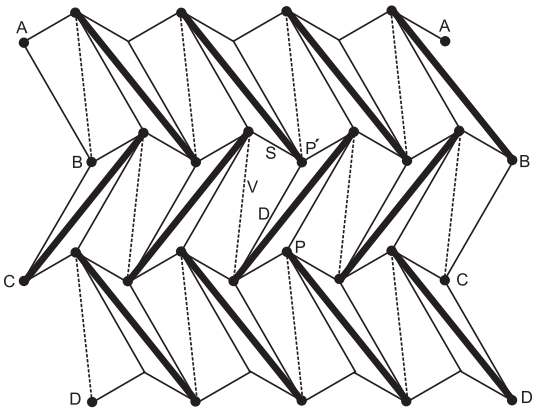

lllFIGURE 17.42 Unfolded tensegrity architecture.

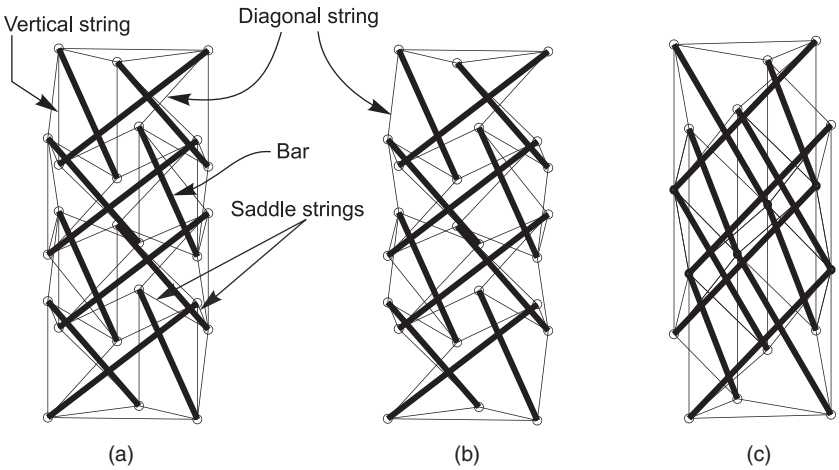

FIGURE 17.43 Types of structures with three bars in one stage. (a) 3-Bar SVD tensegrity; (b) 3-bar SD tensegrity, (c) 3-bar SS tensegrity.

Even with only three bars in one stage, which represents the simplest form of a three-dimensional tensegrity unit, various types of tensegrities can be constructed depending on how these bars have been held in space to form a beam that satisfies the definition of tensegrity. Three variations of a 3-bar per stage structure are described below.

17.4.1.1 3-Bar SVD Class 1 Tensegrity

A typical two-stage 3-bar SVD tensegrity is shown in Figure 17.43(a) in which the bars of the bottom stage are twisted in the counter-clockwise direction. As is seen in Figure 17.42 and Figure 17.43(a), these tensegrities are constructed by using all three types of strings, saddle strings (S), vertical strings (V), and the diagonal strings (D), hence the name SVD tensegrity.

17.4.1.2 3-Bar SD Class 1 Tensegrity

These types of tensegrities are constructed by eliminating the vertical strings to obtain a stable equilibrium with the minimal number of strings. Thus, a SD-type tensegrity only has saddle (S) and the diagonal strings (D), as shown in Figure 17.42 and Figure 17.43(b).

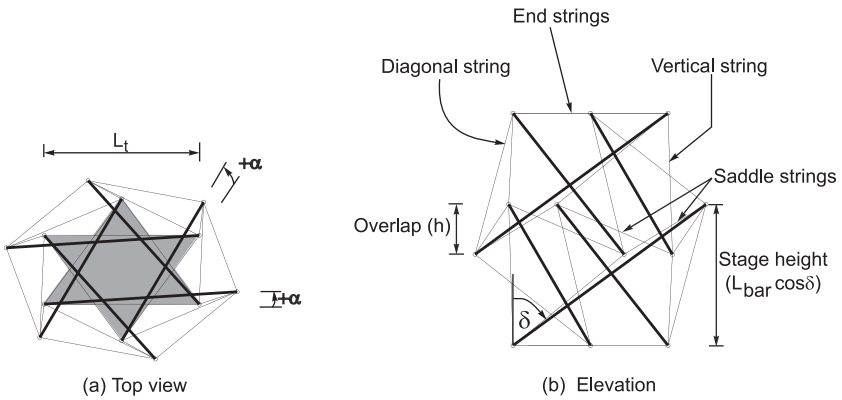

FIGURE 17.44 Top view and elevation of a two-stage 3-bar SVD tensegrity.

17.4.1.3 3-Bar SS Class 2 Tensegrity

It is natural to examine the case when the bars are connected with a ball joint. If one connects points P and P′ in Figure 17.42, the resulting structure is shown in Figure 17.43(c). The analysis of this class of structures is postponed for a later publication.

The static properties of a 3-bar SVD-type tensegrity is studied in this chapter. A typical two-stage 3-bar SVD-type tensegrity is shown in Figure 17.44 in which the bars of the bottom stage are twisted in the counter-clockwise direction. The coordinate system used is also shown in the same figure. The same configuration will be used for all subsequent studies on the statics of the tensegrity. The notations and symbols, along with the definitions of angles α and δ, and overlap between the stages, used in the following discussions are also shown in Figure 17.44.

The assumptions related to the geometrical configuration of the tensegrity structure are listed below:

1. The projection of the top and the bottom triangles (vertices) on the horizontal plane makes a regular hexagon.
2. The projection of bars on the horizontal plane makes an angle α with the sides of the base triangle. The angle α is taken to be positive (+) if the projection of the bar lies inside the base triangle, otherwise α is considered as negative (–).
3. All of the bars are assumed to have the same declination angle δ.
4. All bars are of equal length, L.

17.4.2 Existence Conditions for 3-Bar SVD Tensegrity

The existence of a tensegrity structure requires that all bars be in compression and all strings be in tension in the absence of the external loads. Mathematically, the existence of a tensegrity system must satisfy the following set of equations:

$$\mathbf{A}(\bar{q})\mathbf{t}_0 = 0, \qquad \mathbf{t}_{0\_strings} > 0, \qquad \bar{q}: stable \quad equilibrium. \tag{17.129}$$

For our use, we shall define the conditions stated in (17.129) as the "tensegrity condition."

Note that $\mathbf{A}$ of (17.129) is now a function of α, δ, and h, the generalized coordinates, labeled q generically. For a given q, the null space of $\mathbf{A}$ is computed from the singular value decomposition of $\mathbf{A}$.[36,37] Any singular value of $\mathbf{A}$ smaller than 1.0×10^{-10} was assumed to be zero and the null vector $\mathbf{t}_0$ belonging to the null space of $\mathbf{A}$ was then computed. The null vector was then checked against the requirement of all strings in tension. The values of α, δ, and h that satisfy (17.129)

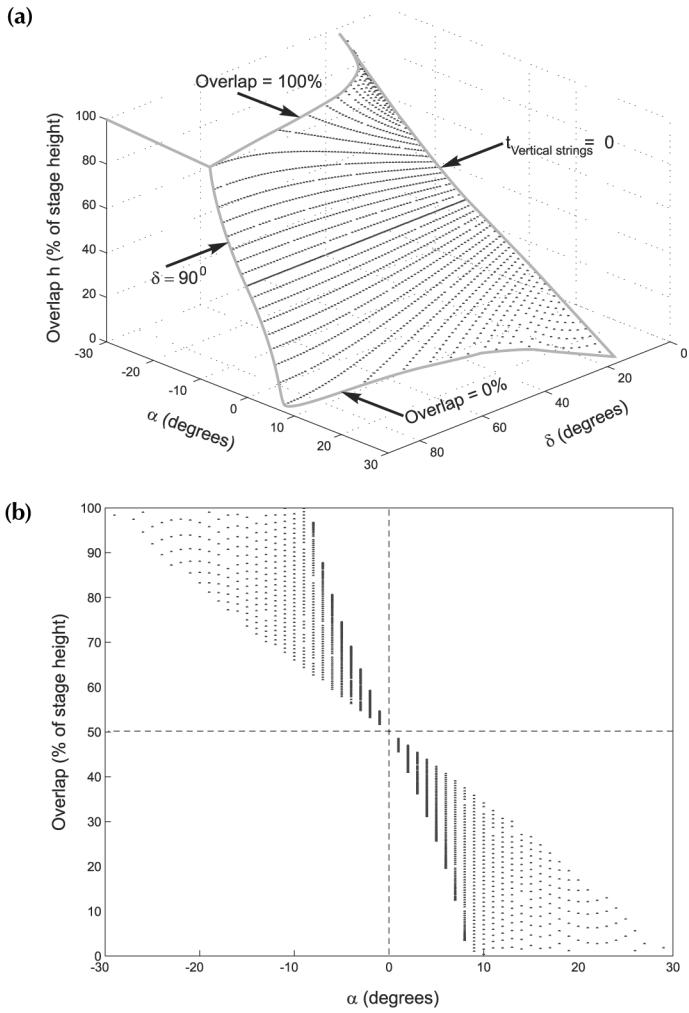

FIGURE 17.45 Existence conditions for a two-stage tensegrity. Relations between (a) α, δ, and the overlap, (b) α and overlap, (c) δ and overlap, and (d) δ and α giving static equilibria.

yield a tensegrity structure. In this section, the existence conditions are explored for a two-stage 3-bar SVD-type tensegrity, as shown in Figure 17.44, and are discussed below.

All of the possible configurations resulting in the self-stressed equilibrium conditions for a two-stage 3-bar SVD-type tensegrity are shown in Figure 17.45. While obtaining Figure 17.45, the length of the bars was assumed to be 0.40 m and L_t, as shown in Figure 17.44, was taken to be 0.20 m.

Figure 17.45 shows that out of various possible combinations of α–δ–*h*, there exists only a small domain of α–δ–*h* satisfying the existence condition for the two-stage 3-bar SVD-type tensegrity studied here. It is interesting to explore the factors defining the boundaries of the domain of α–δ–*h*. For this, the relation between α and *h*, δ and *h*, and also the range of α and δ satisfying the existence condition for the two-stage 3-bar SVD-type tensegrity are shown in Figures 17.45(b), (c), and (d). Figure 17.45(b) shows that when $\alpha = 30°$, there exists a unique value of overlap equal to 50% of the stage height. Note that $\alpha = 0°$ results in a perfect hexagonal cylinder. For any value of α other than 0°, multiple values of overlap exist that satisfies the existence condition. These overlap values for any given value of α depend on δ, as shown in Figure 17.45(c). It is also observed in Figure 17.45(b) and (c) that a larger value of negative α results in a large value of overlap and a

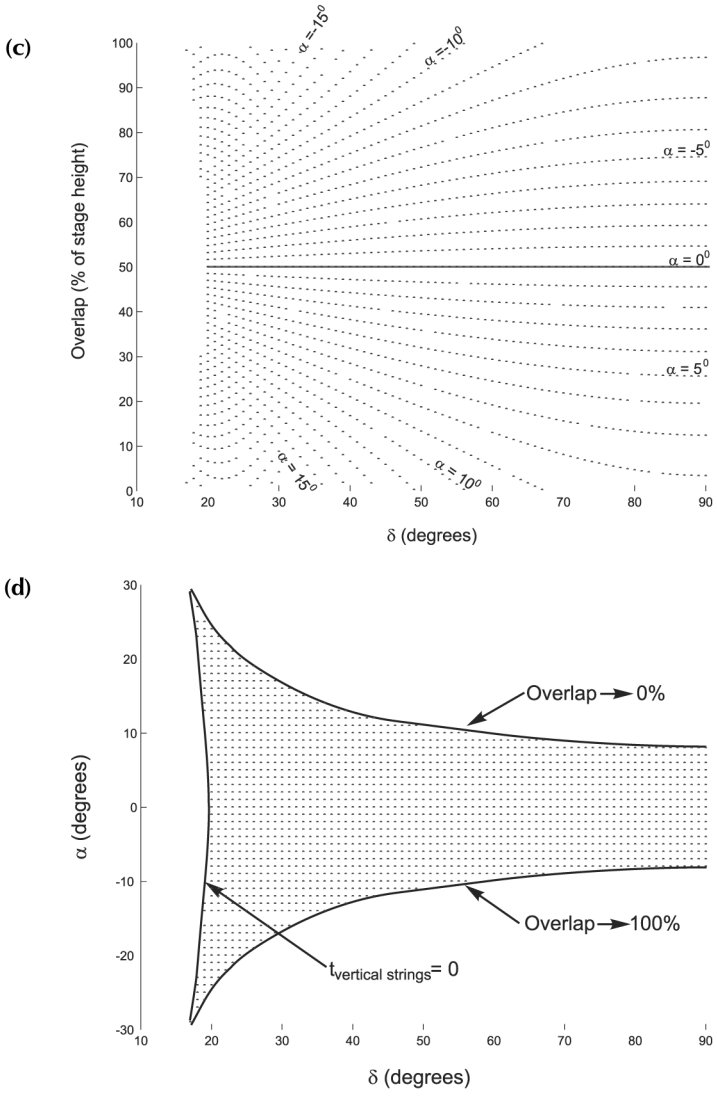

FIGURE 17.45 (Continued)

larger value of positive α results in a smaller value of overlap. Note that a large value of negative α means a "fat" or "beer-barrel" type structure, whereas larger values of positive α give an "hourglass" type of structure. It can be shown that a fat or beer-barrel type structure has greater compressive stiffness than an hourglass type structure. Therefore, a tensegrity beam made of larger values of negative α can be expected to have greater compressive strength.

Figure 17.45(d) shows that for any value of δ, the maximum values of positive or negative α are governed by overlap. The maximum value of positive α is limited by the overlap becoming 0% of the stage height, whereas the maximum value of negative α is limited by the overlap becoming 100% of the stage height. A larger value of negative α is expected to give greater vertical stiffness. Figure 17.45(d) shows that large negative α is possible when δ is small. However, as seen in Figure 17.45(d), there is a limit to the maximum value of negative α and to the minimum δ that would satisfy the existence conditions of the two-stage 3-bar SVD-type tensegrity. To understand this limit of the values of α and δ, the distribution of the internal pretensioning forces in each of the members is plotted as a function of α and δ, and shown in Figures 17.46 and 17.47.

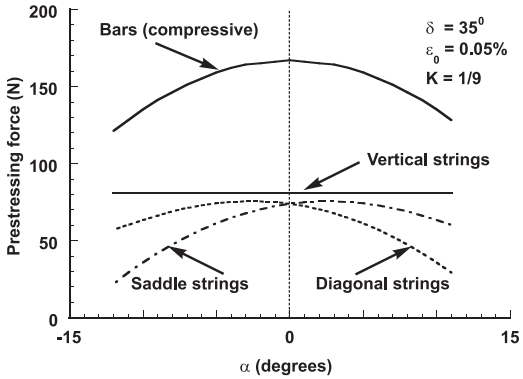

FIGURE 17.46 Prestressing force in the members as a function of α.

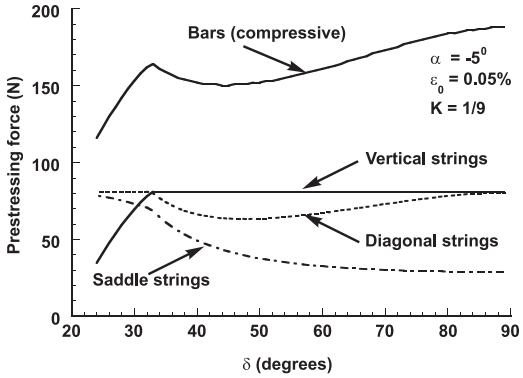

FIGURE 17.47 Prestressing force in the members as a function of δ.

Figure 17.46 shows the member forces as a function of α with δ= 35°, whereas Figure 17.47 shows the member forces as a function of δ with α= –5°. Both of the figures are obtained for K = 1/9, and the prestressing force in the strings is equal to the force due to a maximum prestrain in the strings ε_0 = 0.05% applied to the string which experiences maximum prestressing force. It is seen in both of the figures that for large negative α, the prestressing force in the saddle strings and the diagonal strings decreases with an increase in the negative α. Finally, for α below certain values, the prestressing forces in the saddle and diagonal strings become small enough to violate the definition of existence of tensegrity (i.e., all strings in tension and all bars in compression).

A similar trend is noted in the case of the vertical strings also. As seen in Figure 17.47, the force in the vertical strings decreases with a decrease in δ for small δ. Finally, for δ below certain values, the prestressing forces in the vertical strings become small enough to violate the definition of the existence of tensegrity. This explains the lower limits of the angles α and δ satisfying the tensegrity conditions.

Figures 17.46 and 17.47 show very remarkable changes in the load-sharing mechanism between the members with an increase in positive α and with an increase in δ. It is seen in Figure 17.46 that as α is gradually changed from a negative value toward a positive one, the prestressing force in the saddle strings increases, whereas the prestressing force in the vertical strings decreases. These trends continue up to α= 0°, when the prestressing force in both the diagonal strings and the saddle strings is equal and that in the vertical strings is small. For α < 0°, the force in the diagonal strings is always greater than that in the saddle strings. However, for α > 0°, the force in the diagonal strings decreases and is always less than the force in the saddle strings. The force in the vertical strings is the greatest of all strings.

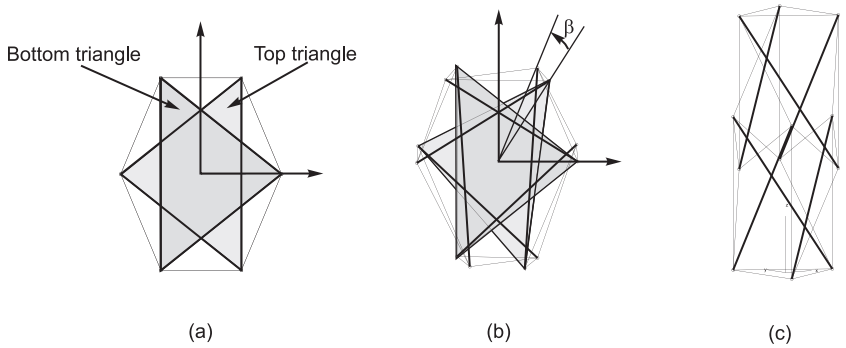

FIGURE 17.48 Rotation of the top triangle with respect to the bottom triangle for a two-stage cylindrical hexagonal 3-bar SVD tensegrity. (a) Top view when $\beta = 0$, (b) top view with β, and (c) elevation.

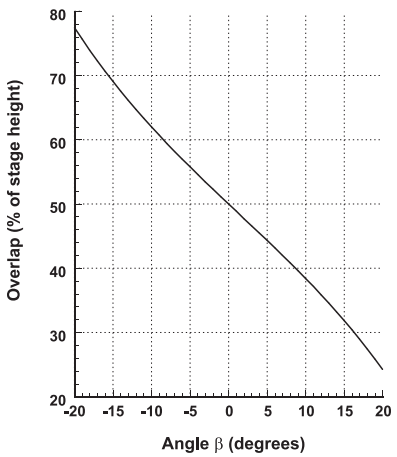

FIGURE 17.49 Existence conditions for a cylindrical two-stage 3-bars SVD tensegrity with respect to the rotation angle of the top triangle (anticlockwise β is positive).

Figure 17.45 showing all the possible configurations of a two-stage tensegrity can be quite useful in designing a deployable tensegrity beam made of many stages. The deployment of a beam with many stages can be achieved by deploying two stages at a time.

The existence conditions for a regular hexagonal cylinder (beam) made of two stages for which one of the end triangles is assumed to be rotated by an angle β about its mean position, as shown in Figure 17.48, is studied next. The mean position of the triangle is defined as the configuration when $\beta = 0$ and all of the nodal points of the bars line up in a straight line to form a regular hexagon, as shown in Figure 17.48. As is seen in Figure 17.49, it is possible to rotate the top triangle merely by satisfying the equilibrium conditions for the two-stage tensegrity. It is also seen that the top triangle can be rotated merely by changing the overlap between the two stages. This information can be quite useful in designing a Stewart platform-type structure.

17.4.3 Load-Deflection Curves and Axial Stiffness as a Function of the Geometrical Parameters

The load deflection characteristics of a two-stage 3-bar SVD-type tensegrity are studied next and the corresponding stiffness properties are investigated.

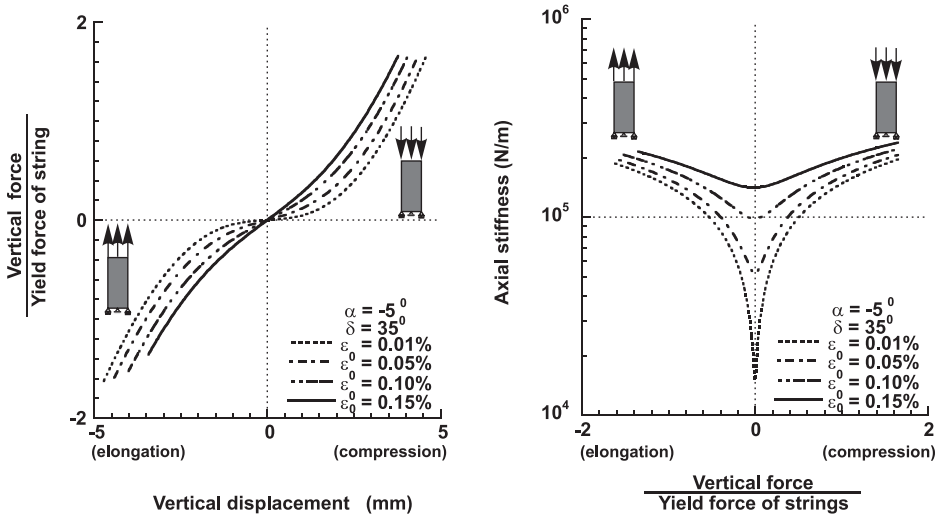

FIGURE 17.50 Load deflection curve and axial stiffness of a two-stage 3-bar SVD tensegrity subjected to axial loading.

Figure 17.50 depicts the load-deflection curves and the axial stiffness as functions of prestress, drawn for the case of a two-stage 3-bar SVD-type tensegrity subjected to axial loading. The axial stiffness is defined as the external force acting on the structure divided by the axial deformation of the structure. In another words, the stiffness considered here is the "secant stiffness."

Figure 17.50 shows that the tensegrity under axial loading behaves like a nonlinear spring and the nonlinear properties depend much on the prestress. The nonlinearity is more prominent when prestress is low and when the displacements are small. It is seen that the axial stiffnesses computed for both compressive and tensile loadings almost equal to each other for this particular case of a two-stage 3-bar SVD-type tensegrity. It is also seen that the axial stiffness is affected greatly by the prestress when the external forces are small (i.e., when the displacements are small), and prestress has an important role in increasing the stiffness of the tensegrity in the region of a small external load. However, as the external forces increase, the effect of the prestress becomes negligible.

The characteristics of the axial stiffness of the tensegrity as a function of the geometrical parameters (i.e., α, δ) are next plotted in Figure 17.51. The effect of the prestress on the axial stiffness is also shown in Figure 17.51. In obtaining the Figure 17.51, vertical loads were applied at the top nodes of the two-stage tensegrity. The load was gradually increased until at least one of the strings exceeded its elastic limit. As the compressive stiffness and the tensile stiffness were observed to be nearly equal to each other in the present example, only the compressive stiffness as a function of the geometrical parameters is plotted in Figure 17.51. The change in the shape of the tensegrity structure from a fat profile to an hourglass-like profile with the change in α is also shown in Figure 17.51(b).

The following conclusions can be drawn from Figure 17.51:

1. Figure 17.52(a) suggests that the axial stiffness increases with a decrease in the angle of declination δ (measured from the vertical axis).
2. Figure 17.51(b) suggests that the axial stiffness increases with an increase in the negative angle α. Negative α means a fat or beer-barrel-type structure whereas a positive α means an hourglass-type structure, as shown in Figure 17.51(b). Thus, a fat tensegrity performs better than an hourglass-type tensegrity subjected to compressive loading.
3. Figure 17.51(c) suggests that prestress has an important role in increasing the stiffness of the tensegrity in the region of small external loading. However, as the external forces are increased, the effect of the prestress becomes almost negligible.

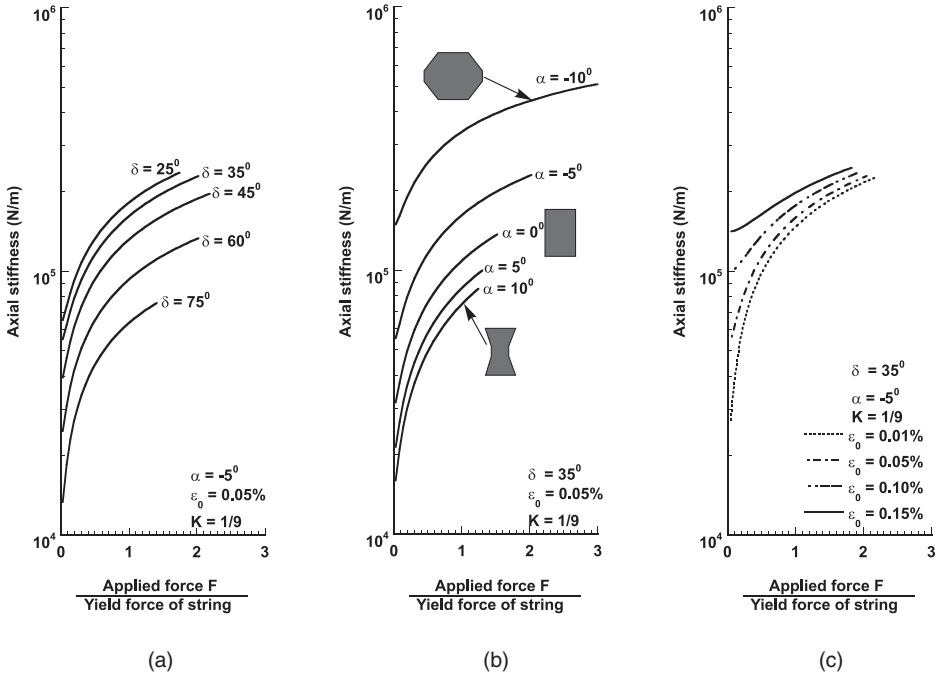

FIGURE 17.51 Axial stiffness of a two-stage 3-bar SVD tensegrity for different α, δ, and pretension.

17.4.4 Load-Deflection Curves and Bending Stiffness as a Function of the Geometrical Parameters

The bending characteristics of the two-stage 3-bar SVD tensegrity are presented in this section. The force is applied along the x-direction and then along the y-direction, as shown in Figure 17.52. The force is gradually applied until at least one of the strings exceeds its elastic limit.

The load deflection curves for the load applied in the lateral are plotted in Figure 17.52 as a function of the prestress. It was observed that as the load is gradually increased, one of the vertical strings goes slack and takes no load. Therefore, two distinct regions can be clearly identified in Figure 17.52. The first region is the one where none of the strings is slack, whereas the second region, marked by the sudden change in the slope of the load deflection curves, is the one in which at least one string is slack. It is seen in Figure 17.52 that in contrast to the response of the tensegrity subjected to the vertical axial loading, the bending response of the tensegrity is almost linear in the region of tensegrity without slack strings, whereas it is slightly nonlinear in the region of tensegrity with slack strings. The nonlinearity depends on the prestressing force. It is observed that the prestress plays an important role in delaying the onset of the slack strings.

The characteristics of the bending stiffness of the tensegrity as a function of the geometrical parameters (i.e., α, δ) are plotted next in Figures 17.53 and 17.54. Figure 17.53 is plotted for lateral force applied in the x-direction, whereas Figure 17.54 is plotted for lateral force applied in the y-direction. The effect of the prestress on the bending stiffness is also shown in Figures 17.53 and 17.54. The following conclusions about the bending characteristics of the two-stage 3-bar tensegrity could be drawn from Figures 17.53 and 17.54:

1. It is seen that the bending stiffness of the tensegrity with no slack strings is almost equal in both the x- and y-directions. However, the bending stiffness of the tensegrity with slack string is greater along the y-direction than along the x-direction.
2. The bending stiffness of a tensegrity is constant and is maximum for any given values of α, δ, and prestress when none of the strings are slack. However, as soon as at least one string goes

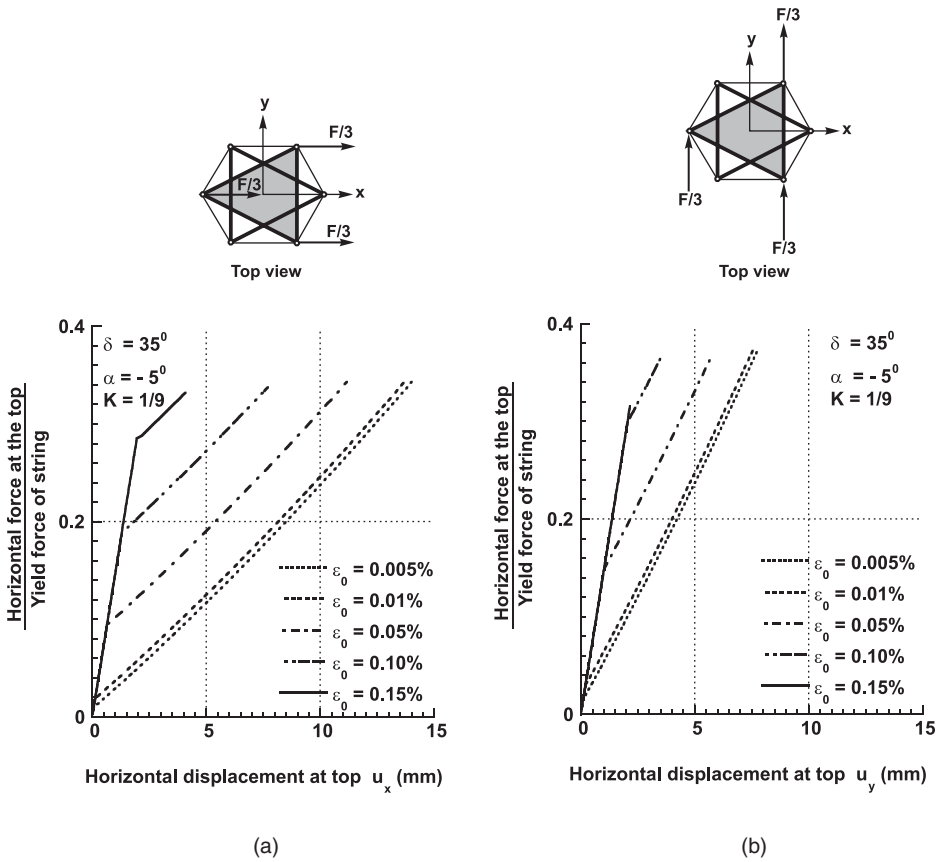

FIGURE 17.52 Load deflection curve of a two-stage 3-bar SVD tensegrity subjected to lateral loading, (a) loading along x-direction, and (b) loading along y-direction.

slack (marked by sudden drop in the stiffness curves in Figures 17.53 and 17.54), the stiffness becomes a nonlinear function of the external loading and decreases monotonically with the increase in the external loading. As seen in Figures 17.53 and 17.54, the onset of strings becoming slack, and hence the range of constant bending stiffness, is a function of α, δ, and prestress.

3. Figures 17.53(a) and 17.54(a) suggest that the bending stiffness of a tensegrity with no slack strings increases with the increase in the angle of declination δ (measured from the vertical axis). The bending stiffness of a tensegrity with a slack string, in general, increases with increase in δ. However, as seen in Figure 17.53(a), a certain δ exists beyond which the bending stiffness of a tensegrity with slack string decreases with an increase in δ. Hence, tensegrity structures have an optimal internal geometry with respect to the bending stiffness and other mechanical properties.
4. Figures 17.53(b) and 17.54(b) suggest that the bending stiffness increases with the increase in the negative angle α. As negative α means a fat or beer-barrel-type structure whereas a positive α means an hourglass-type structure, a fat tensegrity performs better than an hourglass-type tensegrity subjected to lateral loading.
5. Figures 17.53(a,b) and 17.54(a,b) indicate that both α and δ play a very interesting and important role in not only affecting the magnitude of stiffness, but also the onset of slackening of the strings (robustness to external disturbances). A large value of negative α and a large value of δ (in general) delay the onset of slackening of the strings, thereby increasing the range of constant bending stiffness. However, a certain δ exists for which the onset of the slack strings is maximum.

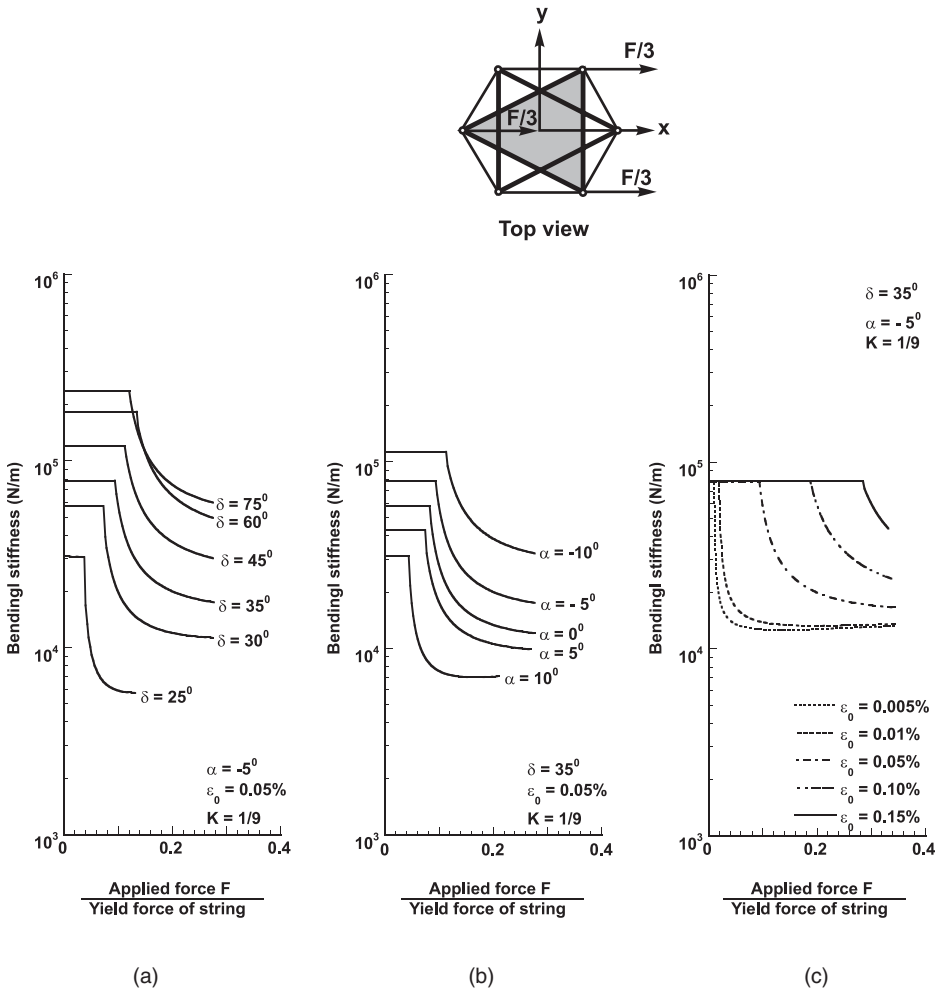

FIGURE 17.53 Bending stiffness of a two-stage 3-bar SVD tensegrity for different α, δ, and pretension. L-bar for all cases = 0.4 in.

6. Figures 17.53(c) and 17.54(c) suggest that prestress does not affect the bending stiffness of a tensegrity with no slack strings. However, prestress has an important role in delaying the onset of slack strings and thus increasing the range of constant bending stiffness.

17.4.5 Summary of 3-Bar SVD Tensegrity Properties

The following conclusions could be drawn from the present study on the statics of a two-stage 3-bar SVD-type tensegrities.

1. The tensegrity structure exhibits unique equilibrium characteristics. The self-stressed equilibrium condition exists only on a small subset of geometrical parameter values. This condition guarantees that the tensegrity is prestressable and that none of the strings is slack.
2. The stiffness (the axial and the bending) is a function of the geometrical parameters, the prestress, and the externally applied load. However, the effect of the geometrical parameters on the stiffness is greater than the effect of the prestress. The external force, on the other hand, does not affect the bending stiffness of a tensegrity with no slack strings, whereas it does affect the axial stiffness. The axial stiffness shows a greater nonlinear behavior even

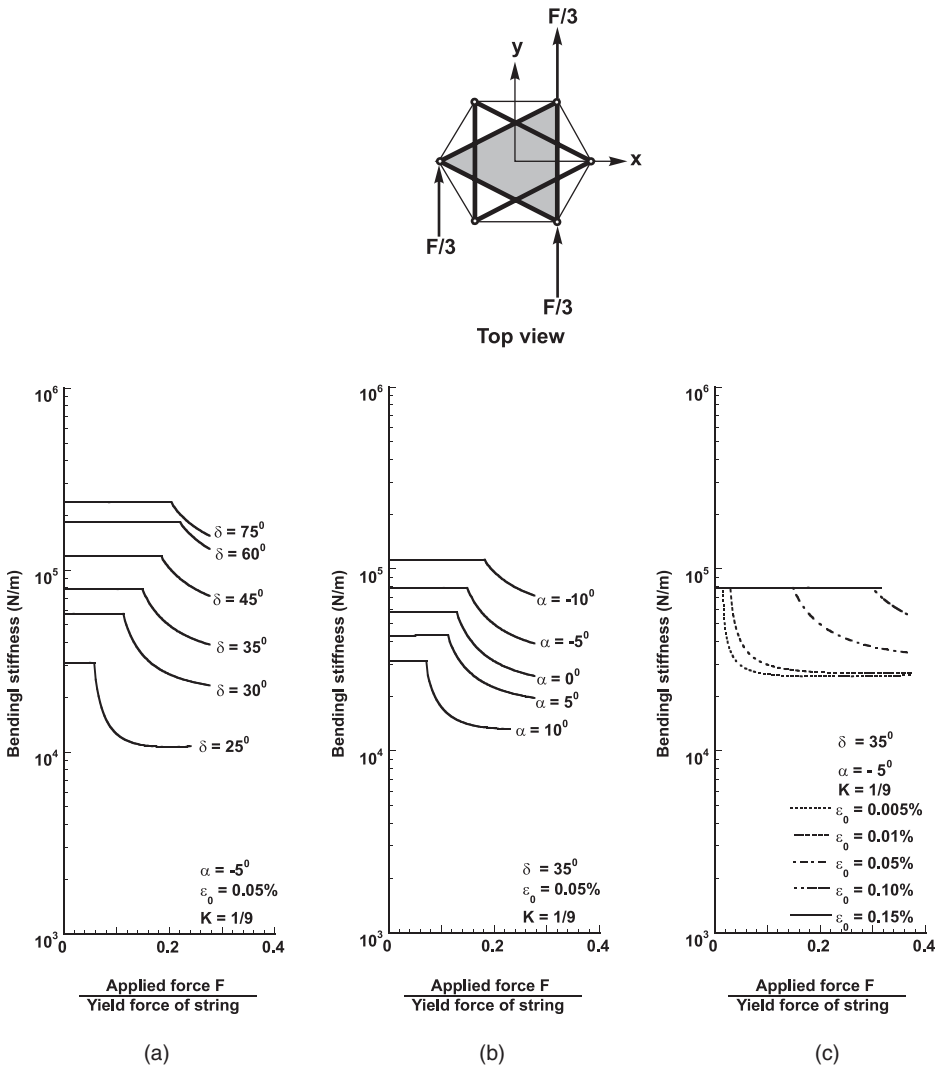

FIGURE 17.54 Bending stiffness of a two-stage 3-bar SVD tensegrity for different α, δ, and pretension.

up to the point when none of the strings are slack. The axial stiffness increases with an increase in the external loading, whereas the bending stiffness remains constant until at least one of the strings go slack, after which the bending stiffness decreases with an increase in the external loading.

3. Both the axial and the bending stiffness increase by making α more negative. That is, both the axial and the bending stiffness are higher for a beer-barrel-type tensegrity. The stiffness is small for an hourglass-type tensegrity.
4. The axial stiffness increases with a decrease in the vertical angle, whereas the bending stiffness increases with an increase in the vertical angle. This implies that the less the angle that the bars make with the line of action of the external force, the stiffer is the tensegrity.
5. Both the geometrical parameters α and δ, and prestress play an important role in delaying the onset of slack strings. A more negative α, a more positive δ, and prestress, all delay the onset of slack strings, as more external forces are applied. Thus, both α and δ also work as a hidden prestress. However, there lies a δ beyond which an increase in δ hastens the onset of slack strings, as more external force is applied.

17.5 Concluding Remarks

Tensegrity structures present a remarkable blend of geometry and mechanics. Out of various available combinations of geometrical parameters, only a small subset exists that guarantees the existence of the tensegrity. The choice of these parameters dictates the mechanical properties of the structure. The choice of the geometrical parameters has a great influence on the stiffness. Pretension serves the important role of maintaining stiffness until a string goes slack. The geometrical parameters not only affect the magnitude of the stiffness either with or without slack strings, but also affect the onset of slack strings. We now list the major findings of this chapter.

17.5.1 Pretension vs. Stiffness Principle

This principle states that increased pretension increases robustness to uncertain disturbances. More precisely, for all situations we have seen (except for the $C4T2$):

When a load is applied to a tensegrity structure, the stiffness does not decrease as the loading force increases unless a string goes slack.

The effect of the pretension on the stiffness of a tensegrity without slack strings is almost negligible. The bending stiffness of a tensegrity without slack strings is not affected appreciably by prestress.

17.5.2 Small Control Energy Principle

The second principle is that the shape of the structure can be changed with very little control energy. This is because shape changes are achieved by changing the equilibrium of the structure. In this case, control energy is not required to hold the new shape. This is in contrast to the control of classical structures, where shape changes required control energy to work against the old equilibrium.

17.5.3 Mass vs. Strength

This chapter also considered the issue of strength vs. mass of tensegrity structures. We found planar examples to be very informative. We considered two types of strength: the size of bending forces and the size of compressive forces required to break the object. We studied the ratio of bending strength to mass and compression strength to mass. We compared this for two planar structures, one the $C2T4$ unit and the other a $C4T1$ unit, to a solid rectangular bar of the same mass.

We find:

- Reasonably constructed $C2T4$ units are stronger in bending than a rectangular bar, but they are weaker under compression.
- The $C2T4$ has worse strength under compression than a solid rectangular bar.
- The simple analysis we did indicates that $C4T2$ and $C4T1$ structures with reasonably chosen proportions have larger compression strength-to-mass ratios than a solid bar.
- On the other hand, a $C4T1$, while strong (not easily broken), need not be an extremely stiff structure.
- $C4T2$ and $C4T1$ structures can be designed for minimal mass subjected to a constraint on both strength and stiffness.

It is possible to amplify the effects stated above by the use of self-similar constructions:

- **A 2D Tensegrity Beam.** After analyzing a $C2T4$ tensegrity unit, we lay n of them side by side to form a beam. In principle, we find that one can build beams with arbitrarily great bending strength. In practice, this requires more study. However, the favorable bending properties found for $C2T4$ bode well for tensegrity beams.

- **A 2D Tensegrity Column.** We take the *C*4*T*2 structure and replace each bar with a smaller *C*4*T*1 structure, then we replace each bar of this new structure by a yet smaller *C*4*T*1 structure. In principle, such a self-similar construction can be repeated to any level. Assuming that the strings do not fail and have significantly less mass than the bars, we find that we have a class of tensegrity structures with unlimited compression strength-to-mass ratio. Further issues of robustness to lateral and bending forces have to be investigated to ensure practicality of such structures.

The total mass including string and bars (while preserving strength) can be minimized by a finite numer of self-similar iterations, and the number of iterations to achieve minimal mass is usually quite small (less that 10). This provides an optimization of tensegrity structures that is analytically resolved and is much easier and less complex than optimization of classical structures. We emphasize that the implications of overlapping of the bars were not seriously studied.

For a special range of geometry, the stiffness-to-mass ratio increases with self-similar iterations. For the remaining range of geometry the stiffness-to-mass ratio decreases with self-similar iterations. For a very specific choice of geometry, the stiffness-to-mass ratio remains constant with self-similar iterations.

Self-similar steps can preserve strength while reducing mass, but cannot preserve stiffness while reducing mass. Hence, a desired stiffness bound and reconciliation of overlapping bars will dictate the optimal number of iterations.

17.5.4 A Challenge for the Future

In the future, the grand challenge with tensegrity structures is to find ways to choose material and geometry so that the thermal, electrical, and mechanical properties are specified. The tensegrity structure paradigm is very promising for the integration of these disciplines with control, where either strings or bars can be controlled.

Acknowledgment

This work received major support from a DARPA grant monitored by Leo Christodoulou. We are also grateful for support from DARPA, AFOSR, NSF, ONR, and the Ford Motor Company.

Appendix 17.A Nonlinear Analysis of Planar Tensegrity

17.A.1 Equations of Static Equilibrium

17.A.1.1 Static Equilibrium under External Forces

A planar tensegrity under external forces is shown in Figure 17.A.1, where F_i are the external forces and t_i represent the internal forces in the members of the tensegrity units. Note that **t** represents the net force in the members which includes the pretension and the force induced by the external forces. The sign convention adopted herein is also shown in Figure 17.A.1, where t_{ki} represents the member force t acting at the i-th node of the member k. We assume that $i < j$ and $t_{ki} = -t_{kj}$. With this convention, we write the force equilibrium equations for the planar tensegrity.

The equilibrium of forces in the x-direction acting on the joints yields the following equations

$$\begin{aligned} t_{1i}\cos\delta_{x1} + t_{4i}\cos\delta_{x4} + t_{6i}\cos\delta_{x6} &= F_1, \\ t_{1j}\cos\delta_{x1} + t_{2i}\cos\delta_{x2} + t_{5i}\cos\delta_{x5} &= -F_2, \\ t_{2i}\cos\delta_{x2} + t_{3i}\cos\delta_{x3} + t_{6j}\cos\delta_{x6} &= -F_3, \\ t_{3j}\cos\delta_{x3} + t_{4j}\cos\delta_{x4} + t_{5j}\cos\delta_{x5} &= F_4. \end{aligned} \tag{17.A.1}$$

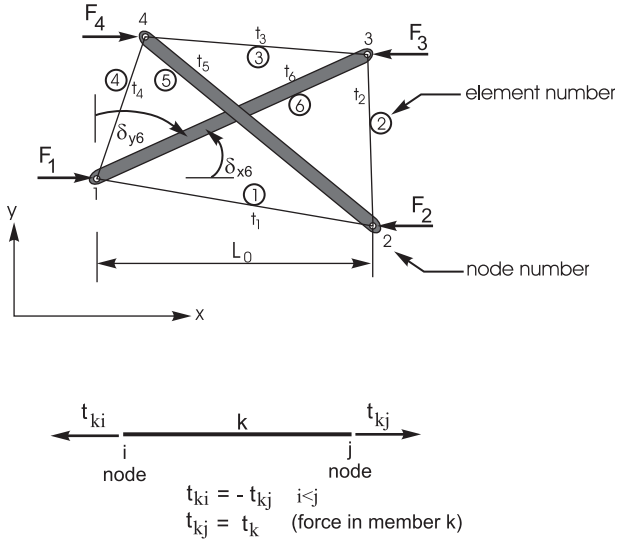

FIGURE 17.A.1 Forces acting on a planar tensegrity and the sign convention used.

Similarly, the equilibrium of forces in the y-direction acting on the joints yields the following equations

$$\begin{aligned} t_{1i}\cos\delta_{y1} + t_{4i}\cos\delta_{y4} + t_{6i}\cos\delta_{y6} &= 0,\\ t_{1j}\cos\delta_{y1} + t_{2i}\cos\delta_{y2} + t_{5i}\cos\delta_{y5} &= 0,\\ t_{2i}\cos\delta_{y2} + t_{3i}\cos\delta_{y3} + t_{6j}\cos\delta_{y6} &= 0,\\ t_{3j}\cos\delta_{y3} + t_{4j}\cos\delta_{y4} + t_{5j}\cos\delta_{y5} &= 0. \end{aligned} \tag{17.A.2}$$

In the above equations, $\cos\delta_{xk}$ represents the direction cosine of member k taken from the x-axis, whereas $\cos\delta_{yk}$ represents the direction cosine of member k taken from the y-axis.

The above equations can be rearranged in the following matrix form:

$$\mathbf{At} = \mathbf{f}, \tag{17.A.3}$$

where $\mathbf{t}$ is a vector of forces in the members and is given by $\mathbf{t}^T = [t_1\ t_2\ t_3\ t_4\ t_5\ t_6]$, matrix $\mathbf{A}$ (of size 8×6) is the equilibrium matrix, and $\mathbf{f}$ is a vector of nodal forces. For convenience, we arrange $\mathbf{t}$ such that the forces in the bars appear at the top of the vector, i.e.,

$$\mathbf{t}^T = [\mathbf{t}_{bars}\ \mathbf{t}_{strings}] = [t_5\ t_6\ t_1\ t_2\ t_3\ t_4]. \tag{17.A.4}$$

Matrix $\mathbf{A}$ and vector $\mathbf{f}$ are given by

$$\mathbf{A} = \begin{bmatrix} \mathbf{C}^T & \vdots & \mathbf{0} \\ \cdots & \cdots & \cdots \\ \mathbf{0} & \vdots & \mathbf{C}^T \end{bmatrix} \begin{bmatrix} \mathbf{H}_x \\ \cdots \\ \mathbf{H}_y \end{bmatrix}, \quad \mathbf{f} = \begin{Bmatrix} \mathbf{f}_x \\ \cdots \\ \mathbf{f}_y \end{Bmatrix}. \tag{17.A.5}$$

In the above equation, matrices $\mathbf{H}_x$ and $\mathbf{H}_y$ are diagonal matrices containing the direction cosines of each member taken from the x-axis or y-axis, respectively, i.e., $H_{xii} = \cos\delta_{xi}$ and $H_{yii} = \cos\delta_{yi}$.

Similar to the arrangement of $\mathbf{t}$, $\mathbf{H}_x$ and $\mathbf{H}_y$ are also arranged such that the direction cosines of bars appear at the top of $\mathbf{H}_x$ and $\mathbf{H}_y$ whereas the direction cosines of strings appear at the bottom of $\mathbf{H}_x$ and $\mathbf{H}_y$. Vectors $\mathbf{f}_x$ and $\mathbf{f}_y$ are the nodal forces acting on the nodes along x- and y-axes, respectively. Matrix $\mathbf{C}$ is a 6×4 (number of members $\times$ number of nodes) matrix. The k-th row of matrix $\mathbf{C}$ contains -1 (for i-th node of the k-th member), $+1$ (for j-th node of the k-th member) and 0. Matrix $\mathbf{C}$ for the present case is given as

$$\mathbf{C} = \begin{bmatrix} 0 & -1 & 0 & 1 \\ -1 & 0 & 1 & 0 \\ -1 & 1 & 0 & 0 \\ 0 & -1 & 1 & 0 \\ 0 & 0 & -1 & 1 \\ -1 & 0 & 0 & 1 \end{bmatrix} \begin{matrix} \left.\vphantom{\begin{matrix}0\\0\end{matrix}}\right\} \text{Bars} \\ \left.\vphantom{\begin{matrix}0\\0\\0\\0\end{matrix}}\right\} \text{Strings} \end{matrix} \tag{17.A.6}$$

It should be noted here that matrix $\mathbf{A}$ is a nonlinear function of the geometry of the tensegrity unit, the nonlinearity being induced by the matrices $\mathbf{H}_x$ and $\mathbf{H}_y$ containing the direction cosines of the members.

17.A.2 Solution of the Nonlinear Equation of Static Equilibrium

Because the equilibrium equation given in (17.A.3) is nonlinear and also $\mathbf{A}$ (of size 8×6) is not a square matrix, we solve the problem in the following way.

Let $\tilde{\mathbf{t}}$ be the member forces induced by the external force $\mathbf{f}$, then from (17.A.3)

$$\begin{aligned} &\mathbf{A}\mathbf{t} = \mathbf{f} \\ \Rightarrow\ &\mathbf{A}(\mathbf{t}_0 + \tilde{\mathbf{t}}) = \mathbf{f} \\ \Rightarrow\ &\mathbf{A}\tilde{\mathbf{t}} = \mathbf{f} - \mathbf{A}\mathbf{t}_0 \\ \Rightarrow\ &\mathbf{A}\mathbf{K}\mathbf{e} = \mathbf{f} - \mathbf{A}\mathbf{t}_0 \end{aligned} \tag{17.A.7}$$

where $\mathbf{e}$ is the deformation from the initial prestressed condition of each member, and from Hooke's law $\tilde{\mathbf{t}} = \mathbf{K}\mathbf{e}$, where $\mathbf{K}$ is a diagonal matrix of size 6×6, with $K_{ii} = (EA)_i/L_i$. $(EA)_i$ and L_i are the axial rigidity and the length of the i-th member. Note that $\mathbf{A}$ expressed above is composed of both the original $\mathbf{A}_0$ and the change in $\mathbf{A}_0$ caused by the external forces $\mathbf{f}$.

$$\mathbf{A} = \mathbf{A}_0 + \tilde{\mathbf{A}} \tag{17.A.8}$$

where $\tilde{\mathbf{A}}$ is the change in $\mathbf{A}_0$ caused by the external forces $\mathbf{f}$.

The nonlinear equation given above can be linearized in the neighborhood of an equilibrium. In the neighborhood of the equilibrium, we have the linearized relationship,

$$\mathbf{e}_k = \mathbf{A}_k^T \mathbf{u}_k \tag{17.A.9}$$

Let the external force $\mathbf{f}$ be gradually increased in small increments ($\mathbf{f}_k = \mathbf{f}_{k-1} + \Delta\mathbf{f}$ at the k-th step), and the equilibrium of the planar tensegrity be satisfied for each incremental force, then (17.A.7) can be written as

$$\mathbf{A}(\mathbf{u}_k)\mathbf{K}\mathbf{A}\ (\mathbf{u}_k)^T\ \mathbf{u}_k = \mathbf{f}_k - \mathbf{A}(\mathbf{u}_k)\mathbf{t}_0 \tag{17.A.10}$$

The standard Newton–Raphson method can now be used to evaluate $\mathbf{u}_k$ of (17.A.10) for each incremental load step $\Delta\mathbf{f}_k$. The external force is gradually applied until it reaches its specific value

and $\mathbf{u}_k$ is evaluated at every load step. Matrix $\mathbf{A}$, which is now a nonlinear function of $\mathbf{u}$, is updated during each load step.

To compute the external force that would be required to buckle the bars in the tensegrity unit, we must estimate the force being transferred to the bars. The estimation of the compressive force in the bars following full nonlinear analysis can be done numerically. However, in the following we seek to find an analytical expression for the compressive force in the bars. For this we adopt a linear and small displacement theory. Thus, the results that follow are valid only for small displacement and small deformation.

Appendix 17.B Linear Analysis of Planar Tensegrity

17.B.1 EI of the Tensegrity Unit with Slack Top String

17.B.1.1 Forces in the Members

A tensegrity with a slack top string does not have prestress. As mentioned earlier, we adopt the small displacement assumptions, which imply that the change in the angle δ due to the external forces is negligible. Therefore, in the following, we assume that δ remains constant. The member forces in this case are obtained as

$$\begin{aligned} t_1 &= 2F, \\ t_2 &= F\tan\delta, \\ t_3 &= 0, \\ t_4 &= F\tan\delta, \\ t_5 &= -\frac{F}{\cos\delta}, \\ t_6 &= -\frac{F}{\cos\delta}. \end{aligned} \tag{17.B.1}$$

The strain energy in each of the members is computed as

$$\begin{aligned} U_1 &= \frac{1}{2}\frac{4L_0F^2}{(EA)_s}, \\ U_2 &= \frac{1}{2}\frac{L_0F^2\tan^3\delta}{(EA)_s}, \\ U_3 &= 0, \\ U_4 &= \frac{1}{2}\frac{L_0F^2\tan^3\delta}{(EA)_s}, \\ U_5 &= \frac{1}{2}\frac{L_0F^2}{(EA)_b\cos^3\delta}, \\ U_6 &= \frac{1}{2}\frac{L_0F^2}{(EA)_b\cos^3\delta}. \end{aligned} \tag{17.B.2}$$

The total strain energy is then obtained as

$$U = \sum_i U_i = \frac{1}{2}\frac{L_0}{(EA)_s}\frac{2F^2}{\cos^3\delta}[\sin^3\delta + 2\cos^3\delta + K], \tag{17.B.3}$$

where K is defined as

$$K = \frac{(EA)_s}{(EA)_b}. \tag{17.B.4}$$

Thus, large values of K mean that the strings are stiffer than the bars, whereas small values of K mean that the bars are stiffer than the strings. $K \to 0$ means bars are rigid.

17.B.1.2 External Work and Displacement

External work W is given by

$$W = 4\frac{1}{2}Fu = 2Fu, \tag{17.B.5}$$

where u is the displacement as shown in Figure 17.11.

Equating the total strain energy given by (17.B.3) to the work done by the external forces given by (17.B.5), and then solving for u yields

$$u = \frac{FL_0}{2(EA)_s \cos^3\delta}[\sin^3\delta + 2\cos^3\delta + K]. \tag{17.B.6}$$

17.B.1.3 Effective EI

Because $EI = M\rho$, we have

$$EI = FL_0 \tan\delta\left(\frac{L_0}{2}\right)^2 \tan\delta\frac{1}{u}. \tag{17.B.7}$$

Substitution of $\tilde{u}$ from (17.B.6) into (17.B.7) yields

$$EI = \frac{1}{2}\frac{L_0^2(EA)_s \sin^2\delta\cos\delta}{(\sin^3\delta + 2\cos^3\delta + K)}. \tag{17.B.8}$$

Substituting $L_0 = L_{bar}\cos\delta$ in (17.B.7) and (17.B.8) yields the following expressions for the equivalent bending rigidity of the planar section in terms of the length of the bars L_{bar},

$$EI = FL_{bar}\sin\delta\left(\frac{L_{bar}}{2}\right)^2 \cos\delta\sin\delta\frac{1}{u}. \tag{17.B.9}$$

or equivalently,

$$EI = \frac{1}{2}\frac{{L_{bar}}^2(EA)_s \sin^2\delta\cos^3\delta}{(\sin^3\delta + 2\cos^3\delta + K)}. \tag{17.B.10}$$

Appendix 17.C Derivation of Stiffness of the $C4T1^i$ Structure

17.C.1 Derivation of Stiffness Equation

For a $C4T1^i$ structure under the buckling load F, the compressive load of bar in the i-th iteration is

$$F_i = \frac{F}{\prod_{j=1}^{i} 2\cos\delta_j}. \tag{17.C.1}$$

Similarly, the tension of strings in the i-th iteration is

$$t_j = \frac{2F\sin\delta_j}{\prod_{s=1}^{j} 2\cos\delta_s} \text{ for } j = 1,2,3,...,i-1,i. \tag{17.C.2}$$

So, the buckling load F can be written in terms of any one of the compressive bar loads or tension of strings in i-th iteration

$$F = F_i \prod_{s=1}^{i} 2\cos\delta_s = \frac{t_j}{2\sin\delta_j} \prod_{p=1}^{j} 2\cos\delta_p \quad \text{for } j = 1,2,3,...,i-1,i. \tag{17.C.3}$$

From the geometry of the structure,

$$\begin{aligned} \sin\delta_j &= \frac{L_{tj}}{2L_j}, \\ \cos\delta_j &= \frac{L_{j-1}}{2L_j}. \end{aligned} \tag{17.C.4}$$

Equation (17.C.3) can be simplified to

$$F = F_i \frac{L_0}{L_i} = t_j \frac{L_0}{L_{tj}}. \tag{17.C.5}$$

From this,

$$\frac{F}{L_0} = \frac{F_i}{L_i} = \frac{t_j}{L_{tj}} = \frac{t_1}{L_{t1}}. \tag{17.C.6}$$

This means the force-to-length ratio of every compressive or tensile members is the same. It is assumed that all the bars and strings have constant stiffness and, hence, are linear. With this assumption,

$$\begin{aligned} F_i &= k_{bi}(L_{i0} - L_i), \\ t_j &= k_{tj}(L_{tj} - L_{tj0}). \end{aligned} \tag{17.C.7}$$

So (17.C.6) becomes

$$k_{bi}\left(\frac{L_{i0}}{L_i} - 1\right) = k_{tj}\left(1 - \frac{L_{tj0}}{L_{tj}}\right) = k_{t1}\left(1 - \frac{L_{t10}}{L_{t1}}\right). \tag{17.C.8}$$

Taking the infinitesimal of all the length quantities yields

$$-k_{bi}\frac{L_{i0}}{L_i^2}dL_i = k_{tj}\frac{L_{tj0}}{L_{tj}^2}dL_{tj} = k_{t1}\frac{L_{t10}}{L_{t1}^2}dL_{t1},$$

and hence,

$$\begin{aligned} dL_i &= -\frac{k_{t1}L_{t10}}{k_{bi}L_{i0}}\frac{L_i^2}{L_{t1}^2}dL_{t1}, \\ dL_{tj} &= \frac{k_{t1}L_{t10}}{k_{tj}L_{tj0}}\frac{L_{tj}^2}{L_{t1}^2}dL_{t1}. \end{aligned} \tag{17.C.9}$$

From the geometry of the structure,

$$\begin{aligned} L_0^2 &= 4L_1^2 - L_{t1}^2 \\ &= 4(4L_2^2 - L_{t2}^2) - L_{t1}^2 \\ &= \ldots \\ &= 4^i L_i^2 - \sum\nolimits_{j=1}^{i} 4^{j-1}L_{tj}^2. \end{aligned} \tag{17.C.10}$$

Taking the infinitesimal of (17.C.10), noting that L_i is length of bars, yields

$$dL_0 = 4^i\frac{L_i}{L_0}dL_i - \frac{1}{L_0}\sum_{j=1}^{i}4^{j-1}L_{tj}dL_{tj}. \tag{17.C.11}$$

Combining the (17.C.11) with (17.C.9) yields

$$\frac{dL_0}{dL_{t1}} = \frac{k_{t1}L_{t10}}{L_0L_{t1}^2}\left(4^i\frac{L_i^3}{k_{bi}L_{i0}} + \sum_{j=1}^{i}4^{j-1}\frac{L_{tj}^3}{k_{tj}L_{tj0}}\right). \tag{17.C.12}$$

From (17.C.5), it is natural to choose F in terms of the tension in the first iteration, i.e.,

$$F = t_1\frac{L_0}{L_{t1}} = k_{t1}\left(1 - \frac{L_{t10}}{L_{t1}}\right)L_0.$$

The derivative of F w.r.t. L_0 yields

$$\frac{dF}{dL_0} = k_{t1}\left(1 - \frac{L_{t10}}{L_{t1}}\right) + k_{t1}L_0\frac{L_{t10}}{L_{t1}^2}\frac{dL_{t1}}{dL_0}. \tag{17.C.13}$$

With (17.C.12), the stiffness of $C4T1^i$ will be

$$\begin{aligned} K_i &= -\frac{dF}{dL_0} = k_{t1}\left(\frac{L_{t10}}{L_{t1}} - 1\right) + L_0^2\left(4^i\frac{L_i^3}{k_{bi}L_{i0}} + \sum_{j=1}^{i}4^{j-1}\frac{L_{tj}^3}{k_{tj}L_{tj0}}\right)^{-1} \\ &= k_{t1}\left\{\left(\frac{L_{t10}}{L_{t1}} - 1\right) + \left[4^i\frac{k_{t1}}{k_{bi}}\frac{L_i}{L_{i0}}\left(\frac{L_i}{L_0}\right)^2 + \sum_{j=1}^{i}4^{j-1}\frac{k_{t1}}{k_{tj}}\frac{L_{tj}}{L_{tj0}}\left(\frac{L_{tj}}{L_0}\right)^2\right]^{-1}\right\}. \end{aligned} \tag{17.C.14}$$

17.C.2 Some Mathematical Relations in Buckling Design

In the strength-preserving design, the $C4T1^i$ system is designed to buckle at the same load as the original bar $C4T1^0$. The angles δ_j, where $j = 1, 2, \ldots, i–1, i$ are free variables to be specified to fix the geometry. Therefore, it is important to find out all the lengths and ratio quantities in terms of these angles.

17.C.2.1 Length of Structure and Strings

From the geometry of the structure, it can be shown that

$$\begin{aligned} L_0 &= L_i \prod\nolimits_{s=1}^{i} 2\cos\delta_s, \\ L_{tj} &= 2L_i \sin\delta_j \prod\nolimits_{s=j+1}^{i} 2\cos\delta_s. \end{aligned} \tag{17.C.15}$$

17.C.2.2 Computing the Stiffness Ratio of Strings, $\frac{k_{ts}}{k_{tj}}$ *for* $s, j = 1,2,3,..., i-1, i$

Consider the ratio

$$\begin{aligned} \frac{k_{t(j+1)}}{k_{tj}} &= \frac{E_{t(j+1)}A_{t(j+1)}}{L_{t(j+1)}} \frac{L_{tj}}{E_{tj}A_{tj}} \\ &= \frac{E_{t(j+1)}}{E_{tj}} \left(\frac{\pi r_{t(j+1)}^2}{\pi r_{tj}^2} \right) \left(\frac{L_{tj}}{L_{t(j+1)}} \right). \end{aligned}$$

From (17.109)

$$\frac{k_{t(j+1)}}{k_{tj}} = \frac{E_{t(j+1)}}{E_{tj}} \left(\frac{\sigma_{tj} t_{j+1}}{\sigma_{t(j+1)} t_j} \right) \left(\frac{L_{tj}}{L_{t(j+1)}} \right).$$

With (17.C.2) and (17.C.15), the ratio can be simplified to

$$\frac{k_{t(j+1)}}{k_{tj}} = \frac{E_{t(j+1)}}{E_{tj}} \left(\frac{\sigma_{tj}}{\sigma_{t(j+1)}} \right).$$

From this,

$$\frac{k_{ts}}{k_{tj}} = \frac{E_{ts}\sigma_{tj}}{E_{tj}\sigma_{ts}}. \tag{17.C.16}$$

In particular, if $E_{tj} = E_t$ and $\sigma_{tj} = \sigma_t$, then

$$\frac{k_{ts}}{k_{tj}} = 1. \tag{17.C.17}$$

So, in the strength-preserving design, if the same material is used, then all strings have the same stiffness.

17.C.2.3 Computing the Stiffness Ratio of String to Bar

$$\frac{k_{tj}}{k_{bi}} \text{ where } j = 1, 2, 3, ..., i-1, i$$

The stiffness of bar and strings are defined by

$$k = \frac{EA}{L},$$

where E is the Young's modulus, A is the cross-section area, and L is the length of bar or strings at the buckling load. With this definition and (17.C.16),

$$\frac{k_{tj}}{k_{bi}} = \frac{k_{tj}}{k_{ti}} \frac{k_{ti}}{k_{bi}} = \frac{E_{tj}\sigma_{ti}}{E_{ti}\sigma_{tj}} \frac{E_{ti}\pi r_{ti}^2}{L_{ti}} \frac{L_i}{E_i \pi r_i^2}$$

$$= \frac{E_{tj}\sigma_{ti}}{E_i \sigma_{tj}} \left(\frac{1}{L_{ti} L_i} \right) \frac{L_i^2}{r_i^2} r_{ti}^2 .$$

From (17.106), (17.109), and (17.C.15),

$$\frac{k_{tj}}{k_{bi}} = \frac{E_{tj}\sigma_{ti}}{E_i \sigma_{tj}} \left(\frac{t_i}{\pi \sigma_{ti}} \right) \left(\frac{4 l_i^2}{2 L_i^2 \sin \delta_i} \right)$$

$$= \frac{E_{tj}\sigma_{ti}}{E_i \sigma_{tj}} \left(\frac{2F \sin \delta_i}{\pi \sigma_{ti} \Pi_{s=1}^{i} 2 \cos \delta_s} \right) \left(\frac{2}{L_i^2 \sin \delta_i} \right) \left(\frac{E_i}{E_0} \right)^{\frac{1}{2}} \left(\frac{1}{\Pi_{p=1}^{i} 2 \cos \delta_p} \right)^{\frac{1}{2}} l_0^2 .$$

Substitute F from (17.66) into the above equation to obtain

$$\frac{k_{tj}}{k_{bi}} = \frac{E_{tj}\pi^2}{16 \sigma_{tj} l_0^2} \sqrt{\frac{E_0}{E_i}} \left(\prod_{s=1}^{i} 2 \cos \delta_s \right)^{\frac{1}{2}} . \tag{17.C.18}$$

For some materials of bars and strings, (17.C.18) reduces to

$$\frac{k_{tj}}{k_{bi}} = \frac{E_{tj}\pi^2}{16 \sigma_{tj} l_0^2} \left(\prod_{s=1}^{i} 2 \cos \delta_s \right)^{\frac{1}{2}} . \tag{17.C.19}$$

17.C.2.4 Computing the Rest Length-to-Length Ratio of Strings, L_{tj0}/L_{tj}

The tension in the strings is given by

$$t_j = k_{tj}(L_{tj} - L_{tj0}),$$

$$t_j = \frac{E_{tj}\pi r_{tj}^2}{L_{tj}}(L_{tj} - L_{tj0}).$$

From (17.109),

$$t_j = \frac{E_{tj}t_j}{L_{tj}\sigma_{tj}}(L_{tj} - L_{tj0}).$$

So,

$$\frac{L_{tj0}}{L_{tj}} = 1 - \frac{\sigma_{tj}}{E_{tj}}. \tag{17.C.20}$$

17.C.2.5 Computing the Rest Length to Length Ratio of Bars, L_{i0}/L_i

From (17.C.6),

$$\frac{F_i}{L_i} = \frac{t_1}{L_{t1}}$$

Hence,

$$k_{bi}\left(\frac{L_{i0}}{L_i} - 1\right) = k_{t1}\left(1 - \frac{L_{t10}}{L_{t1}}\right)$$

leading to

$$\frac{L_{io}}{L_i} = 1 + \frac{k_{t1}}{k_{bi}}\left(1 - \frac{L_{t10}}{L_{t1}}\right). \tag{17.C.21}$$

Using (17.C.20) and (17.C.21) reduces to

$$\frac{L_{i0}}{L_i} = 1 + \frac{k_{t1}}{k_{bi}}\frac{\sigma_{t1}}{E_{t1}}. \tag{17.C.22}$$

17.C.2.6 Computing the String Stiffness, k_{t1}

Recall that the string stiffness is given by

$$k_{t1} = \frac{E_{t1}\pi r_{t1}^2}{L_{t1}}.$$

$$= 1 + \frac{t1^2}{161_0^2}$$

Using (17.66), (17.108), and (17.109) yields

$$
\begin{aligned}
k_{t1} &= \frac{E_{t1}}{L_{t1}} \frac{t_1}{\sigma_{t1}} \\
&= \frac{E_{t1}}{\sigma_{t1}} \frac{F \tan \delta_1}{L_0 \tan \delta_1} \\
&= \frac{E_{t1}}{\sigma_{t1}} \frac{E_0 \pi^3 r_0^4}{4 L_0^3} \\
&= \frac{E_0 E_{t1} \pi^3 L_0}{64 \sigma_{t1} l_0^4}.
\end{aligned}
\tag{17.C.23}
$$

References

1. K. Snelson, Continuous tension, discontinous compression structures, US Patent 3, 169, 611, 1965.
2. B. Fuller. *Tensile-integrity structures,* US Patent, 3, 063, 521, 1962.
3. R. Adhikari, R. E. Skelton, and W. J. Helton, *Mechanics of Tensegrity Beams,* UCSD, Structural System and Control Lab., Report No. 1998-1, 1998.
4. D. M. Campbell, D. Chen, P. A. Gossen, and K. P. Hamilton, *Effects of spatial triangulation on the behavior of "tensegrity" domes,* 652–663, IASS-ASCE International Symposium, April 24–28, Atlanta, GA, 1994.
5. R. Chu, Tensegrity, *Journal of Synergetics,* 2(l), 1988.
6. M. F. Coughlin and D. Stamenovic, A tensegrity structure with buckling compression elements: Application to cell mechanics, *Transactions of ASME, Journal of Applied Mechanics,* 64, 480–486, 1997.
7. D. E. Ingber, Tensegrity: The architectural basis of cellular mechanotransduction, *Annual Review of Physiology,* 59, 575–599, 1997.
8. I. J. Oppenheim and W. J. Williams, Tensegrity prisms as adaptive structures, ASME Annual meeting, Dallas, November 1997.
9. A. Pugh, *An Introduction to Tensegrity,* University of California Press, Berkeley, 1976.
10. R. Motro et al., Form finding numerical methods for tensegrity systems*,* IASS-ASCE International Symposium, Atlanta, GA, April 24–28, 706–713, 1994.
11. H. Faruya, Concept of deployable tensegrity structures in space applications, *International Journal of Space Structures*, 7(2), 143–151, 1992.
12. S. Pellegrino, Analysis of prestressed mechanisms, *International Journal of Solids and Structures*, 26(12), 1329–1350, 1989.
13. S. Pellegrino, A class of tensegrity domes, *International Journal of Space Structures*, 7(2), 1992.
14. A. Hanaor, Double-layer tensegrity grids as deployable structures, *International Journal of Space Structures*, 8, 1992.
15. S. Pellegrino, Foldable bar structures, *International Journal of Solids and Structures*, 34(15), 1825–1847, 1996.
16. D. Williamson and R. E. Skelton, A general class of tensegrity systems: Equilibrium analysis, Engineering Mechanics for the 21st Century, ASCE Conference, La Jolla, 1998.
17. R. E. Skelton, J. P. Pinaud, and D. L. Mingori, Dynamics of the shell class of tensegrity structures, *Journal of the Franklin Institute*, 338(2–3), 255–320, 2001.
18. H. Murakami and Y. Nishimura, Static and dynamic characterization of regular truncated icosahedral and dodecahedral tensegrity modules, *International Journal of Solids and Structures*, 2001 (to appear).
19. B. de Jager and R. E. Skelton, Optimizing stiffness properties of tensegrity structures, *Proceedings of International Mechanical Engineering Congress and Exposition,* 3330, New York, 2001.
20. C. Sultan, Modeling, design, and control of tensegrity structures with applications*,* Ph.D. dissertation, Purdue University, Lafayette, Indiana, 1999.

21. C. Sultan, M. Corless, and R. E. Skelton, The prestressability problem of tensegrity structures: Some analytical solutions, *International Journal of Solids and Structures,* 2001 (to appear).
22. C. Sultan, M. Corless, and R. E. Skelton, Tensegrity flight simulator, *Journal of Guidance, Control, and Dynamics,* 23(6), 1055–1064, 2000.
23. C. Sultan, M. Corless, and R. E. Skelton. Linear dynamics of tensegrity structures, *Engineering Structures*, 2001 (to appear).
24. C. Sultan, M. Corless, and R. E. Skelton, Symmetrical reconfiguration of tensegrity structures, *International Journal of Solids and Structures,* 2001 (to appear).
25. L. Caviglione, Modellazione statica e dinamica di una tensegrity nell'ambito di una strategia di controllo attivo, Laurea thesis, University of Genoa*,* 1999.
26. M. Pedretti, Smart tensegrity structures for the Swiss expo, *Smart Structures and Materials*, 3330, San Diego, 1998.
27. L. Caviglione, A. Del Grosso, and M. Pedretti, Stabilisation and control of large tensegrity structures, private communication.
28. A. G. M. Michell, The limits of economy in frame structures, *Philosophical Magazine,* 8, 589–597, 1904.
29. M. P. Bendsoc and N. Kikuchi, Generating optimal topologies in structural design using a homozenization method, *Computer Methods in Applied Mechanics and Engineering*, 71, 197–224, 1988.
30. F. Jarre, M. Koevara, and J. Zowe, Optimal truss design by interior-point methods, *SIAM Journal on Optimization*, 8(4), 1084–1107, 1998.
31. J. Lu and R. E. Skelton, Optimal hybrid control for structures, *Computer-Aided Civil and Infrastructure Engineering*, 13, 405–414, 1998.
32. A. H. Simmons, C. A. Michal, and L. W. Jelinski, Molecular orientation and two-component nature of the crystalline fraction of dragline silk, *Science*, 271, 84–87, 1996.
33. Y. Termonia, Molecular modeling of spider silk elasticity, *Macromolecules,* 27, 7378–7381, 1994.
34. D. E. Ingber, Architecture of life, *Scientific American*, 48–57, January 1998.
35. D. E. Ingber, Cellular tensegrity: Defining new rules of biological design that govern the cytoskeleton, *Journal of Cell Science,* 104(3), 613–627, 1993.
36. R.E. Skelton, *Dynamic Systems Control — Linear Systems Analysis and Synthesis,* John Wiley & Sons, New York, 1988.
37. S. Pellegrino and C. R. Calladine, Matrix analysis of statistically and kinematically indeterminate frameworks, *International Journal of Solids and Stru*ctures, 22(4), 409–428, 1985.